NTNU – Trondheim
Norwegian University of
Science and Technology

Development of the Hybrid Absorption Heat Pump Process at High Temperature Operation

Anders Borgås

Master of Energy and Environmental Engineering
Submission date: June 2014
Supervisor: Trygve Magne Eikevik, EPT

Norwegian University of Science and Technology
Department of Energy and Process Engineering

NTNU
Norwegian University
of Science and Technology

Department of Energy
and Process Engineering

EPT-M-2014-17

MASTER THESIS

for

Student Anders Borgås

Spring 2014

Development of the hybrid absorption heat pump process at high temperature operation
Utvikling av hybrid absorpsjonsvarmepumpeprosess for høytemperatur drift

Background and objective

The heat pump market has so far mainly focused on residential heat pumps for space heating and domestic hot water production. Less focus has been on heat pumps for higher temperature applications and industrial use due to high initial investment costs, competition with alternative investments, and non-mature or non-existing technologies for the applications to be served. New developments in compact high pressure components, e.g. compressors, ejectors and heat exchangers for CO_2, ammonia and hydrocarbon heat pump systems, are important drivers for change of this situation.

This master work will concentrate on the design of a high temperature hybrid heat pump for production of hot water from surplus heat. The cases for calculation will be taken from the food industry.

The following tasks are to be considered:

1. Literature review of high temperature heat pumps with special focus on hybrid heat pumps
2. Develop a simulation tools for calculation of the hybrid heat pump systems, eventually use commercial software
3. Optimize different heat exchanger design for the hybrid process utilizing the temperature glide (plate, plate and shell or other heat exchanger design)
4. Evaluate different system designs to utilize the absorption heat to achieve higher temperature than the discharge gas temperature from the compressor
5. Make a scientific paper from the main results of the work
6. Make suggestion for further work

-- " --

Within 14 days of receiving the written text on the master thesis, the candidate shall submit a research plan for his project to the department.

When the thesis is evaluated, emphasis is put on processing of the results, and that they are presented in tabular and/or graphic form in a clear manner, and that they are analyzed carefully.

The thesis should be formulated as a research report with summary both in English and Norwegian, conclusion, literature references, table of contents etc. During the preparation of the text, the candidate should make an effort to produce a well-structured and easily readable report. In order to ease the evaluation of the thesis, it is important that the cross-references are correct. In the making of the report, strong emphasis should be placed on both a thorough discussion of the results and an orderly presentation.

The candidate is requested to initiate and keep close contact with his/her academic supervisor(s) throughout the working period. The candidate must follow the rules and regulations of NTNU as well as passive directions given by the Department of Energy and Process Engineering.

Risk assessment of the candidate's work shall be carried out according to the department's procedures. The risk assessment must be documented and included as part of the final report. Events related to the candidate's work adversely affecting the health, safety or security, must be documented and included as part of the final report. If the documentation on risk assessment represents a large number of pages, the full version is to be submitted electronically to the supervisor and an excerpt is included in the report.

Pursuant to "Regulations concerning the supplementary provisions to the technology study program/Master of Science" at NTNU §20, the Department reserves the permission to utilize all the results and data for teaching and research purposes as well as in future publications.

The final report is to be submitted digitally in DAIM. An executive summary of the thesis including title, student's name, supervisor's name, year, department name, and NTNU's logo and name, shall be submitted to the department as a separate pdf file. Based on an agreement with the supervisor, the final report and other material and documents must be given to the supervisor in digital format. All relevant data collected and produced during the project shall be delivered to the supervisor on a CD at the end of the project.

☐ Work to be done in lab (Water power lab, Fluids engineering lab, Thermal engineering lab)
☐ Field work

Department of Energy and Process Engineering, January 14th 2014

Prof. Olav Bolland
Department Head

Prof. Trygve M. Eikevik
Academic Supervisor

Research Advisor:
Armin Hafner, SINTEF Energi AS, e-mail: armin.hafner@sintef.no

NTNU
Norwegian University
of Science and Technology

Department of Energy
and Process Engineering

EPT-M-2014-17

CORRECTION OF TASKS TO BE CONSIDERED

In agreement with the project supervisor, the optimization of heat exchanger design was only conducted for a plate-fin heat exchanger. Development of simulation tools required more time than expected, and the simulations conducted was focused on thermodynamic aspect of the hybrid heat pump for high temperature application. **Therefore the new tasks to be considered are:**

1. Literature review of high temperature heat pumps with special focus on hybrid heat pumps
2. Develop a simulation tools for calculation of the hybrid heat pump systems, eventually use commercial software
3. Evaluate the hybrid compression/absorption heat pump for heating water to 150 °C
4. Optimize a plate-fin heat exchanger design for an absorption process heating air
5. Make a scientific paper from the main results of the work
6. Make suggestion for further work

These task are specified in agreement with the project advisor

Prof. Trygve M. Eikevik
Supervisor

Anders Borgås
Student

Preface

This master thesis is written to conclude the five year master Degree Program at The Department of Energy and Process Engineering at NTNU. The thesis investigates the compression/absorption heat pump with an ammonia/water mixture for high temperature applications utilizing low grade waste heat.

I would like to thank my supervisor Trygve M. Eikevik for his guidance during the work on the thesis. I would also like to thank Stein Rune Nordtvedt at Hybrid Energy AS for his assistance on the topic.

Finally, I wish to express gratitude towards my fellow students Martin Bergland and Bjørn-Ole Grønneflåta, who also wrote their thesis on compression/absorption heat pumps, for important discussions and exchange of views during the process.

Anders Borgås

Abstract

Recovering waste heat from industrial processes is beneficial in order to reduce primary energy demands. Waste heat temperatures; however, are often too low to directly utilize in processes with high temperature demands, thus high temperature heat pumps might be useful. Hybrid heat pumps with ammonia/water mixtures as working fluid are identified as one of the most promising heat temperature heat pump technologies. The hybrid heat pump process combines the conventional vapour-compression heat pump cycle and the absorption heat pump cycle, and is especially suited for process with large temperature lifts due to the fact that binary mixtures evaporates and condenses with varying tempeatures. Moreover, saturation pressures of ammonia/water mixtures is significantly lower than saturation pressure of pure ammonia, which enables of ammonia at higher temperatures than in conventional vapour-compression heat pumps. Hybrid heat pump systems are also distinguished by high performances and are flexible considering capacity control and external changes.

A two-stage compression/absorption heat pump simulation model was developed in order to evaluate the thermodynamic process for high temperature operation. In the simulation scenarios, waste heat was available at 50 °C and the goal was to heat process water from 100 °C to 150 °C. Heat pump performance, temperature levels and pressure levels were some of the key results of the simulation scenarios. Secondary, it was developed a simulation model of a finned, annular tube cross-flow absorber in order to assess the dimensions of an absorber for heating air with an ammonia/water mixture. Both models were used in a simulation case where the compression/absorption heat pump was integrated in a spray drying process using waste heat air at 35 °C as heat source.

Simulations with the two-stage model showed that the scenarios with high water content in the vapour before the compressor, achieved the highest performances. Circulation ratios were higher, which resulted in a larger fraction of the mixture mass flow went through the compressor circuit, hence smaller compressor work. Although pressure ratios were higher, resulting absorber pressures were significantly lower. Some of the disadvantages with high water content were higher discharge temperatures, although discharge temperatures were high in all scenarios, and considerably lower vapour densities. In simulations were the discharge temperature was limited to 180 °C, the highest achieved COP was 1.81, while in simulations with no limitations to the discharge temperature, the highest COP was 2.53. Moreover, simulation scenarios without limitations to the discharge temperature resulted in lower absorber pressures, hence lower pressure ratios and higher performances. However, it resulted in discharge temperatures as high as 310 °C. Simulations with a desuperheater showed, provided that the minimum temperature difference between solution and heat sink does not occur at the absorber inlet, that a desuperheater provides no gain. Even when the minimum temperature difference occurs at the absorber inlet, there is only a small gain and it gets smaller with increasing circulation ratios.

Dimensioning the absorber gave some unrealistic results in terms of an extreme ratio between absorber height and width/length. Even with the smallest obtained ratio, the

height was 10 times the width, and the required surface area was significantly higher than for larger ratios. It is difficult to determine whether the results are due to errors in the simulation model or if it is difficult to obtain a noteworthy result with the simulation inputs. However, it is worth mentioning that the air mass flow rate was 15 times as high as the mixture mass flow rate. In the spray drying simulation case, the heat pump performance was 1.40 including the fan work. This performance was calculated with no limitation to the discharge temperature and with more realistic limitations, the performance would have been lower. The required temperature lift in the case may have been somewhat high for the heat pump process.

Sammendrag

Gjenvinning av overskuddsvarme i industrielle prosesser er gunstig for å kunne redusere den primære energibruken, men ofte er temperaturen på varmen for lav til å direkte kunne nyttes i prosesser med høye temperaturkrav, dermed vil høytemperaturvarmepumper være nødvendig. Hybride varmepumper med ammoniakk/vannblandinger som arbeidsmedium er identifisert som en av de mest lovende teknologiene for høytemperaturvarmepumper. Hybride varmepumper kombinerer konvensjonelle kompresjonsvarmepumper og absorbsjonsvarmepumper, og er særdeles egnet for prosesser med store temperaturløft idet binære blandinger fordamper og kondenserer med varierende temperaturer. Videre er metningstrykkene til ammoniakk/vannblandinger betydelig lavere en for ren ammoniakk, noe som fører til at ammoniakk kan brukes som arbeidsmedie for høyere temperaturer en i konvensjonelle kompresjonsvarmepumper. Hybride varmepumper kjennetegnes også av høy ytelse og stor fleksibilitet med tanke på kapasitetsregulering og ytre forandringer.

Det ble utviklet en simuleringsmodell av en to-trinns kompresjons/absorbsjonsvarmpumpe for å kunne vurdere prosessen termodynamisk, ved høytemperaturdrift. I simuleringsscenarioene ble blant annet varmepumpens ytelse, trykknivåer og temperaturnivåer vurdert når overskuddsvarme ved 50 °C ble gjenvunnet og prosessvann varmet opp fra 100 °C til 150 °C. Det sekundære målet var å utvikle en simuleringsmodell for dimensjonering av en rør-finnevarmeveksler for oppvarming av luft. Videre ble begge modellene brukt i en case der varmepumpen ble integrert i en spraytørkeprosess hvor overskuddsvarmen fra luft ved 35 °C ble brukt som varmekilde i desorberen.

Simuleringer med to-trinns modellen viste at varmepumpen hadde høyest ytelse når ammoniakk konsentrasjonen i gassen i kompresjonskretsen var den laveste av de vurderte scenarioene. Det førte til at sirkulasjonsraten ble høy og en større andel av massestrømmen til blandingen gikk i løsningskretsen, dermed ble kompressorarbeidet mindre. Selv om trykkforholdet var noe større, ble absorbertrykkene betydelig lavere. Ulempene med en høy andel vann var at trykkgasstemperaturene ble høyere, selv om trykkgasstemperaturene ble veldig høye for alle simuleringene, og at gasstettheten er betraktelig mindre. Med trykkgasstemperaturen begrenset til 180 °C, var den høyeste ytelsen 1.81, mens uten begrensinger ble en ytelse på 2.53 oppnådd. Videre viste simuleringsresultatene at ved å øke grensen til trykkgasstemperaturen kunne absorbertrykkene reduseres, dermed lavere trykkforhold og høyere ytelse. Men det førte samtidig til trykkgasstemperaturer opp mot 310 °C. Simuleringer med overhetningsvarmeveksler viste at, såfremt den minste temperaturdifferansen mellom blandingen og varmesluket ikke forekommer ved innløpet til absorberen, vil ikke overhetningsvarmeveksleren gi noen gevinst. Selv når den minste temperaturdifferansen forekommer ved innløpet, vil gevinsten være liten og den blir mindre når sirkulasjonsraten øker.

Dimensjoneringen av absorberen ga noe urealistiske resultater i form av det ekstreme forholdet mellom høyden og bredden/lengden på absorberen. Selv med det minste forhol- det, var høyden 10 ganger så stor som bredden, i tillegg krevde det et betraktelig større varmevekslerareal en ved større forskjeller mellom høyde og bredde/lengde. Det

er vanskelig å avgjøre om det er et resultat av feil i simuleringsmodellen, eller om det er vanskelig å oppnå gode resultater med inngangsparameterene brukt i simuleringene. Det er verdt å nevne at massestrømmen til luft vil kunne være 15 ganger så stor som massestrømmen til blandingen under disse forholdene, samtidig er hastigheten til luften begrenset. Simuleringscasen med spraytørke ga en varmepumpeytelse på 1.40, inkludert viftearbeidet. Denne ytelsen ble beregnet uten begrensing til trykkgasstemperaturen, og med mer realistiske begrensinger til trykkgasstemperaturen ville ytelsen vært betraktelig lavere. Det er mulig at temperaturløftet i simuleringscasen var i overkant stor for varmepumpeprosessen.

Contents

List of Figures

List of Tables

Nomenclature

Latin letters

A	Area	m^2
$\dot{C}$	capacitance rate	kW/K
c_p	specific heat capacity	kJ/kg-K
D	diameter	m
h	enthalpy	kJ/kg
H	height	m
L	length	m
$\dot{m}$	mass flow rate	kg/s
$N_{t,col}$	number of tube columns	-
$N_{t,row}$	number of tube rows	-
P	pressure	bar
P_{HX}	LMTD effectiveness	-
p_{fin}	fin pitch	m
Pr	Rrandtl number	-
q	vapour mass fraction	-
$\dot{Q}$	heat transfer rate	kW
r	radius	m
R_{HX}	LMTD capacitance ratio	-
Re	Reynolds number	-
s	entropy	kJ/kg-K
s_h	horizontal tube spacing	mm
s_v	vertical tube spacing	mm
u	internal energy	kJ/kg
T	temperature	°C or K
th_{fin}	fin thickness	m
u_m	mean velocity	m/s
U_y	overall heat transfer coefficient (air-side surface area)	W/m^2-K
v	specific volume	m^3/kg
$\dot{V}$	volumetric flow rate	m^3/s
W	width / work	m / kW
x	ammonia concentration	-
ZZ	overall ammonia concentration	-

Greek letters

α	heat transfer coefficient	W/m^2-K
ε	thermal efficiency	-

η	fin efficiency	-
θ	reduced temperature	-
λ	thermal conductivity	W/m-K
μ	dynamic viscosity	Pa-s
ρ	density	kg/m^3
Subscripts		
abs	absorber	-
avg	average	-
C	cold	-
cf	correction factor	-
comp	compressor	-
cond	conduction	-
crit	critical	-
des	desorber	-
dsh	desuperheater	-
eff	effective	-
H	hot	-
ihx	internal heat exchanger	-
in	inner	-
liq	liquid	-
m	mean	-
max	maximum	-
min	minimum	-
mix	mixture	-
s	surface	-
out	outer	-
thr	throttling	-
tot	total	-
vap	vapour	-
Superscripts		
-	-	-
Abbreviations		
CFC	Chlorofluorocarbon	-
COP	Coefficient Of Performance	-
CR	Circulation Ratio	-
EES	Engineering Equation Solver	-
GWP	Global Warming Potential	-
HCFC	Hydrochlorofluorocarbon	-
HFC	Hydrofluorocarbon	-
HP	High-Pressure	-
IHX	Internal Heat Exchanger	-
LMTD	Log Mean Temperature Difference	K
LP	Low-Pressure	-
ODP	Ozone Depletion Potential	-
SHX	Solution Heat Exchanger	-

Introduction

1.1 Background

Global energy demands are increasing and concerns of global warming brings major challenges considering the future of energy production and consumption. Industry requires energy at high temperatures and produces vast amounts of waste heat, often disposed without further use. Recovering waste heat is environmentally benign as it reduces primary energy use. However, waste heat temperatures are often too low to directly utilize and in order to make use of low grade waste heat for processes with high temperature requirements, heat pumps are necessary (Stene, 1993). Heat pumps are the only heat recovering system able to deliver heat at a higher temperature than the temperature of the waste heat (Dinçer and Kanoğlu, 2010). In the last two decades, heat pump technology has become a mature technology (Chua et al., 2010). Heat pumps with output temperatures below 50 °C are widely used for residential purposed. However, heat pumps for industrial use and high temperature applications are rarely used. High initial costs as well as low energy costs has been some of the main factors for the slow development. Nevertheless, there is a large potential and it is estimated that 40% of the primary industrial energy demand in industrialised countries can be reduced by the use of heat pumps. If the use of heat pumps in industry should prevail, initial cost must be decreased. (Dinçer and Kanoğlu, 2010). Heat pumps have to be financially competitive with technologies such as boilers, heat pipes and regenerators. Moreover, heat pumps must be able to deliver heat at 150 °C to 300 °C and process technologies must be adapted to heat pump applications. While the residential market may be satisfied with standardized solutions and installations, most industrial heat pump applications need to be adapted to unique conditions (Jakobs et al., 2010). Heat pumps can be used for space heating, process water heating and cooling, steam production, drying and humidification processes, evaporation, distillation and concentration processes in a wide range of industrial sectors, and different processes requires energy in wide ranges of temperature levels and temperature lifts, which sets requirements to heat pump technology. The phase-out of CFCs and HFCs challenges the development of high temperature heat pumps as it results in fewer applicable refrigerants. Brunin et al. (1997) vindicated that conventional vapour-compression heat pumps with hydrocarbons and compression/absorption heat pumps with ammonia/water mixtures offers the two most promising heat pump technologies for high temperature applications. Compression/absorption heat pumps with ammonia/water mixtures presents an interesting alternative, not only because of the use of two natural working fluids, but it combines the vapour-compression heat pump

cycle and absorption heat pump cycle. Vapour-compression heat pumps have limited temperature lifts, inflexible operating ranges, limited capacity control and mismatches between temperature curves, while absorption heat pumps have limited temperature ranges (Kim et al., 2013). By combining the two systems in a hybrid compression/absorption heat pump, the individual limitations are reduced. Compression/absorption heat pumps are characterized as heat pump systems especially suited for processes with large temperature lifts, due to evaporation and condensation with temperature glides, and distinguished by high performance and flexibility considering capacity control and external changes.

1.2 Main goal of the thesis

The main goal of the thesis is to develop a calculation tool in order to evaluate the compression/absorption heat pump process with an ammonia/water mixture as working fluid, for high temperature application. Simulation scenarios will address thermodynamic performances, pressure levels, temperature levels and other important properties when utilizing surplus heat at 50 °C in order to heat process water from 100 °C and 150 °C. The approach of the simulations will address what is necessary for the process to be realised rather than what is possible with current components and limitations.

The secondary focus is developing a simulation tool for the absorber process in order to evaluate dimensions of an finned-tube absorber for heating air. Finally, both models will be used to assess the compression/absorption heat pump as measure to reduce the energy demand in a spray drying process.

A scientific paper is also written presenting the most important results and conclusion of the thesis.

1.3 Structure of the thesis

Chapter 2 provides an short overview of current heat pump technology for high temperature application.

Chapter 3 provides a literature review compression/absorption heat pump cycle, and characteristic features of the compression/absorption process and the ammonia/water mixture. The chapter also gives a brief overview of the development of compression/absorption process for high temperature application and the absorption process with ammonia/water mixtures.

Chapter 4 gives a description of the two simulation models. A two-stage compression/absorption model for heating water and an absorber model for heating air.

Chapter 5 presents the results from the simulations and discussions.

Chapter 6 gives the conclusion and suggestions for future work.

High Temperature Heat Pumps

2.1 Introduction

Heat pumps for industrial purposes and high temperature application have a great variation in type of drive energy, heat pump size, operating conditions, heat sources and type of application, and as previously noted, this causes heat pumps to be customized for the specific application (IEA-HPC, 2014). Figure 2.1 displays heat pump installations in industry (LeonardoEnergy, 2007).

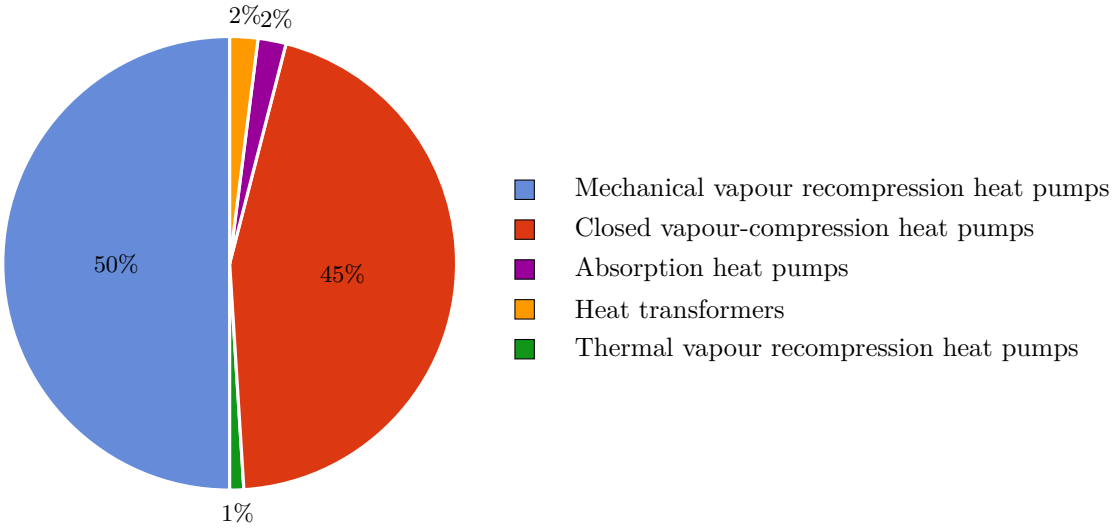

FIGURE 2.1: Industrial heat pump installations divided according to heat pump type

2.2 Closed vapour-compression heat pumps

A simple closed-cycle mechanical compression heat pump consists of four components; a condenser, an evaporator, a compressor and a expansion device. The term closed-cycle refers to the circulation of the cycle refrigerant/working fluid. Closed-cycle compression heat pumps utilizes the latent heat of evaporation and condensation to conduct isothermal heat exchanges. Heat is absorbed by the refrigerant from the heat source isothermally by evaporation in the evaporator, before entering the compressor and compressed to a higher pressure stage, hence the temperature increases. Refrigerant exiting

the compressor enters the condenser with a higher temperature than the heat sink, thus heat is rejected to the heat sink by condensation, before it is expanded to the low-pressure stage of the cycle.

A great majority of heat pumps in operation are simple vapour-compression heat pumps, but as figure 2.1 shows, vapour-compression systems is not as dominant in the industrial sector as in the residential sector. One of the main challenges for high temperature vapour-compression cycles are suitable working fluids with favourable thermodynamic and environmental properties. R114 was exclusively used for industrial applications with temperature requirements up to 120 °C, while R11 was used for even higher temperature demands (Zhou et al., 2012). Both refrigerants are pure substances of CFCs and are refrigerants included in the Montreal Protocol, and it has been extensive research to reveal suitable replacements for the refrigerants. Among R124, R141a and R123, the latter was the most promising interim alternative to R11, while R245ca and R143 were considered as long term substitutes. R134 and R143 were potential replacements for R114. In later years systems with R245fa as refrigerant has been introduced in high-temperature heat pump applications and steam generation (Watanabe, 2012). Even with zero ODP and significantly lower GWP than R114, R245fa still has a substantial contribution on global warming and can be viewed as an interim alternative.

Natural working fluids has gained a great amount of attention, due to the environmental impact of many other refrigerants. The most significant natural working fluids are ammonia, water, CO_2 and hydrocarbons. Ammonia is an excellent working fluid, preferable to most CFCs, HCFCs and HFCs (Bolaji and Huan, 2013; Lorentzen, 1995). However, pressure limitations of system components prevents the use of NH_3 at high temperatures. A saturation pressure of 40 bar results in condensation at 78.5 °C. Ammonia will also have considerably higher discharge temperatures than conventional refrigerants, due to relatively low densities and specific heat in the vapour phase. Water is also an excellent working fluid for high temperature heat pump applications. Besides not being toxic or flammable, water has favourable thermodynamic properties and a critical temperature of 374.1 °C. The heat of vaporization is about fifteen times higher than that of R134a at 50 °C (Pearson, 2012). Other advantages is that water is thermally stable and chemically inert at high temperatures, which may cause problems for other refrigerants (Bolaji and Huan, 2013). The major disadvantage with water in vapour-compression cycles, is low volumetric heat capacity due to low vapor density and low operating pressures, resulting in large required swept volume to the compressor. However, there has been progression in developing compressors with good efficiencies for this purpose (Yuan and Blaise, 1988). Many hydrocarbons are suitable refrigerants due to good thermodynamic and transport properties. Butane and isobutane with critical temperatures of 152.0 °C and 134.7 °C respectively, are particularly interesting when considering high temperature heat pump applications. The only objection against the usage of hydrocarbons is their flammability.

2.2.1 Multistage vapour-compression heat pumps

Large temperature lifts in heat pump systems results in high pressure ratios, which entails lower compression efficiencies, higher discharge temperatures and lower system performances. In multistage heat pump systems, compression and expansion are divided into several steps to reduce disadvantages of high temperature lifts (Stene, 1997). Multistage vapour-compression heat pumps are expanded closed vapour-compression heat pumps, and can be classified as either compound or cascade systems (Chua et al., 2010). Compound systems are essentially extended single-stage systems. The condenser and the evaporator operates as in a single-stage system, but compression and expansion is carried out in two or several system. The most usual configuration is a two-stage system. In this configuration a low-pressure compressor compresses the refrigerant from the condenser-pressure to an intermediate pressure before the high-pressure compressor compresses the refrigerant to the condenser pressure. Cascade systems applies two (or several) different working fluid in separate single-stage compression cycles allowing the individual cycles to operate within systems boundaries were it can provide good system efficiency with reasonable pressures (Fornasieri et al., 2009). A cascade condenser/evaporator connects the cycles, which adds an extra temperature loss.

2.2.2 Transcritical cycles

Conventional vapour-compression cycles operates subcritically in order to utilize the latent heat of evaporation and condensation. In a transcritical cycle, heat rejection occurs in supercritical phase, where the fluid is neither gas nor liquid. Contrary to subcritical heat rejection where temperature is constant at constant pressure, the temperature is independent of the pressure. The result is a heat rejection with a temperature glide. CO_2 has re-emerged as a refrigerant in the development of transcritical heat pump cycles. Both subcritical and transcritical CO_2 cycles have a relative low theoretical COP, but high compressor efficiency and excellent transport properties, results in a competitive efficiency in reality. CO_2 systems have operating pressures typically 5-10 times higher that conventional refrigerants. Development in components has allowed higher system pressure and more compact design of systems due to high vapour density and there are no extra safety risk concerning the high pressure in CO_2 systems. CO_2 systems have been introduced to the commercial market in heat pump water heaters and in different system solutions in commercial refrigeration and are becoming an competitive alternative. One pre-condition for an effective CO_2 system is a heat sink with low inlet temperature to ensure a low CO_2 temperature before expansion. CO_2 evaporating temperatures is limited to approximately 25 °C due to the critical temperature and waste heat recovering in industrial processes will often have heat source temperatures above the critical temperature of CO_2, thus resulting in an infeasible solution (Kim et al., 2004; Stene, 1997).

2.3 Vapour-recompression systems

There are two types of vapour-recompression heat pump systems; Mechanical vapour-recompression (MVR) and thermal vapour-recompression (TVR). MVR systems are the most common of industrial heat pumps (Laue, 2006) and is used to mechanically compress waste gases in order to reclaim surplus heat. MVR systems can be classified as open or semi-open systems. In an open MVR-system, the compressed waste gas delivers heat by condensation to the heat sink. Semi-open systems are less usual configuration were the compressed gas delivers heat to a heat sink, which in turn delivers heat to another process stream. MVR systems does not apply a separate working fluid, like vapour compression systems, but uses process streams directly. Water vapour is the most common working fluid, although other process fluids are used, notably in the chemical industry (LeonardoEnergy, 2007). The configuration of MVR systems require fewer components than conventional vapour compression systems, thus a lower investment and maintenance cost, and easier implementation. MVR systems are able to work with heat source temperatures at 70 - 80 °C and deliver useful heat at 110 - 150 °C, in some cases as high as 200 °C. Compared to vapour-compression heat pumps, MVR systems have a much higher COP, typically between 10 - 30. TVR systems are not as widely applied as MVR systems. System efficiency is general low and rapidly decreasing with increasing temperature lift. Investment and maintenance cost for these applications are low, however, they are best suited for small scale systems. As a thermally driven heat pump system, TVR can be a beneficial system when there is a large difference between fuel and electricity prices (LeonardoEnergy, 2007; Stene, 1993).

2.4 Absorption heat pumps

There are two main configurations of absorption heat pumps. Type I absorption heat pumps are referred to as heat amplifiers, meaning the heat pumping process is a heat increasing process. Type II absorption heat pumps are referred to as heat transformers, meaning the heat pumping process is a temperature increasing process (Stene, 1993). Heat amplifiers and heat transformers consists of the same main components and have the same operating principle. The difference between the systems are the temperature levels of different components and temperature levels of the heat inputs and outputs. The main components of absorption heat pumps are evaporator, condenser, generator/desorber and absorber. The system consists of to circuits; a heat pump circuit and a absorption circuit, where the heat pump circuit with the condenser, evaporator and expansion device, is similar to a vapour-compression. But in a absorption heat pumps, the absorption circuit with absorber, generator and solution pump, replaces the compressor in a vapour-compression heat pump (McMullan, 2003). H_2O/LiBr and NH_3/H_2O are the two most common working pairs in absorption heat pumps. Systems applying H_2O/LiBr in heat amplifiers are able to deliver heat at 100 °C with a COP of 1.6 - 1.7. Heat transformers applying H_2O/LiBr are able to deliver heat at 100 °C with a COP of 0.45 - 0.5. Large capital cost, especially for small scale applications, is the main prevalence for thermally driven heat pumps (Nordtvedt, 2013). Ratio between cost of

electricity and fuel is another important factor. Countries producing electricity at thermal power plants have relatively high electricity prices, thus making thermally driven heat pumps more suitable than in countries where electricity is produced by hydro-power (Stene, 1993)

Compression/Absorption Heat Pumps

3.1 Introduction

Compression/absorption heat pumps are essentially conventional vapour-compression heat pumps employing non-azeotropic (zeotropic) working fluids (Stene, 1993). Non-azeotropic working fluids consists of multiple components with different volatility which causes the composition in liquid and vapour phases to change during evaporation and condensation processes, hence heat exchanging processes with temperature glides (Dinçer and Kanoğlu, 2010). The simplest version of a compression/absorption heat pump cycle is based on the the Osenbrück cycle (figure 3.3). Although the principle of the cycle has been know for over a century, little effort has been done to studying the subject until recent decades (Nordtvedt, 2005). Compression/absorption heat pumps are characterized by flexibility in capacity and temperature range, and is especially suited for processes with heat sink and heat source temperature glides. Combined with the use of environmentally benign working fluids, the system is likely to have an important role in future heat pump application. Absorption heat pump processes utilize the ability of liquids and salts to absorb vapour, thus the working media is often a binary mixture. The two most common working pairs used is water/lithium bromide and ammonia/water. In compression/absorption heat pump processes with ammonia/water mixtures, ammonia is the more volatile component, hence classified as the working fluid, while water is classified as the absorbent. An understanding of the thermodynamic of binary mixtures is important to understand the advantages and particularities of a compression/absorption heat pump system, and to understand the working principle of a compression/absorption heat pump cycle.

3.2 Properties of the ammonia/water mixture

Single component fluids evaporates and condenses isothermally, and the saturation temperature is determined by the pressure. Saturation temperatures for a binary mixtures, however, are not only determined by pressure, but by both pressure and mixture composition. Moreover, the different volatility of the component causes one component to evaporate/condense more quickly causing the concentration to change during evaporation and condensation, thus the saturation temperature changes. In chemical terms this phenomenon is described as a boiling point elevation. Boiling point elevation is a collagative property of mixtures which means that the property is dependant on the

presence of dissolved particles and their number, but not their identity. The presence of solvent in a solute causes the boiling point of the solution to increase (Atkins and Paula, 2010). In an absorption process with an ammonia/water mixture, ammonia, being more volatile than water, is referred to as the refrigerant/working fluid, while water is referred to as the absorbent. When ammonia is dissolved in water, the boiling point of the mixture is higher than for pure ammonia at the same pressure and temperature, while it is lower than for pure water under the same conditions. The phenomenon of boiling point elevation is the foundation of two of the most prominent characteristics of compression/absorption heat pumps with ammonia/water mixtures; evaporation and condensation processes with temperature glides, and it enables the use of ammonia at higher temperatures than in conventional vapour-compression heat pump cycles.

Temperature-concentration diagrams are useful tools for visualising evaporation and condensation processes in binary mixtures. Figure 3.1 shows the temperature-concentration for an ammonia/water mixture at 5 bar, where the bubble point curve indicates at which temperature, for a given concentration, the first bubbles starts to form in the liquid. The concentration in the bubbles is found by drawing a horizontal line from the bubble point curve to the dew point curve. Similarly the dew point curve indicates, for a given concentration, at which temperature the first droplets starts to form, and by drawing a horizontal line from the dew point curve to the bubble point curve, the concentration of the liquid droplet is found. The diagram shows that the concentration of bubbles and droplets is not equal to the liquid and vapour concentrations, thus the concentration changes as bubbles and droplets are formed. When liquid evaporates, more ammonia evaporates than water, thus the liquid properties moves to the left along the bubble point curve. The boiling point of the mixture increases, while evaporating bubbles will have an increasing water concentration. Figure 3.1 illustrates an evaporation process for an ammonia/water mixture at 5 bar (Alefeld and Radermacher, 1993):

- An ammonia/water mixture with a 50 weight-% concentration of ammonia and a temperature of 10.0 °C is subcooled liquid, denoted by point 1 in figure 3.1.
- When adding heat to the mixture, the temperature increases until it reaches the bubble point temperature for the given concentration. In this case the temperature is 39.8 °C, denoted by point 2_b. The first bubble starts to form and the ammonia concentration of the bubble, which is in thermal equilibrium with the surroundings, is 99.6 weight-%, denoted by point 2_d.
- More heat is added to the mixture, and more of the mixture evaporates, until it reaches a temperature of 102.3 °C, denoted by point 3. If all the evaporated mixture remains in contact with the liquid, the mixture is two-phase. The ammonia concentration of the vapour is 81.3 weight-%, denoted by point 3_d, while the concentration of the liquid is 18.3 weight-%, denoted by point 3_b.
- More heat is added until the mixture of the temperature reaches 128.8 °C denoted by point 4_d. The evaporation process is completed and the concentration of the last droplet to evaporate is 8.2 weight-%, denoted by point 4_b. In other words, if saturated vapour with a 50 weight-% concentration of ammonia condensates, the first droplet would have a 8.2 weight-% concentration of ammonia.

- Further heating would result in a superheated vapour. In figure 3.1 superheated vapour at 158.6 °C is denoted by point 5.

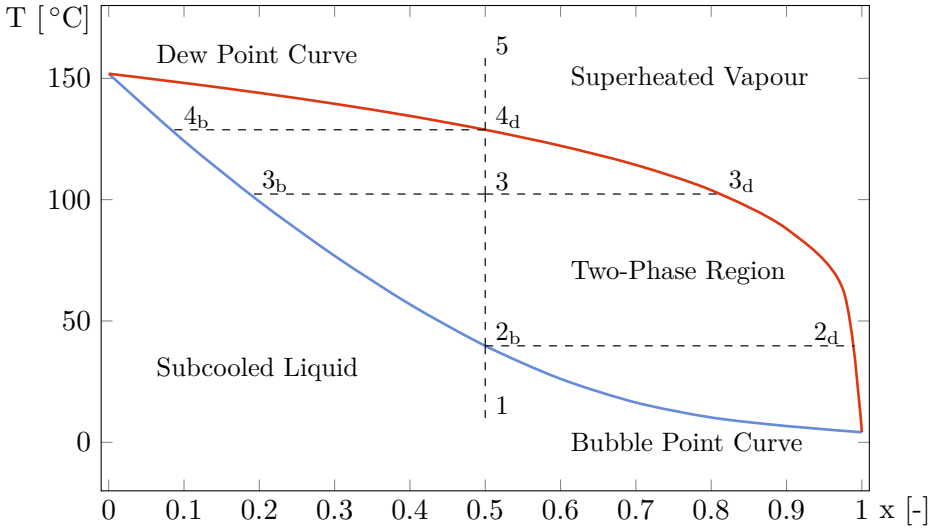

FIGURE 3.1: Temperature-concentration diagram of an ammonia/water mixture at 5 bar

When a working fluid and an absorbent at the same temperature is adiabatically mixed into a solution, the temperature of the solution will either decrease or increase depending on the pressure and concentration of each component. If the mixing is isothermal, heat is either rejected to or absorbed from the surroundings. The energy production or energy required in the process is called the solution enthalpy, and the total enthalpy of the solution is given by (Stene, 1993):

$$h = (1 - x) \cdot h_a + x \cdot h_r + (\Delta h)_i \tag{3.1}$$

where h_a is the absorbent enthalpy, h_r is the refrigerant enthalpy, x is the mass fraction of the refrigerant and $(\Delta h)_i$ is the solution enthalpy. The total heat production during condensation and evaporation of binary mixtures is determined by the latent heat and the solution enthalpy:

$$(\Delta h)_{tot} = (\Delta h)_i + (\Delta h)_{latent} \tag{3.2}$$

Figure 3.2 shows the significance of the solution enthalpy for an ammonia/water mixture. However, it is a less useful representation for evaluating an absorber or desorber process since the temperature and concentration vary during the process.

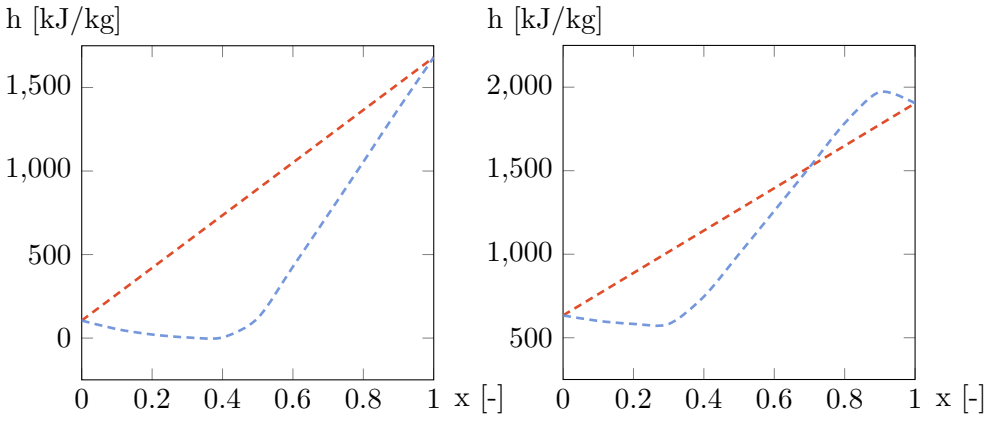

(A) 2.5 bar 25 °C (B) 25 bar 150 °C

FIGURE 3.2: The red curve shows the enthalpy for each component as if there where separated, while the blue curve shows the total enthalpy of the solution. The difference between the curve is the solution enthalpy.

3.3 Characteristic features of the compression/absorption heat pump

The Osenbrück cycle, shown in figure 3.3, is the most basic compression/absorption heat pump cycle. Compared to conventional vapour-compression heat pump cycles, the main difference is the solution circuit. Solution exiting the desorber is not fully evaporated, thus a two-phase mixture. Saturated vapour and saturated liquid is separated before the vapour is compressed to the high-pressure side of the cycle (1 - 2). Liquid solution, characterized as a "weak" solution due low ammonia concentration, increases its pressure through the solution pump (3 - 4). Liquid solution runs through the solution heat exchanger to increase cycle performance and increase solution temperature (4 - 5). In the absorber, vapour is absorbed into the liquid rejecting heat to the heat sink. Ammonia concentration in the liquid gradually increases and saturated liquid out of the absorber is characterized as a "strong" solution (2/5 - 6). Heat is rejected to the "weak" solution in the solution heat exchanger (6 - 7) before the solution is expanded to the low-pressure side of the cycle (7 - 8). During evaporation, the ammonia concentration in the liquid decreases, and at the desorber outlet the liquid solution is characterized as a "weak" solution (8 - 1/3).

The Osenbrück cycle shows the basic elements and working principle of compression/absorption cycles, and Morawetz (1989) gives further overview on different sorption compression heat pumps. Stokar and Trepp (1987) design a compression heat pump with a solution circuit and their results stated that heat pump offers two major advantages over a single fluid Rankine cycle. The first advantages is that the heating capacity of the heat pump can be easily adjusted by varying the composition. The other is that due to the temperature glide, the COP of the heat pump can be substantially higher for application with heat sources and heat sinks with temperature glides.

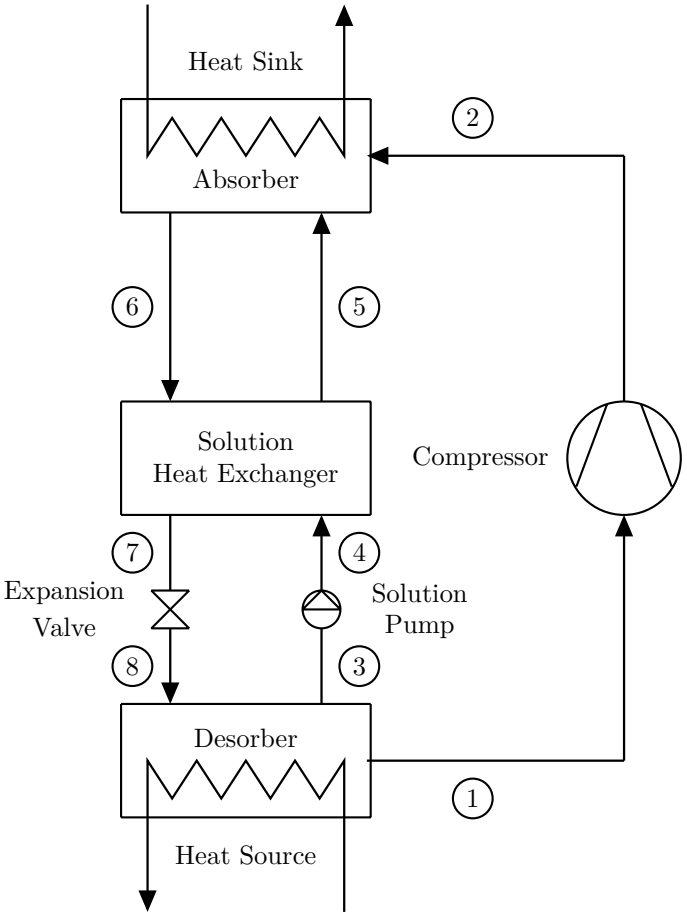

FIGURE 3.3: The Osenbrück cycle

Several studies have shown that the compression/absorption heat pump exhibits some interesting advantages to conventional vapour-compression heat pumps. Hultén and Berntsson (1999; 2002) studied the compression/absorption heat pump cycle theoretically and summarized the advantages and disadvantages of the cycle compared to vapour-compression cycles:

- Small swept volume to the compressor.
- High heat transfer coefficients.
- Environmentally benign working fluids.
- High COP
- The possibility of varying the working fluid composition increases the flexibility an making it easier adaptable to variations in temperature levels and capacities.
- High working temperatures that can be obtained, at least 150 °C.
- Working fluid temperature glides can be matched to the gliding temperatures of heat sinks and heat sources, lowering the system irreversibility and leading to a higher COP.

- No gain from an economizer coupling.
- Leakage will change the composition.
- Ammonia is flammable and toxic.

Generally, ammonia is considered a favourable working fluid despite toxicity and flammability. However, ammonia as working fluid in high temperature heat pump application is limited due to relatively high saturation pressure. One of the most beneficial aspects of the compression/absorption cycle with ammonia/water mixture is that it enables the possibility to use ammonia at higher temperatures. Saturation pressure for pure ammonia at 100 °C is 62.6 bar, while the saturation pressure of a liquid mixture with 90 weight-% of ammonia at 100 °C is 54.4 bar, and the saturation pressure with 50 weight -% of ammonia is 23.6 bar. Only a small concentration of water causes the saturation pressure to decrease significantly. Figure 3.9 shows an arbitrary compression/absorption process in a Clapeyron diagram. Evaporation at 2.2 bar and a mixture desorber outlet temperature at 45 °C with an overall ammonia concentration of 50 weight-% results in a 97.5 weight-% ammonia concentration in the vapour and 33 weight-% ammonia in the liquid. With an absorber pressure at 25 bar, it results in temperature glide from 130 °C to 100 °C. Compared with pure ammonia, condensation at 130 °C results in a pressure of 109 bar.

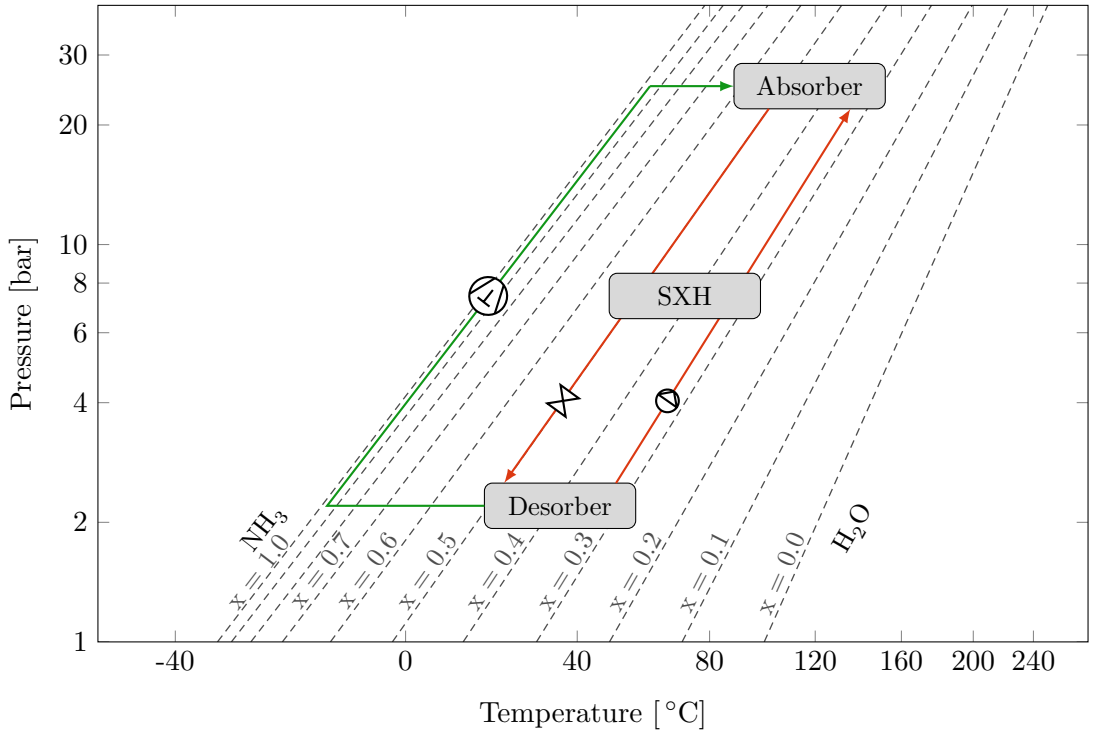

FIGURE 3.4: Clapeyron diagram of a compression/absorption cycle with components

As previously noted, compression/absorption systems are especially suitable for processes with heat sources and heat sink with temperature glides. As the composition in liquid and vapour phases changes during evaporation and condensation, saturation

temperatures changes resulting in mixture temperature glides. The Lorenz cycle represents the ideal theoretical reference process, and as figure 3.5 displays, heat exchanging processes with heat sinks and heat sources with temperature glide has smaller temperature losses when evaporation and condensation processes are non-isothermal (Granryd et al., 2009). Moreover, the temperature profiles can be matched to further reduce the temperature loss.

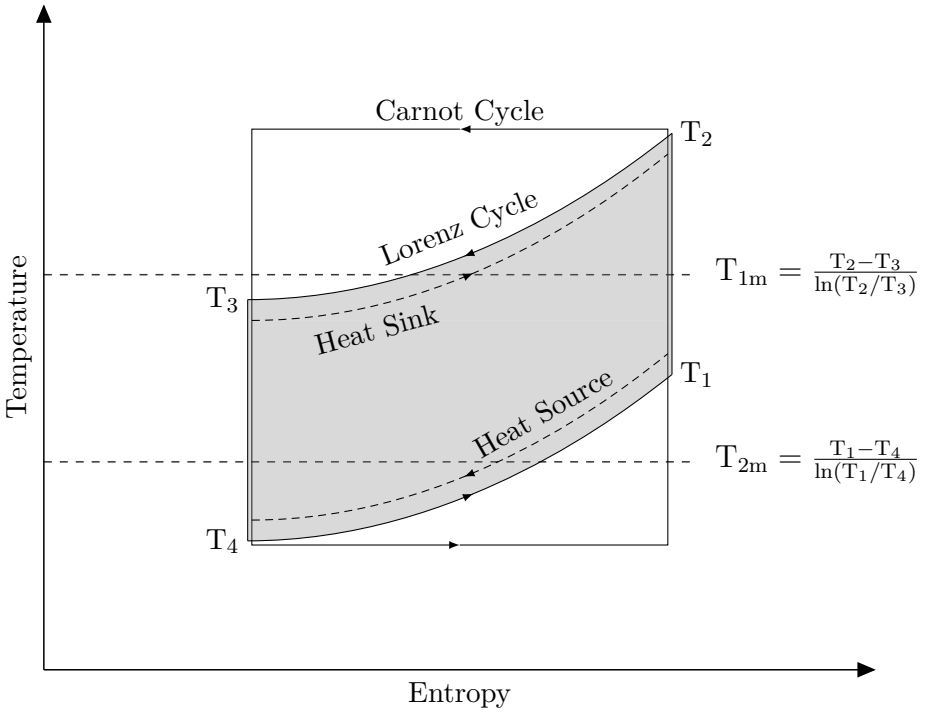

Figure 3.5: Comparison of ideal cycles with high temperature gradient heat source and heat sink (Granryd et al., 2009)

Early studies on compression/absorption heat pump used the LMTD method as an approach to model the heat exchangers. Itard and Machielsen (1994) argued that the use of temperature-entropy diagrams of mixtures shows that mixture temperature profiles in the desorber and absorber is strongly dependant on the overall concentration and that it is not linear. Hence, the LMTD method can not be applied for modelling heat exchangers nor calculating the performance of the system. This is especially important in processes with large temperature glides and or small temperature differences between hot and cold streams. Figure 3.6 shows how the temperature profiles can appear under certain conditions, and it shows that the mixture temperature profile in the desorber results in a minimum temperature difference either at the desorber inlet outlet. However, in the absorber process, the minimum temperature difference occur somewhere in the heat exchange, thus modelling the process with the minimum temperature difference either at the inlet or outlet will result in infeasible temperature profiles.

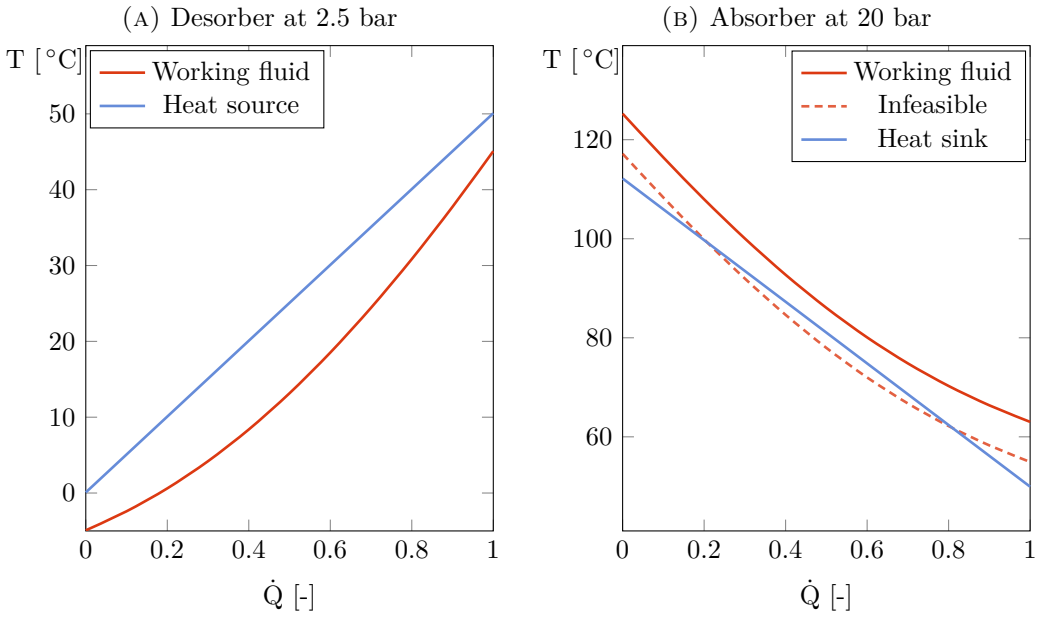

FIGURE 3.6: Temperature versus the cumulative heat load in desorber and absorber with an overall ammonia mass fraction of 0.75

The normalised temperature-enthalpy diagram in figure 3.7 shows the non-linearity in saturation temperatures versus enthalpy. Fluids with constant specific heat capacities will form a straight curve, while the ammonia/water mixture forms a non-linear curve in a temperature-enthalpy diagram (Nordtvedt, 2005). Figure 3.7 shows that the non-linearity is more significant at low pressures and high ammonia concentrations, and that the curve have a certain S-shaped which crosses the constant curve, while lower concentration does not. Figure 3.8 shows the cumulative heat load from saturated vapour to saturated liquid assuming a linear enthalpy decrease from inlet to outlet. The mixture at the absorber inlet will not be saturated vapour in a compression/absorption heat pump process, however, contrary to the normalised temperature-enthalpy diagram where the temperature curves shows saturation properties for a constant ammonia concentration, figure 3.8 shows the temperature profile shows how the mixture temperature can appear during a condensation process. Lower overall ammonia concentrations have higher saturation temperature and temperature curves are more linear. Temperature curves also become more linear when increasing the pressure. It is mentionable that low vapour fractions at the start of the absorption process will reduce to temperature difference more for high overall ammonia concentration than lower concentration. A vapour fraction of 0.5 means that the mixture temperature curve for an overall ammonia concentration of 0.5 at 5 bar starts at $\dot{Q} = 0.49$ and a temperature difference from 103 °C to 38 °C. For an overall ammonia concentration of 0.8 a vapour fraction of 0.5 at 5 bar means that the temperature curve starts at $\dot{Q} = 0.38$, however, the resulting temperature difference is only from 27 °C to 11 °C.

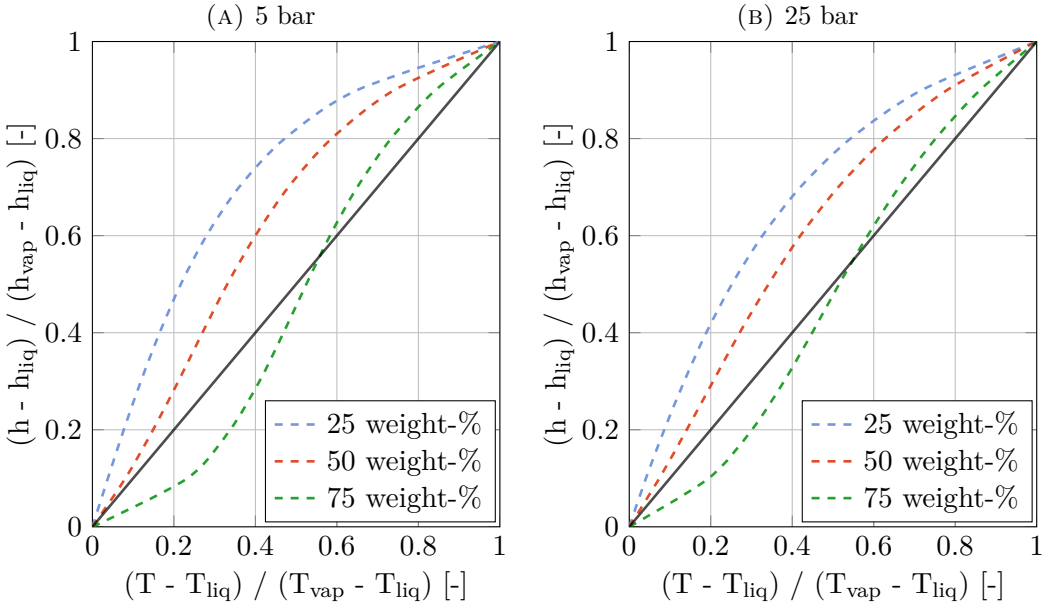

FIGURE 3.7: Normalised temperature-enthalpy diagram

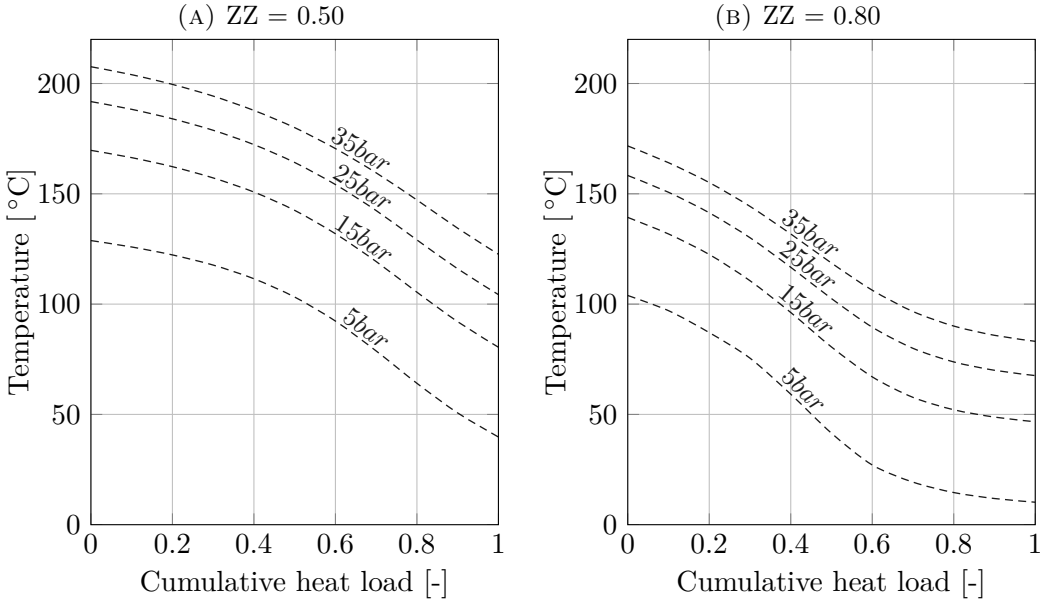

FIGURE 3.8: Temperature profile versus the cumulative heat load for the working fluid at different concentrations and pressures. At $\dot{Q} = 0$ the working fluid is saturated vapour and at $\dot{Q} = 1$ the working fluid is saturated liquid

The ratio between liquid circulating in the solution circuit and vapour to the compressor can be altered, thus changing the overall ammonia concentration in the desorber and absorber. If the pressures remain constant, the saturation temperatures of the mixture will decrease or increase dependant on an increase or decrease in the overall ammonia concentration, thereby adjusting the process to external changes. If the temperature of the heat source and heat sink remain constant, variation in composition will alter the saturation temperatures. However, since the external parameters remains unchanged, the properties of the liquid and vapour after the desorber changes. The compressor is

supplied by vapour of lower or higher density, resulting in a capacity change (Nordtvedt, 2005). Figure 3.9 shows how the variation in composition alter the pressures when both heat source and heat sink temperatures remain constant.

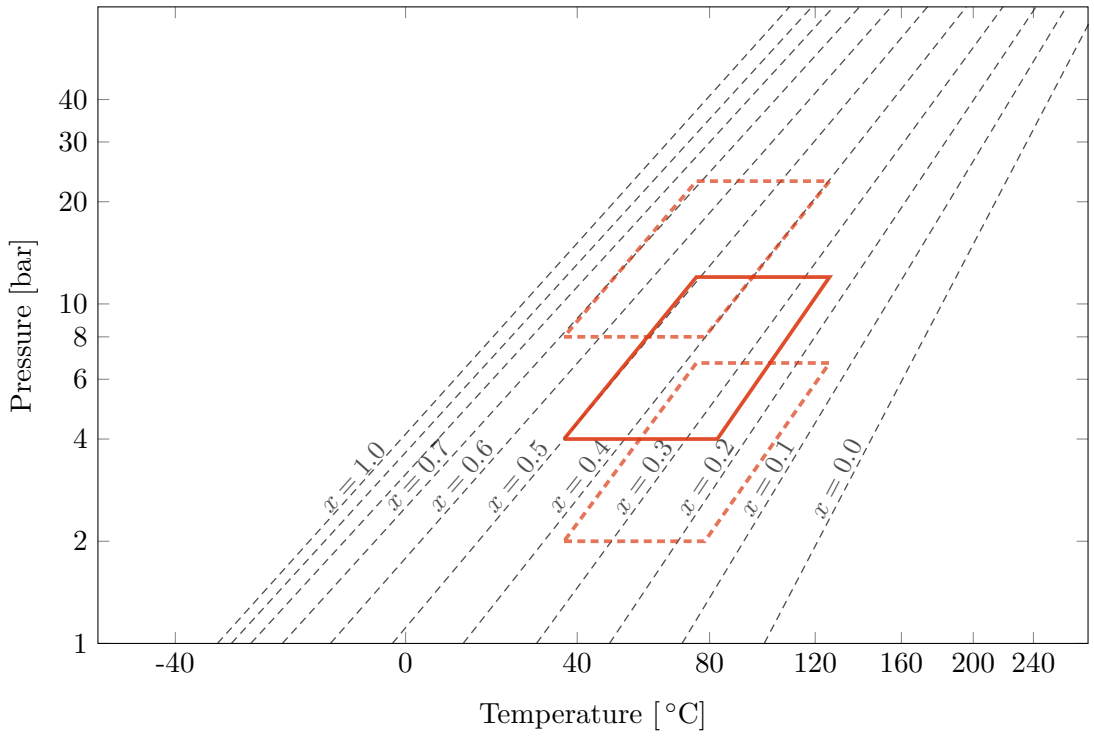

FIGURE 3.9: Capacity control by varying the mixture composition

3.4 Absorption processes with ammonia/water mixtures

The absorber is one of the important components in compression/absorption heat pump systems, and the design of the absorber has a vital impact on system performance and cost (Killion and Garimella, 2001). As previously noted, the complex mass and heat transfer process during evaporation and condensation of ammonia/water mixtures results in non-linear temperature profiles, and it has led to difficulties in developing valid mathematical models for the absorption processes. To understand the complex process in taking place in the absorber requires an understanding the thermodynamics of fluid mixtures, phase equilibria, heat transfer and mass transfer (Vuddagiri and Eubank, 1998). The combined effect of heat and mass transfer determines the absorption rate in the process, which ultimately decides the size of the absorber. Generally, two absorption modes are recommended to enhance heat and mass transfer; the falling film absorption mode and bubble absorption mode. Falling film absorption provides relatively high heat transfer coefficients and is stable during operation. However, falling film absorption have wettability problems and require good liquid distributors at the liquid inlet (Kang et al., 2000). Bubble absorption provides high heat transfer coefficients, good mixing between vapour and liquid, and good wettability. Generally, vapour distribution required in bubble absorption is easier to accomplish than liquid distribution. However, bubble

absorption require a pressure difference on the vapour side to drive the vapour through the pool of liquid, which rules out bubble absorption in low-pressure systems. This problem is less severe in ammonia/water systems, but must be taken into account (Lee et al., 2002a).

Kang et al. (2000) performed an analytical investigation focusing on variables affecting the absorption rate of the two absorption modes, in a plate heat exchanger. They reported that the bubble absorption mode had better overall characteristics. The local absorption rate of the bubble mode is always higher due to better mixing and higher heat transfer coefficients. Consequently the heat transfer area with bubble absorption is smaller, almost 50 %. Moreover, the heat transfer coefficient have a more significant effect on the absorption rate in falling film absorption than bubble absorption, while mass transfer coefficients have a more significant effect in bubble absorption than falling film absorption. Lee et al. (2002a,b) performed an experimental analysis comparing falling film absorption and bubble absorption in a plate heat exchanger focusing on how solution flow rates and vapour flow rates affected the absorber performance. The found that more heat is generated in bubble absorption and that the bubble absorption mode is superior to the falling film absorption mode in terms of mass transfer performance. Moreover, they reported that an increasing solution flow rate will result in a significant increase in heat transfer performance, and a slightly increase in mass transfer performance. When vapour flow rate increases, the mass transfer performance increases. While the heat transfer performance increases in the bubble absorption mode, it would remain or get worse in falling film absorption. The experiments showed that bubble absorption mode showed good performance in plate-type absorbers, especially when the solution flow rate is low and vapour flow rate is high.

Fernández-Seara et al. (2005) analysed the heat and mass transfer processes during absorption of ammonia into water in a co-current vertical absorber. The absorber configuration was a shell and tube type with water as coolant medium. Later they continued their work with an analysis of a air-cooled tubular absorber (Fernández-Seara et al., 2007). The vapour/liquid co-current absorption process of an ammonia/water mixture is distinguished by a changing two-phase flow pattern. At the start of the absorber there is a churn flow followed by a slug flow and finally a bubbly flow until all the vapour is absorber into the liquid. The results showed that the absorption process progress rapidly in the churn and slug flow regions, but slows down in the in the bubbly flow region. Tube diameters and lengths are key parameters for the absorber design, and their results reviled that there exist an optimum inner diameter of the tubes which minimizes the absorber length, and diameters smaller than the optimum diameter will have a significant effect on the absorption length. The number of tubes will effect the absorption length, and an increase of tubes will reduce the required tube length. However, the effect on the absorption length will diminish as the number of tubes increases. The analysis of the air-cooled absorber reviled that the absorption process evolved more rapidly at the first tube row where the air hits first, thus the tube length require to accomplish complete absorption is different for each row and that the length of the tubes should be dimensioned for the last tube row. To avoid the detrimental effect of air heating at the first tube row, absorbers should be arranged with as few tube rows as possible. Further,

results showed that the fin pitch had a significant effect on the absorption length, and that a large fin pitch increased the absorption length.

Cerezo et al. (2009) studied how ammonia-water absorption takes place in a channel of a plate heat exchanger operating under typical conditions of absorption chillers, driven by low temperature heat sources. The increase of the cooling water flow rate increased the mass absorption flux, while the effect in the solution heat transfer coefficient was less pronounced. On the other hand, the solution heat transfer coefficient improved as the solution flow rate increased. The mass absorption flux and solution heat transfer were improved when the absorber pressure was increased, while the increase of the solution concentration and the cooling and solution temperature had the opposite effect.

Lee et al. (2012) performed an experimental investigation to measure heat and mass transfer rates in a complete refrigeration/heat pumping unit operating under various conditions. The experiments showed that the absorber duty, overall heat transfer coefficient and solution heat transfer coefficient will increase with increasing solution flow rate. Further, the solution heat transfer coefficient were found to decrease with increasing pressure and solution concentration. Experiments on complete absorption system introduce three major confounding influences. The absorption process is a result of subcooled inlet conditions and the corresponding equilibrium conditions. The definition of driving temperature differences becomes a significant issue. Overall component mass, species and energy balances are affected the whole system, whereas in a single-pressure facility these balances can be established for the component, i.e absorber.

3.5 Compression/absorption heat pumps for high temperature applications

Brunin et al. (1997) discussed the working domain of compression heat pumps and compression/absorption heat pumps. With the limits set by design, fluids considered in the paper, the disappearance of CFCs and HCFCs, the only alternatives for high temperature heat pumps is compression heat pumps with hydrocarbons and compression/absorption heat pumps with ammonia/water mixtures. They highlighted that at the current time, the knowledge of compression/absorption heat pumps made it difficult to evaluate and compare the cost against compression heat pumps. In their calculations they used a concentration difference of 0.1 g/g between strong and weak solution, and predicted that with an overall ammonia concentration of 0.45 heat sink temperatures above 100 °C could be reached.

Rane et al. (1993) researched a two-stage vapour compression heat pump with solution circuits. The system design was to certain degree similar two that system schematic in figure 3.10. The systems operates on the same principle as a conventional cascade system where a low temperature cycle provides heat for a high temperature cycle. In this configuration, external heat is delivered to the evaporator, while the condenser provides heat to the generator. They modified the cycle and investigated how a rectifier, desuperheater and a bleed line affected the performance. The conclusion was that the

cycle with a bleed line and desuperheater had the best performance. Moreover, the analysis showed that such a system can operate at temperatures above 100 °C and conduct temperature lifts beyond 100 K. Compared to a single-stage vapour compression cycle with ammonia, the cooling COPs was twice as high and the pressure ratios only one third. Their experimental work (Rane and Radermacher, 1993) confirmed that the cycle could operate with temperature lifts over 100 K d with a pressure ratio of 6.9 and a cooling COP of 1.04.

Zhou and Radermacher (1997) compared the experimental results of a vapour-compression heat pump with a solution circuit and desorber/absorber heat exchange, single-stage vapour-compression heat pump with a solution circuit and two-stage vapour-compression heat pump a with solution circuit. The first-mentioned heat pump was fairly similar to the cycle given in figure 3.10, however, without the solution heat exchanger. Their results indicated that single-stage system had the highest COP and lowest temperature lift, while the two-stage system had the highest temperature lift and lowest COP. The temperature lift of the heat pump with a desorber/absorber heat exchange was not as high as for the two-stage system. Since the absorber pressure decreases with decreasing concentration it makes it difficult to increase pressure and decrease solution concentration at the same time in order to achieve a high temperature lift.

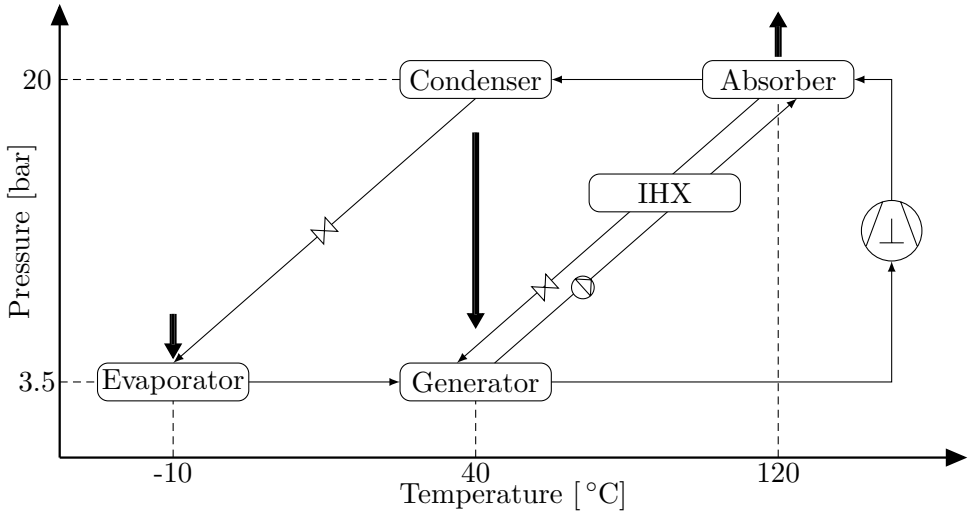

FIGURE 3.10: Schematic diagram of a compression/absorption heat pump with a cascade heat exchanger

Figure 3.10 shows a compression/absorption heat pump system for high temperature lifts. Only a part of the vapour is absorbed in the absorber, while the remaining absorption process occur in the condenser which operates as the heat source for the generator. This system can deliver heat 120 °C with a heat source temperature at -10 °C. The resulting temperature lift is above 100 °C with only one compressor (Stene, 1993).

Sveine et al. (1998) design a two-stage compression/absorption heat pump with ammonia/water as working fluid. The system schematic is shown in figure 3.11. In order to not exceed the maximum discharge temperatures, the maximum pressure was set to 19 bar. In the theoretical calculation they found that with an heat source temperature of

53 °C the heat sink temperature was 117 °C with a COP of 3.8. Moreover, the solution heat exchanger between the compressors had a significant impact on the system performance. While the vapour was cooled down between the compressors, thus reducing the discharge temperatures, the liquid solution was heated to the saturation temperature.

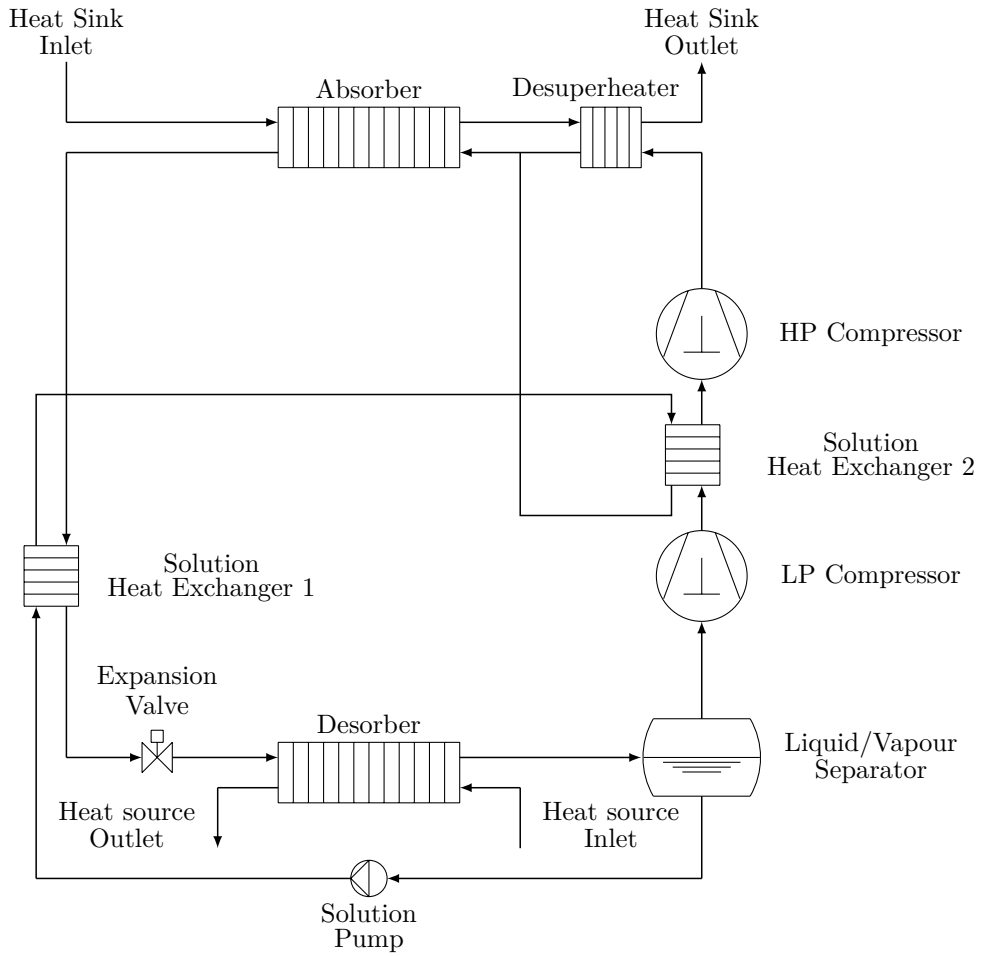

FIGURE 3.11: Schematic diagram of the two-stage compression/absorption heat pump developed by Sveine et al. (1998)

Simulation Models

4.1 Introduction

To assess the compression/absorption heat pump for high temperature application, two separate computer simulation models were developed. The purpose of the first model is to evaluate the thermodynamic performance of a two-stage compression absorption heat pump, while the purpose with the second model is to evaluate the dimensions of a finned, annular tube cross-flow absorber for heating air. Both models are developed in Engineering Equation Solver (EES), and uses an external procedure for calculating the thermodynamic properties of the ammonia/water mixture. The NH3H2O procedure uses correlations of Ibrahim and Klein (1993) for the ammonia/water mixture. EES codes for both models are given in appendix D.

4.2 Two-stage compression/absorption heat pump model

4.2.1 General

a In order to evaluate the compression/absorption heat pump cycle for high temperature application, a two-stage heat pump model is chosen. The heat pump consists of an absorber, desorber, two solution heat exchangers, desuperheater, two compressors, solution pump, expansion valve and a liquid/vapour separator. A schematic diagram is shown in figure 4.1, and the principle of the system is based on the models described by Sveine et al. (1998) and Nordtvedt (2005). In order to simplify the model and calculations, assumptions made by Nordtvedt (2005), are applied in this model:

- Pressure drops in the system are negligible.
- Heat losses to the ambient are negligible.
- Strong solution leaving the absorber is saturated.
- Solution, heat sink and heat source fluid flow counter-currently in absorber and desorber.
- Vapour and liquid are assumed to be in equilibrium in the solution, in absorber and desorber.

- Mixing of the weak solution and vapour at the absorber inlet is adiabatic.
- Vapour at the compressor inlet is assumed to be in thermodynamic equilibrium with the liquid in the liquid/vapour separator.
- Solution pump efficiency is 100 %.

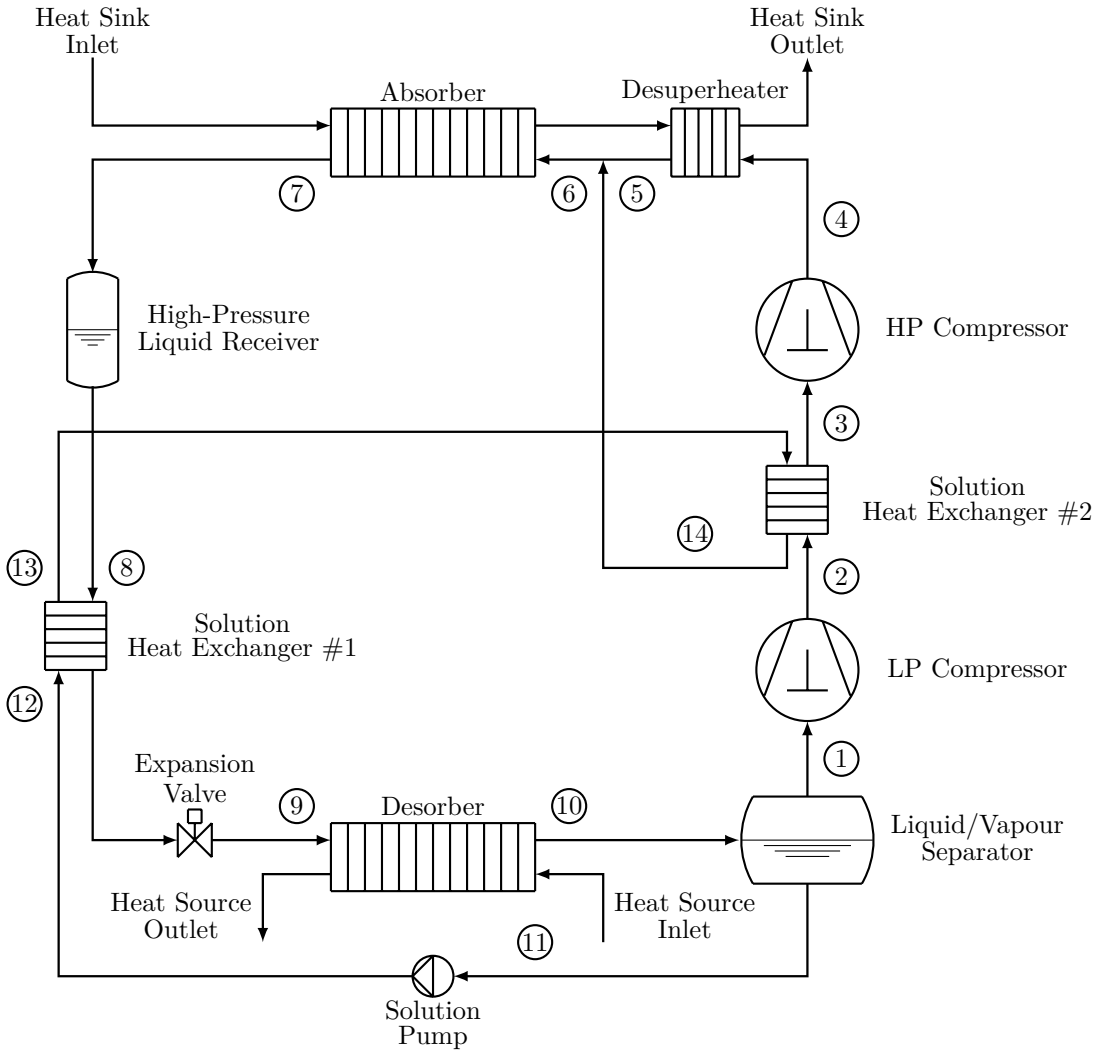

FIGURE 4.1: Schematic diagram of the two-stage compression/absorption heat pump model

TABLE 4.1: Two-stage model inputs and outputs

Inputs	Outputs
Ammonia concentration in vapour	Ammonia concentration in liquid
Overall ammonia concentration	Circulation ratio
Absorber pressure	Desorber pressure
Heat source inlet temperature	Heat sink and source mass flow rates
Heat sink inlet temperature	Heat sink outlet temperature
Minimum temperature difference in heat exchangers	System performance
Isentropic efficiencies of compressors	Thermodynamic state points
Thermal efficiencies of internal heat exchangers	
Absorber capacity	

The computer model uses an external procedure for the ammonia/water mixture, were the thermodynamic properties are calculated using the correlation given by Ibrahim and Klein (1993). The call statement is CALL(CODE;In1;In2;In3:T;P;x;h;s;u;v;q), where the CODE statement consists of a 3 digit integer indicating which 3 of the 8 possible input parameters to be used. In order to calculated any thermodynamic state, 3 properties need to be known, thus assumptions for each state in the heat pump cycle must be made.

T = [K]
P = [bar]
x = [ammonia mass fraction]
h = [kJ/kg]
s = [kJ/kg-K]
u = [kJ/kg]
v = [m^3/kg]
q = [vapour mass fraction]

The calculation procedure for each thermodynamic state point is shown in appendix A, and model inputs and outputs are listen in table 4.1. Total mixture mass flow rate is found by the required heat output in the absorber and the calculated enthalpy difference between the absorber inlet and outlet calculated when running the simulation. Equation (4.1) gives the relation between the overall ammonia concentration, ammonia concentration in the liquid and vapour and the mass flows. Equation (4.2) shows the calculation of the circulation ratio. Energy balance for heat exchangers is given by equation (4.3), while energy balance for compressors and solution pump is given by equation (4.4). Ammonia mass balance in desorber and desorber is given by equation (4.5) (Nordtvedt, 2005).

$$ZZ = \frac{\dot{m}_{vap} \cdot x_{vap} + \dot{m}_{liq} \cdot x_{liq}}{\dot{m}_{tot}} \tag{4.1}$$

$$CR = \frac{\dot{m}_{liq}}{\dot{m}_{vap}} \tag{4.2}$$

$$\sum(\dot{m} \cdot h)_{in} - \sum(\dot{m} \cdot h)_{out} = 0 \tag{4.3}$$

$$\sum(\dot{m} \cdot h)_{in} + W - \sum(\dot{m} \cdot h)_{out} = 0 \tag{4.4}$$

$$\sum(\dot{m} \cdot x)_{in} - \sum(\dot{m} \cdot x)_{out} = 0 \tag{4.5}$$

4.2.2 Desorber

Mixture temperature curves in the desorber is calculated assuming a linear enthalpy increase from desorber inlet to outlet. When overall ammonia concentration and the desorber pressure is known, the enthalpy difference is divided into 50 points with equal difference between each point. Mixture temperature curves is found by calculating the mixture temperature for each point. Heat source temperature curves is calculated assuming a linear temperature decrease from inlet to outlet, where the minimum temperature difference between heat source and mixture is set at the desorber inlet and outlet.

4.2.3 Absorber

Mixture temperature curves in the absorber is calculated similar to the mixture temperature curves in the desorber. The complex process of heat and mass transfer in ammonia/water mixtures causes minimum temperature differences between mixture and heat sink to occur in the heat exchange, not at the inlet or outlet as for the desorber. This model calculates two different heat sink temperature curves with different approaches to maintain the minimum temperature differences. The first approach sets absorber inlet and outlet temperature differences to the minimum temperature differences and calculates a heat sink mass flow rate. The minimum temperature difference for all 50 points is calculated, and if one of the points return a smaller temperature difference than the minimum temperature differences, heat sink inlet and outlet temperature and heat sink mass flow is adjusted until the minimum temperature difference is maintained. The second approach sets temperature differences at absorber inlet and outlet to the minimum temperature difference, but maintains the heat sink outlet temperature. Heat sink inlet temperature and mass flow rate is adjusted until the minimum temperature differences is not violated.

4.2.4 Single-phase heat exchangers

Heat transfer in desuperheater and solution heat exchanger # 1 and # 2 is calculated according to equation (4.6), (4.7) and (4.8) (Incropera et al., 2006). EES does not provide heat capacity for the ammonia/water mixture, and the specific heat capacity for the mixture is calculated as $c_p = \Delta h / \Delta T$.

$$Q_{max} = C_{min} \cdot (T_{H,in} - T_{C,in}) \tag{4.6}$$

$$Q = \varepsilon \cdot C_{min} \cdot (T_{H,in} - T_{H,in}) \tag{4.7}$$

$$\varepsilon \equiv \frac{Q}{Q_{max}} \tag{4.8}$$

4.2.5 Other components

Compressors This thesis does not have the focus on compressor performance in the compression/absorption heat pump, thus there are no implemented calculations for compressor efficiencies. Neither are there are any function for compressor cooling. If the discharge temperature is higher than the limitation set in calculations, the temperature is reduced neglecting the heat which is reduced.

Solution pump The solution pump is assumed to be isentropic.

Expansion valve The expansion process is assumed to be isenthalpic. Further it is assumed that the vapour created by flashing is in thermodynamic equilibrium with the liquid.

4.2.6 System heating performance

The system heating performance is calculated using equation (4.9), (4.10), (4.11), (4.12), (4.13) and (4.14).

$$COP = \frac{Q_{abs} + Q_{dsh}}{W_{LPcomp} + W_{HPcomp} + W_{pump}} \tag{4.9}$$

$$Q_{abs} = \dot{m}_{tot} \cdot (h_6 - h_7) \tag{4.10}$$

$$Q_{dsh} = \dot{m}_{vap} \cdot (h_4 - h_5) \tag{4.11}$$

$$W_{LPcomp} = \dot{m}_{vap} \cdot (h_2 - h_1) \tag{4.12}$$

$$W_{HPcomp} = \dot{m}_{vap} \cdot (h_4 - h_3) \tag{4.13}$$

$$W_{pump} = \dot{m}_{liq} \cdot (h_{12} - h_{11}) \tag{4.14}$$

4.3 Absorber model

4.3.1 General

The absorber model is adapted from an EES model for a finned, annular tube cross-flow heat exchanger given by Nellis and Klein (2009), and consists of 10 segments, where each segments have equal dimensions. Figure 4.2 shows a schematic diagram of each segment, while figure 4.3 shows how the segments are related to one another, and how the air flows through the absorber. The output properties in one segment are the input properties in the next segment for both mixture and air, and model inputs and outputs are listed in table 4.2.

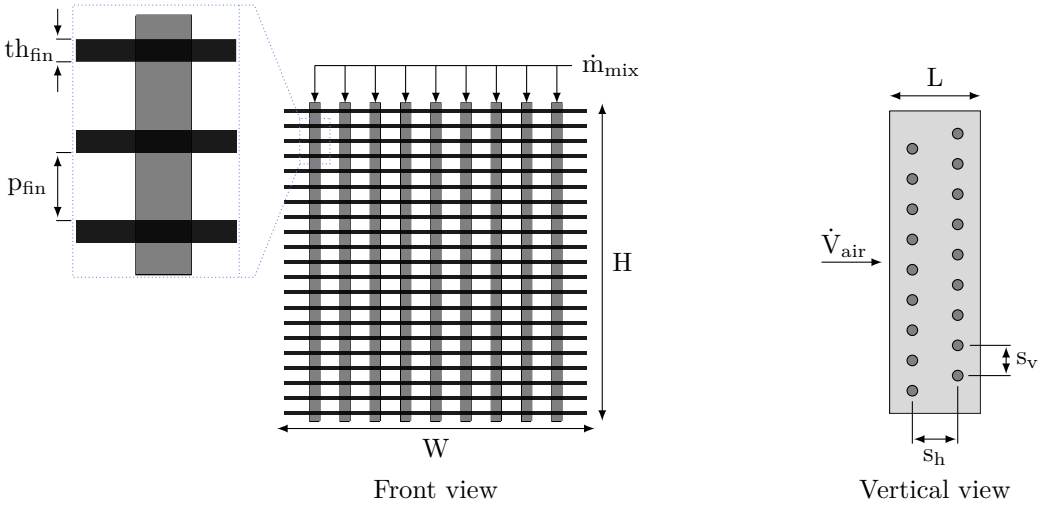

FIGURE 4.2: Schematic diagram of a segment in the finned, annular tube cross-flow absorber

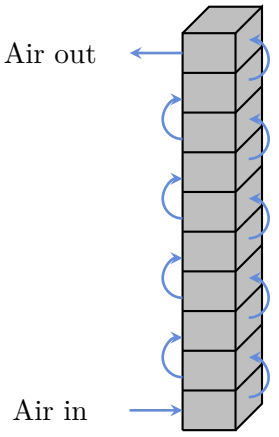

FIGURE 4.3: Air flow through the finned, annular tube cross-flow absorber

Table 4.2: Absorber model inputs and outputs

Inputs	Outputs
Dimensions of the absorber	Overall heat transfer coefficient
Mixture inlet properties	Mixture outlet temperature
Air inlet properties	Air outlet temperature
Absorber duty	Actual heat transferred

The simulation process for the model is:

- Mixture inlet temperature and air inlet temperature is set.
- Mixture outlet temperature and air outlet temperature is guessed.
- In the initial calculation, the temperature decrease for the mixture and temperature increase for the air, is equal for all 10 segments.
- Heat transfer coefficients, actual heat transfer and temperature difference in all 10 segment is calculated using the initial temperatures.
- A new mixture and air temperature is calculated in all 10 segment with the calculated properties.
- Heat transfer coefficients, actual heat transfer and temperature difference in all 10 segment is calculated using the mean temperature of the initial temperature and calculated temperature in the previous iteration.
- The simulation model performs 10 iterations where the input temperature in each segment is the mean value of the input temperature and calculated temperature in the previous segment.

4.3.2 Corrections for cross-flow heat exchanger

The conductance and total thermal resistance between mixture and air in each segment is calculated using equation (4.15) and (4.16). The calculation of the total thermal resistance is shown in section 4.3.3, and as equation (4.16) shows, the model neglects fouling resistance.

$$UA = \frac{1}{R_{tot}} \tag{4.15}$$

$$R_{tot} = R_{in} + R_{cond} + R_{out} \tag{4.16}$$

The absorber model is cross-flow, thus need to be corrected with the $LMTD\ F$ factor. The LMTD effectiveness, P_{HX}, and LMTD capacitance ratio R_{HX} is calculated:

$$P_{HX} = \frac{T_{C,out} - T_{C,in}}{T_{H,in} - T_{C,in}} \tag{4.17}$$

$$R_{HX} = \frac{\dot{C}_C}{\dot{C}_H} = \frac{T_{H,in} - T_{H,out}}{T_{C,out} - T_{C,in}} \tag{4.18}$$

The correction factor is found using a EES function for cross-flow heat exchangers with both fluids unmixed.

$$\Delta T_{lm} = \Delta T_{lm,cf} \cdot F_{HX} \tag{4.19}$$

$$\dot{Q} = UA \cdot \Delta T_{lm} \tag{4.20}$$

The calculated $\dot{Q}$ is used to correct outlet temperatures for mixture and air in each segment.

4.3.3 Thermal resistance

Thermal resistance between mixture and inner surface of the tubes The heat transfer coefficient of the mixture is simplified and calculated with the thermophysical properties of the mixture liquid. The velocity of the liquid is corrected throughout the heat exchange with respect to the ratio between liquid and vapour, and the average density in a segment is calculated according to equation (4.21). ρ_{liq} is the density of saturated liquid at the given temperature and pressure, while ρ_{vap} is the density of saturated vapour at the given temperature and pressure.

$$\rho_{avg} = \rho_{liq} \cdot (1 - q) + \rho_{vap} \cdot q \tag{4.21}$$

Assuming a constant mass flow through the heat exchanger, the velocity of the liquid mixture in each segment is calculated according to equation (4.22).

$$u_m = \frac{4 \cdot \dot{m}}{\rho_{avg} \cdot D_{in}^2} \tag{4.22}$$

The Reynolds number and Prandtl number and heat transfer coefficient is calculated equation (4.23) and (4.24) respectively.

$$Re_D = \frac{\rho_{liq} \cdot u_m \cdot D_{in}}{\mu_{liq}} \tag{4.23}$$

$$Pr = \frac{c_p \cdot \mu_{liq}}{\lambda_{liq}} \tag{4.24}$$

The heat transfer coefficient of the mixture is calculated by the Dittus-Boelter equation (equation (4.25)), assuming it is constant through the segment. Thermal resistance between mixture and tube wall is calculated using equation (4.26).

$$\alpha_{mixture} = 0.023 \cdot Re_D^{0.8} \cdot Pr^{0.4} \cdot \frac{\lambda_{liq}}{D_{in}} \tag{4.25}$$

$$R_{in} = \frac{1}{\alpha_{mixture} \cdot \pi \cdot D_{in} \cdot L} \tag{4.26}$$

Thermal resistances between air and air-side surface Air heat transfer coefficients is calculated using an EES function for external flow over a staggered bank. The model calculates the heat transfer coefficient and pressure drop using the air inlet and outlet temperature for the segment and the tube surface temperature. The tube surface temperature is approximated as the average temperature between air inlet temperature and mixture inlet temperature for the segment. Thermal resistance on the air-side is calculated using equation (4.27). The approach for the overall fin efficiency is shown in section 4.3.4

$$R_{out} = \frac{1}{\eta_{overall} \cdot \alpha_{air} \cdot A_{tot}} \tag{4.27}$$

Conduction resistance in the tube wall Tube wall conduction resistance is found by using equation (4.28). λ is found from an EES function for thermophysical properties.

$$R_{cond} = \frac{ln(\frac{D_{out}}{D_{in}})}{2 \cdot \lambda \cdot \pi \cdot L_{tube}} \tag{4.28}$$

4.3.4 Fin efficiency

The fin efficiency is calculated with an approach that the actual fins acts like annular fins connected to the tube, and is found using the EES function for annular fins (figure 4.4). The effective radius of each fin is found so that the total surface area of the annular fins is equal to the actual fin surface area (equation (4.29)). The overall surface efficiency is found using equation (4.30), (4.31), (4.32) and (4.33).

$$r_{fin,eff} = \sqrt{\frac{A_{s,fin,tot} \cdot p_{fin}}{2 \cdot \pi \cdot L_{tube}} + \frac{D_{out}^2}{4}} \tag{4.29}$$

$$\eta_{overall} = 1 - \frac{A_{s,fin,tot}}{A_{tot}} \cdot (1 - \eta_{fin}) \tag{4.30}$$

$$A_{s,fin,tot} = 2 \cdot \frac{W}{p_{fin}} \left(H \cdot L - N_{t,row} \cdot N_{t,col} \cdot \frac{\pi \cdot D_{out}^2}{4} \right) \tag{4.31}$$

$$A_{s,unfin} = \pi \cdot D_{out} \cdot L_{tube} \left(1 - \frac{th_{fin}}{p_{fin}} \right) \tag{4.32}$$

$$A_{tot} = A_{s,fin,tot} + A_{s,unfin} \tag{4.33}$$

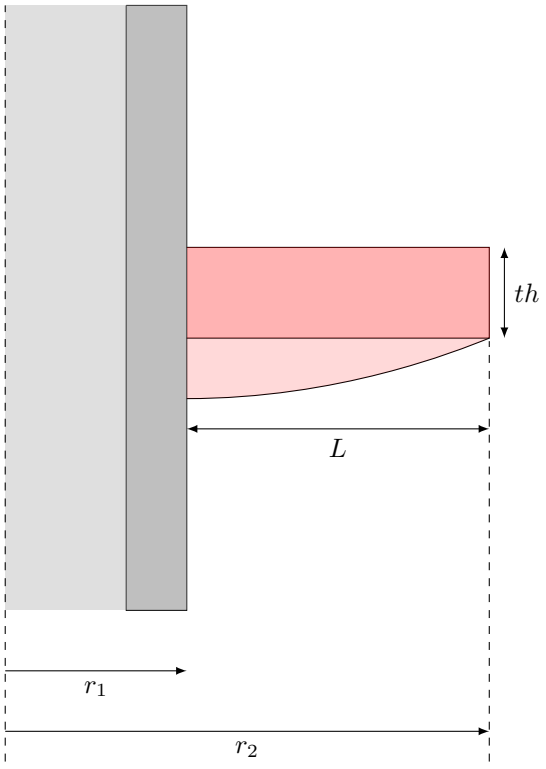

FIGURE 4.4: Annular rectangular fins

4.3.5 Thermophysical properties

The EES procedure for the ammonia/water mixture does not provide thermophysical properties. Thermophysical properties is found using equations given by Thorin (2001) and Conde-Petit (2004) for calculating liquid mixture conductivity and viscosity. The calculation procedure is shown in appendix B.

Simulation Results

5.1 Two-stage compression/absorption cycle

The main aim for the two-stage compression/absorption heat pump cycle simulations are to assess the thermodynamic performance, necessary pressure levels and other parameters for a theoretical heat pump cycle utilising surplus heat at 50 °C and heating process water from 100 °C to 150 °C. Nordtvedt (2005) used a maximum limit of water in the vapour to the compressor to be 2.5 weight-% based on compressor limitations. Forthcoming simulations evaluates the theoretical performance of compression/absorption heat pump cycle and with higher water concentrations than 2.5 weight-%. In order to avoid a sub-atmospheric pressure when the mixture temperature is 45 °C at the desorber outlet, the minimum ammonia concentration in the vapour was found to be slightly below 93 weight-%, and it sets an natural lower boundary for the simulation. In order to evaluate the system performance for different conditions, four simulation scenarios were chosen. The ammonia concentration in the vapour at the compressor inlet was set to 93, 95, 97 and 99 weight-% and the heat sink temperature was constant at 50 °C. Overall ammonia concentration and absorber pressure was found to accommodate the required heat sink temperature lift. Forthcoming figures shows the temperature versus the cumulative heat load for the scenarios and displays two different heat sink temperature curves. Blue heat sink temperature curves shows simulations where the temperature difference between mixture and heat sink is equal at the inlet and outlet, while green heat sink temperature curves shows simulation results when the heat sink outlet temperature is fixed at 5 °C below the mixture temperature and the heat sink inlet temperature and mass flow rate was adjusted to maintain the minimum temperature difference. Compressor efficiencies is set to 0.8 and thermal efficiencies in solution heat exchangers is set to 0.8. The minimum temperature difference in all heat exchangers is set to 5 °C in all simulations.

5.1.1 Simulation scenarios

5.1.1.1 93 weight-% ammonia in the vapour

With a mixture temperature of 45 °C out of the desorber and an ammonia concentration of 93 weight-% in the vapour, the resulting desorber pressure is 1.03 bar. The ammonia concentration in the saturated liquid exiting the desorber is 22 weight-%. If the discharge temperature is limited to 180 °C, in order to achieve the required heat sink temperature lift in the absorber, the absorber pressure needs to be 33 bar and the overall ammonia concentration 56.5 weight-%. Desorber and absorber temperature profiles is shown in figure 5.1. Mixture is cooled from 157.2 °C to 107.5 °C, while water is heated from 100.6 °C to 150.2 °C (heat sink #1), and 99.1 °C to 152.2 °C (heat sink #2). The simulation gave a COP of 1.81.

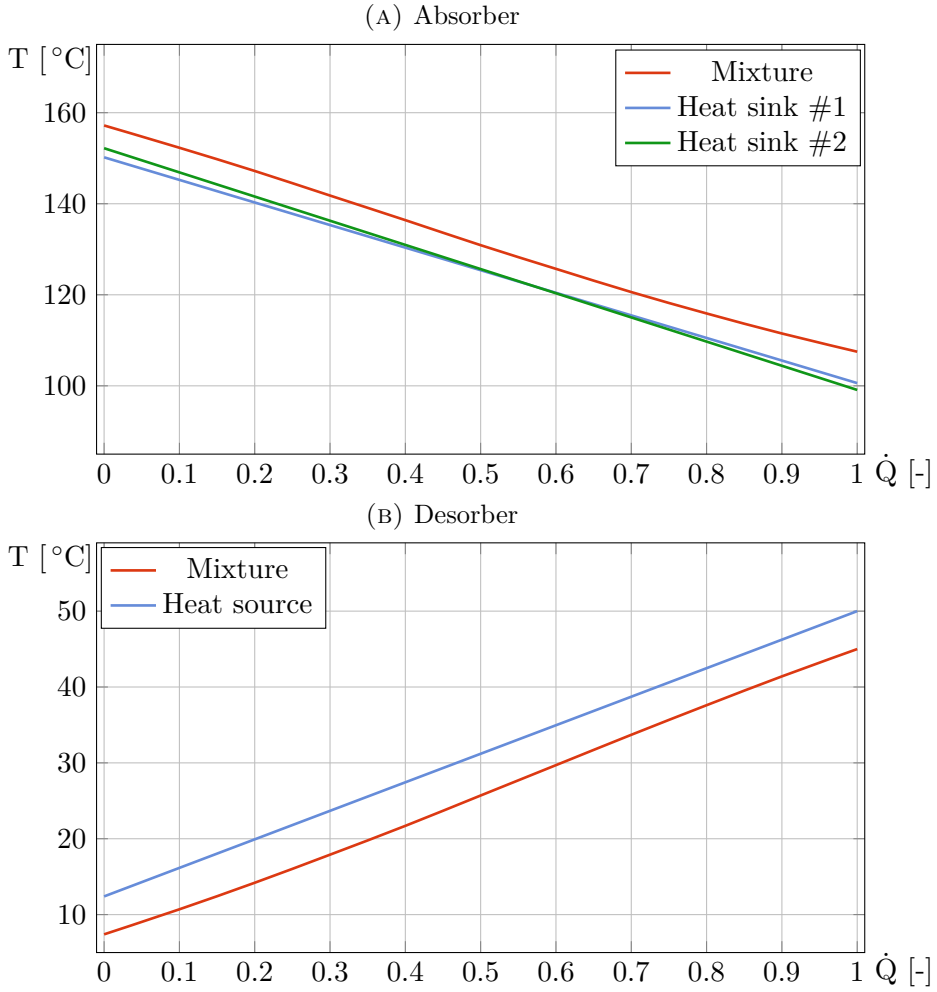

FIGURE 5.1: Temperature versus cumulative heat load for a two-stage compression/absorption cycle with P_{des} = 1.03 bar and P_{abs} = 33 bar. Heat sink # 1 shows the temperature curve for water when the temperature difference between mixture and water is equal at the absorber inlet and outlet. Heat sink # 2 shows the temperature curve for water when the temperature difference between mixture and water is 5 °C at the absorber inlet.

5.1.1.2 95 weight-% ammonia in the vapour

With a mixture temperature of 45 °C out of the desorber and an ammonia concentration of 95 weight-% in the vapour, the resulting desorber pressure is 1.34 bar. The ammonia concentration in the saturated liquid exiting the desorber is 26 weight-%. If the discharge temperature is limited to 180 °C, in order to achieve the required heat sink temperature lift in the absorber, the absorber pressure needs to be 38.5 bar and the overall ammonia concentration 61.5 weight-%. Desorber and absorber temperature profiles is shown in figure 5.2. Mixture is cooled from 158.0 °C to 108.1 °C, while water is heated from 100.2 °C to 150.1 °C (heat sink #1), and 97.1 °C to 153.0 °C (heat sink #2). The simulation gave a COP of 1.79.

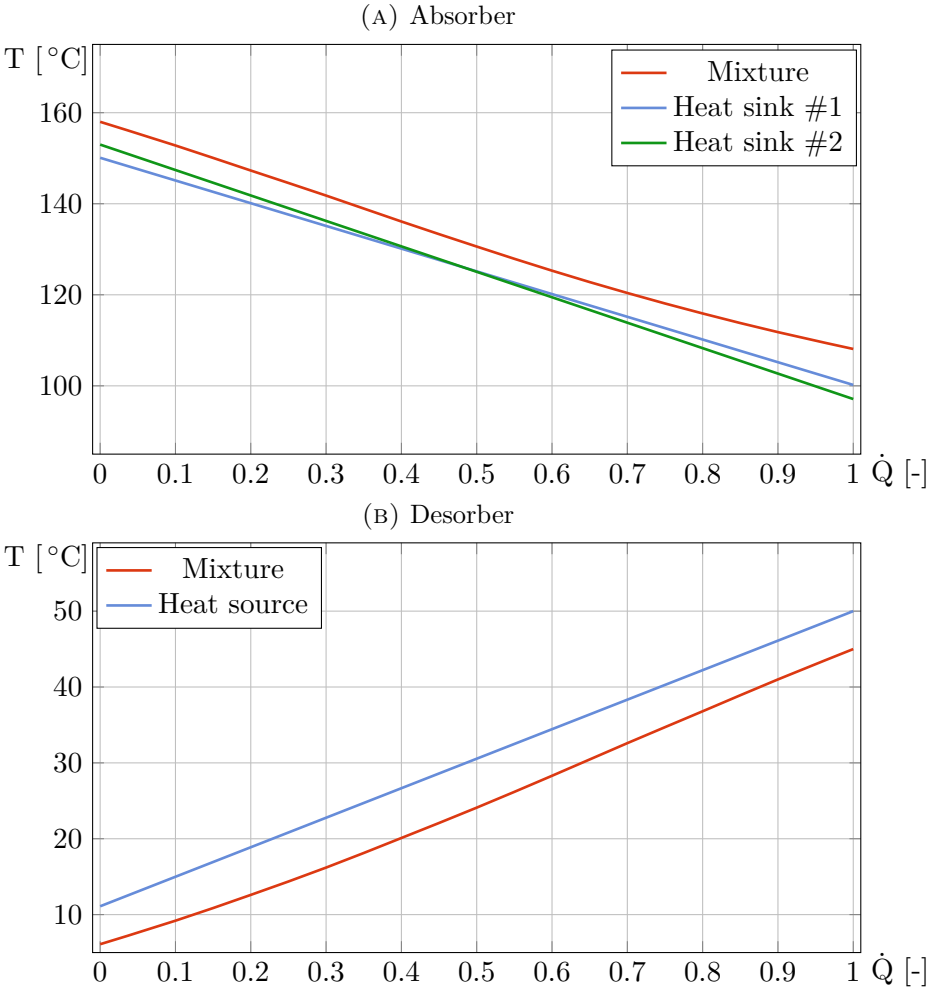

FIGURE 5.2: Temperature versus cumulative heat load for a two-stage compression/absorption cycle with $P_{des} = 1.34$ bar and $P_{abs} = 38.5$ bar. Heat sink # 1 shows the temperature curve for water when the temperature difference between mixture and water is equal at the absorber inlet and outlet. Heat sink # 2 shows the temperature curve for water when the temperature difference between mixture and water is 5 °C at the absorber inlet.

5.1.1.3 97 weight-% ammonia in the vapour

With a mixture temperature of 45 °C out of the desorber and an ammonia concentration of 97 weight-% in the vapour, the resulting desorber pressure is 1.94 bar. The ammonia concentration in the saturated liquid exiting the desorber is 31 weight-%. If the discharge temperature is limited to 180 °C, in order to achieve the required heat sink temperature lift in the absorber, the absorber pressure needs to be 47.5 bar and the overall ammonia concentration 69 weight-%. Desorber and absorber temperature profiles is shown in figure 5.3. Mixture is cooled from 159.6 °C to 109.9 °C, while water is heated from 100.2 °C to 150.0 °C (heat sink #1), and 94.6 °C to 154.6 °C (heat sink #2). The simulation gave a COP of 1.75.

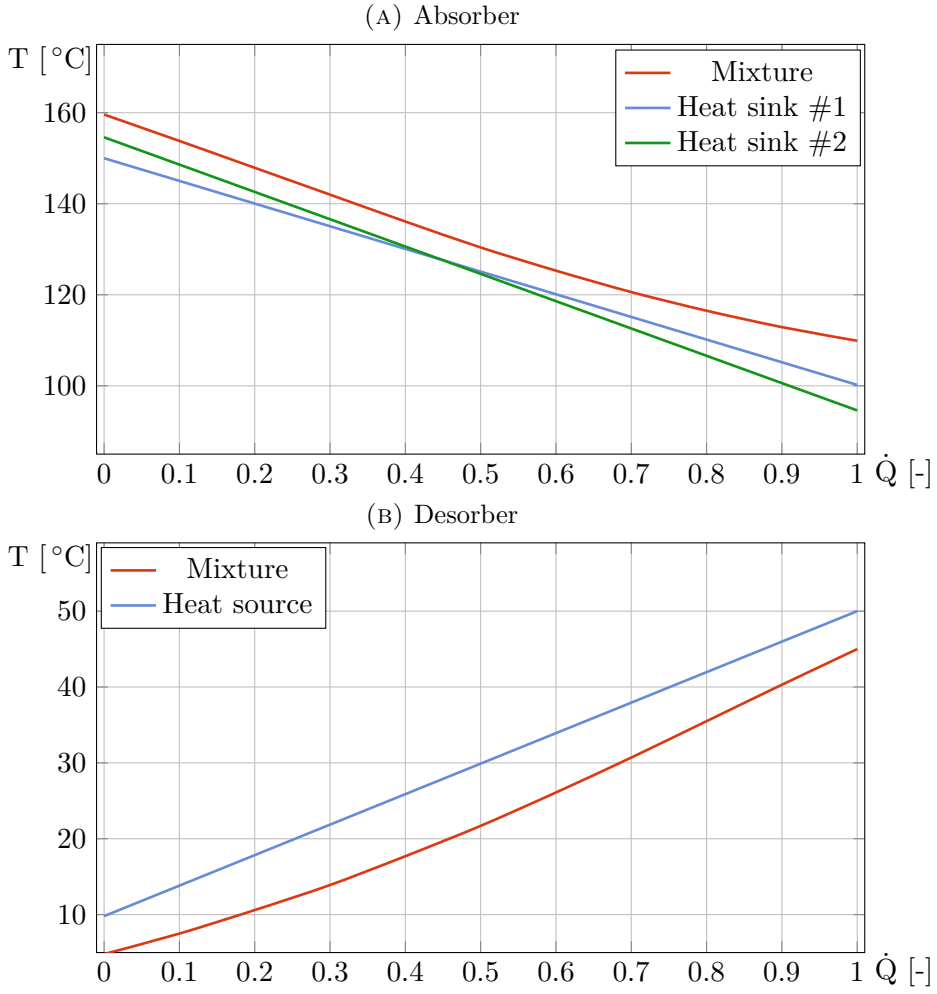

FIGURE 5.3: Temperature versus cumulative heat load for a two-stage compression/absorption cycle with P_{des} = 1.94 bar and P_{abs} = 47.5 bar. Heat sink # 1 shows the temperature curve for water when the temperature difference between mixture and water is equal at the absorber inlet and outlet. Heat sink # 2 shows the temperature curve for water when the temperature difference between mixture and water is 5 °C at the absorber inlet.

5.1.1.4 99 weight-% ammonia in the vapour

With a mixture temperature of 45 °C out of the desorber and an ammonia concentration of 99 weight-% in the vapour, the resulting desorber pressure is 4.0 bar. The ammonia concentration in the saturated liquid exiting the desorber is 33 weight-%. If the discharge temperature is limited to 180 °C, in order to achieve the required heat sink temperature lift in the absorber, the absorber pressure needs to be 70 bar and the overall ammonia concentration 85 weight-%. Desorber and absorber temperature profiles is shown in figure 5.4. Mixture is cooled from 161.8 °C to 116.6 °C, while water is heated from 102.6 °C to 147.9 °C (heat sink #1), and 87.3 °C to 156.6 °C (heat sink #2). The simulation gave a COP of 1.56.

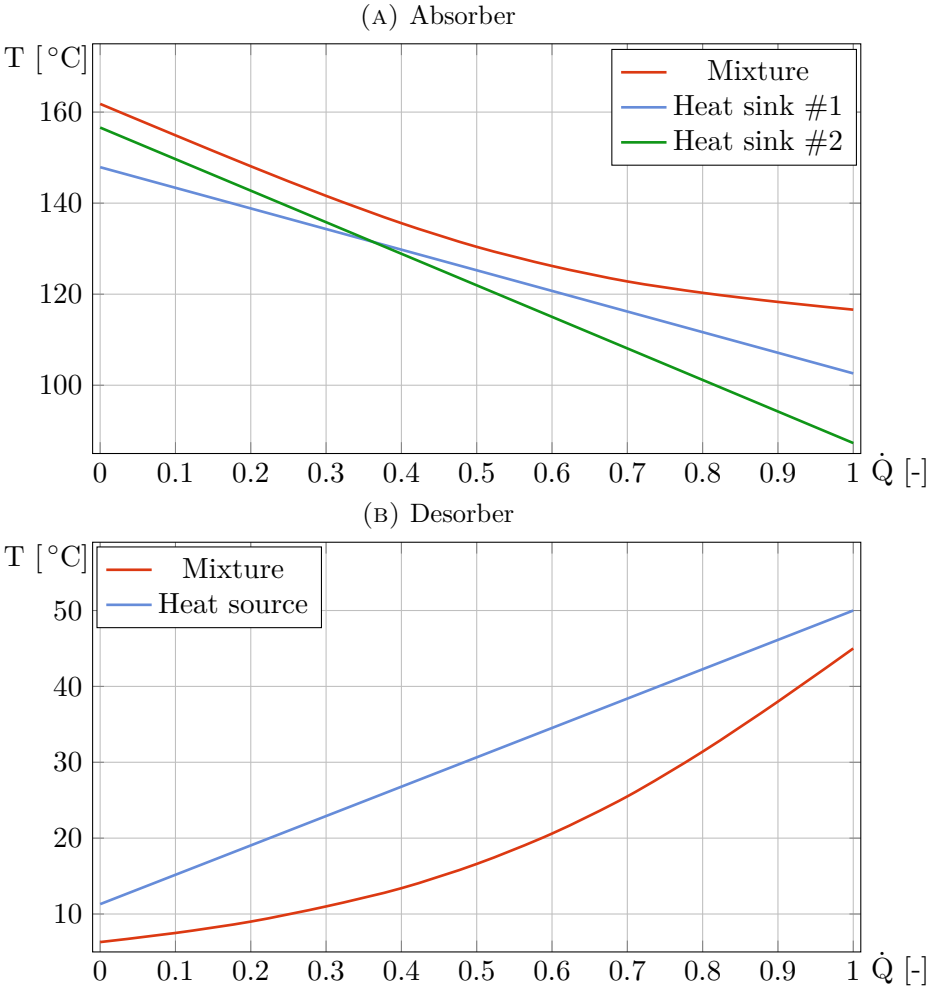

FIGURE 5.4: Temperature versus cumulative heat load for a two-stage compression/absorption cycle with P_{des} = 4.0 bar and P_{abs} = 70 bar. Heat sink # 1 shows the temperature curve for water when the temperature difference between mixture and water is equal at the absorber inlet and outlet. Heat sink # 2 shows the temperature curve for water when the temperature difference between mixture and water is 5 °C at the absorber inlet.

5.1.1.5 Higher discharge temperatures

In all the previous presented simulation results, the discharge temperature has been limited to 180 °C for both compressors. There is no integrated function for compressor cooling in the model, thus the available heat above 180 °C has been "ignored". If there is no upper limit for the discharge temperature, the available heat is larger and the temperature of the vapour before mixing is higher, thus the temperature of the mixture entering the absorber is higher. Consequently the absorber pressure can be reduced and the overall ammonia concentration is reduced to accommodate to required water temperature lift. Figure 5.5, 5.6, 5.7 and 5.8 shows the temperature versus cumulative heat load in the absorber for all four scenarios when the discharge temperature is limited to 220 °C and when the discharge temperature has no limitation. Table 5.1 compares some results between simulations with the discharge temperature limited to 180 °C and simulations with no limitation to the discharge temperature. Table 5.2 shows a brief overview of some results for simulations with no limitations to the discharge temperature. An overview of all the simulation results are listed in appendix C.

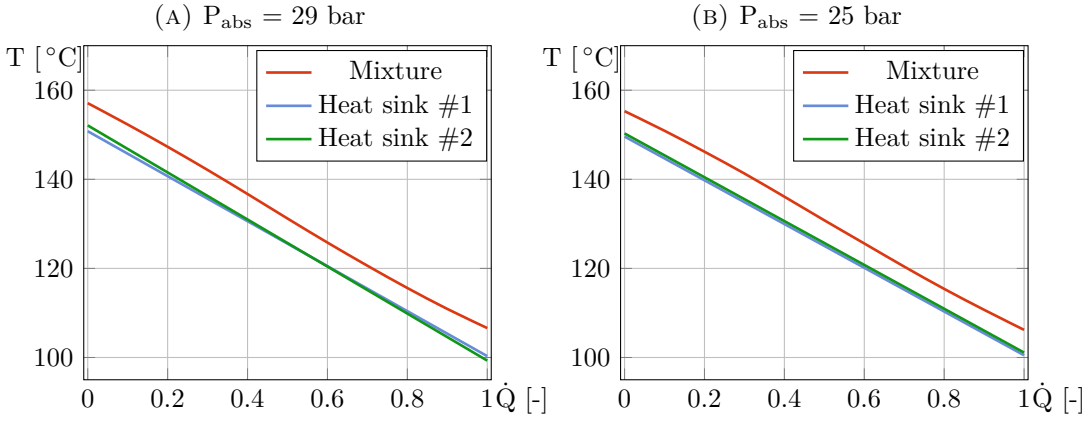

FIGURE 5.5: Temperature versus cumulative heat load with higher discharge temperature and P_{des} = 1.03 bar

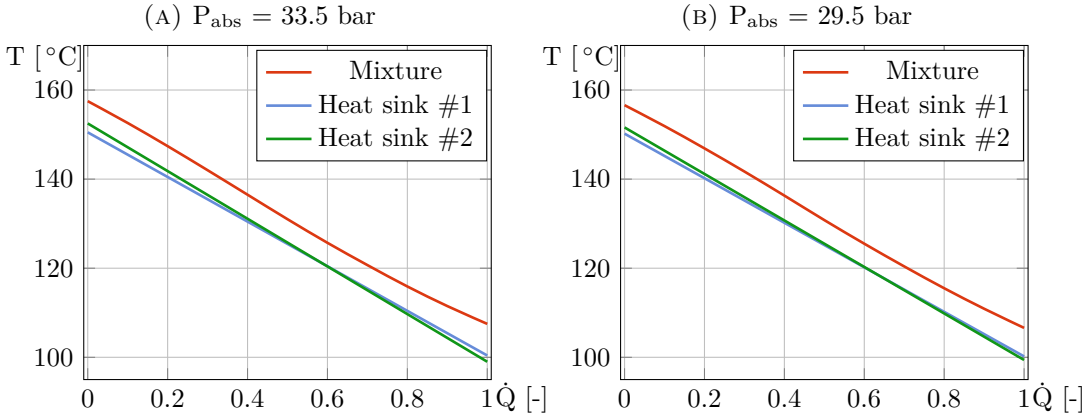

FIGURE 5.6: Temperature versus cumulative heat load with higher discharge temperature and P_{des} = 1.34 bar

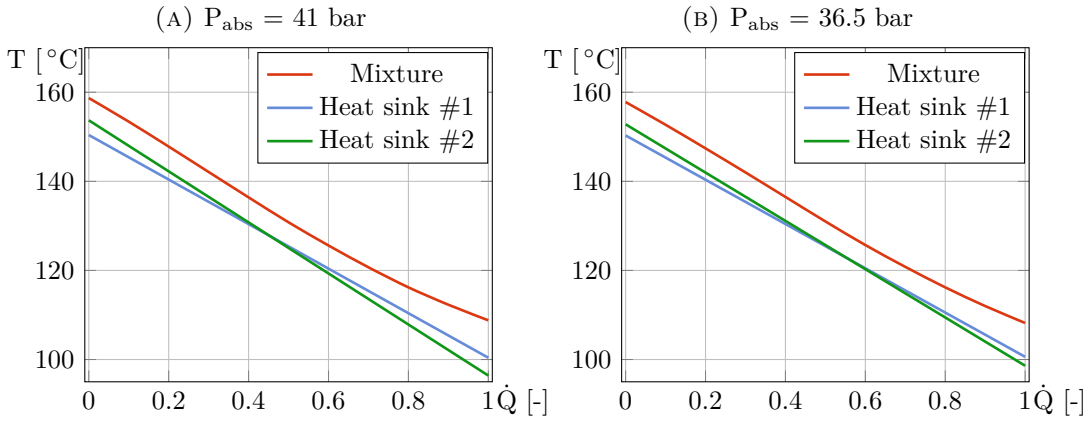

FIGURE 5.7: Temperature versus cumulative heat load with higher discharge temperature and P_{des} = 1.94 bar

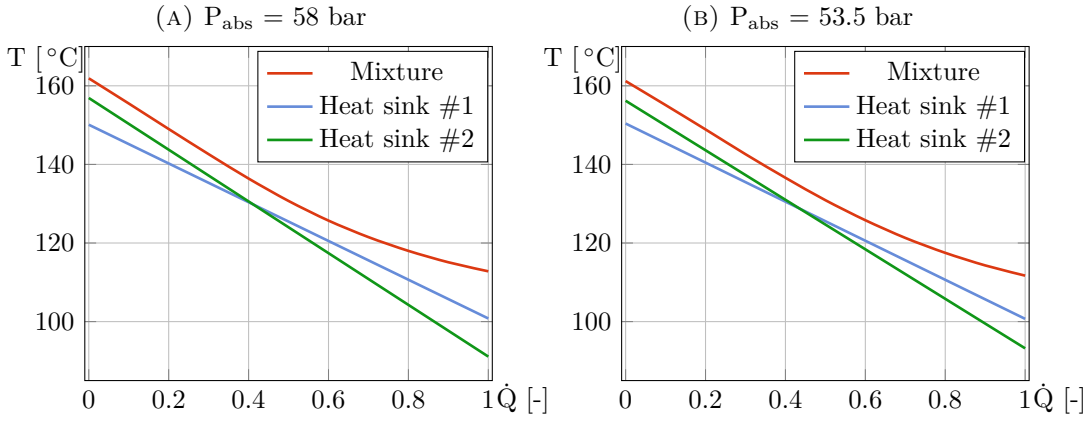

FIGURE 5.8: Temperature versus cumulative heat load with higher discharge temperature and P_{des} = 4.0 bar

TABLE 5.1: Difference in simulation results for the scenarios with discharge temperatures restricted to 180 °C and no limitation

x_1 [-]	0.93	0.95	0.97	0.99
Δ PR[b)]	13.0	12.5	12.3	12.6
Δ COP[a)]	39.6	39.8	40.6	56.8
Δ W_{thr}[b)]	37.4	37.3	38.0	42.5
Δ CR[a)]	54.3	59.5	78.4	149.7
Δ ZZ[b)]	13.3	13.0	13.8	13.5

[a)] Percentage increase

[b)] Percentage decrease

TABLE 5.2: Summary of simulation results with no limitation to the discharge temperature

x_1 [-]	0.93	0.95	0.97	0.99
COP [-]	2.53	2.50	2.47	2.44
CR [-]	1.64	1.49	1.31	0.82
ZZ [-]	0.49	0.54	0.60	0.74
P_{abs} [bar]	25.0	29.5	36.5	53.5
PR [-]	4.92	4.70	4.34	3.66
ρ_1 [kg/m^3]	0.68	0.87	1.27	2.67
ρ_3 [kg/m^3]	2.74	3.40	4.61	8.26
T_4 [°C]	302.6	295.0	283.2	258.8
ΔW_{thr} [kW]	6.0	6.5	7.0	8.0
Q_{des} [kW]	60.5	60.0	59.5	59.0
q_6 [-]	0.40	0.43	0.46	0.61

5.1.1.6 Desuperheater

In previous simulation scenarios, the assumption is that the mixing of vapour exiting the compressor and liquid solution is adiabatic, and that the vapour and liquid phases are in thermodynamic equilibrium. Figure 5.9 shows the temperature curves for a simulation scenario with and without a desuperheater, where figure 5.9 (A) shows the same temperature profile as figure 5.7 (A). The heat delivered in the desuperheater is set to the enthalpy differences between a discharge temperature of 220 °C and 160 °C. Vapour at 160 °C is adiabatically mixed with solution liquid before the absorber. Black encirclements in figure 5.9 illustrates the minimum temperature difference Additional figures with temperature profiles for simulations with desuperheater is shown in appendix C.

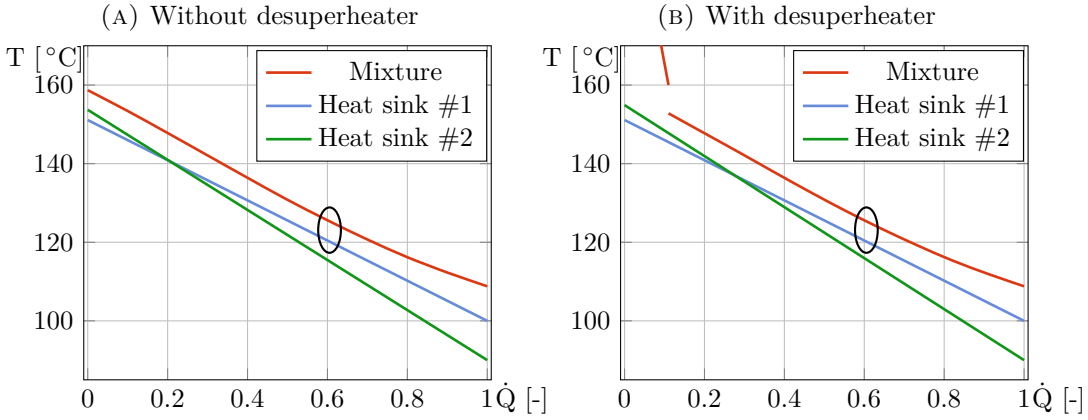

FIGURE 5.9: Temperature versus cumulative heat load for a two-stage compression/absorption cycle with and without desuperheater, when $P_{desorber}$ = 1.94 bar and $P_{absorber}$ = 41 bar. The heat sink # 1 curves shows the water temperature curve when the water inlet temperature is 100 °C. The heat sink # 2 curves shows the water temperature curve when the water inlet temperature is 90 °C.

5.1.2 Summary and discussion

Temperature curves Evaluating figure 5.1, 5.2, 5.3 and 5.4 it is evident that the increasing overall ammonia concentration is a more dominant factor for the linearity of mixture temperature curves than the pressure, which also is shown by the temperaure difference between mixture and heat sink at absorber inlet and outlet. To maintain the minimum temperature difference throughout the process, the temperature at the absorber inlet and outlet increases in the scenarios and the temperature difference at the absorber inlet and outlet is 7 °C, 8 °C, 9.5 °C and 14 °C respectively. The non-linearity of the mixture temperature curve increases with increasing ammonia concentration and causes the inlet/outlet temperature difference in the first scenario to be 2 °C larger than the minimum of 5 °C, while for the last scenario the non-linearity causes the temperature difference to be 9 °C above the minimum. In all the figures, the mixture temperature profile in the absorber is relatively linear for throughout most of the heat exchange before it bends towards the end. It is more significant for the later scenarios, thus the green heat sink temperatures has larger difference between inlet and outlet temperature difference. In the simulation results were the limitation to the discharge temperature is higher, the temperature curves become more linear. Although the absorber pressure is lower, the overall ammonia concentration is lowered and the linearity increases. With 93 weight-% of ammonia in the vapour, removing the limitation to the discharge temperature of 180 °C, the absorber pressure is reduced by 24 % while the overall ammonia concentration is reduced by 13 % resulting in a reduction of the temperature difference at absorber inlet and outlet to 5.7 °C. Simulations with higher ammonia concentration in the vapour also show the same results. For 95, 97 and 99 weight-% of ammonia, the temperature difference at the absorber inlet and outlet is 6.4 °C, 7.5 °C and 10.9 °C respectively, when there is no limitation to the discharge temperature.

Comparisons of the scenarios By summarizing the results in table C.1 and C.2, increasing the ammonia concentration from 93 weight-% to 99 weight-% results in:

- Higher absorber and desorber pressures
- Lower pressure ratios
- Lower COP
- Smaller circulation ratios
- Smaller heat transfer in both solution heat exchangers
- Approximately unchanged mixture, heat sink and heat source mass flow rates
- Higher expansion losses

The results of allowing a higher discharge temperature results in:

- Lower absorber pressures, thus lowering the pressure ratios

- Higher COP
- Larger circulation ratios
- Larger heat transfer in solution heat exchanger # 1, while smaller heat transfer in solution heat exchanger # 2
- Approximately unchanged mixture, heat sink and heat source mass flow rates
- Smaller expansion loss

COP In the simulations the requirement to the heat capacity in the absorber was 100 kW, thus the mass flow was adjusted according to the calculated enthalpy difference in the absorber. However, simulation results showed that the total mass flow of mixture only had minor changes comparing the scenarios. As the pressure ratio decreases for an increasing ammonia concentration in the vapour, the specific compressor work becomes smaller, however, the COP decreases in this case. The varying circulation ratio to achieve the required overall ammonia concentration in each scenario and the approximately constant mixture mass flow rates, results in larger vapour mass flow rates through the compressor circuit. Thus, the compressor work increases as the ammonia concentration increases, resulting in a lower COP. The difference between the scenarios, however, are minor. In simulations with higher limitations to the discharge temperature, COP increased in all scenarios. Also in this case, the increasing COP can be explained a higher circulation ratio. Evaluating the COP results in table 5.1, the increase is quite substantial. Besides the increasing circulation ratio, the smaller compressor work is also explained by a lower pressure ratio. A drawback with the simulation results is that the isentropic efficiency for the compressors has been 0.8 in all simulations. More realistic efficiencies would probably have narrow the difference in COP between the scenarios. One last remark is that with lower heat source temperatures which results in mixture temperatures out of the desorber lower than 45 °C will require larger ammonia concentrations than 93 weight-% to avoid sub-atmospheric pressures.

Discharge temperature Simulation results in table 5.2 shows that there is a close linkage between the pressure ratios and the discharge temperatures in the processes. There are not large differences between scenarios, however, the heat transfer in the solution heat exchanger between the compressors decreases with increasing ammonia concentration in the vapour. One can assume that the larger circulation ratio, hence larger ratio between solution mass flow rate and vapour mass flow rate, results in a larger heat transfer in solution heat exchanger #2, thus a larger reduction of the vapour temperature before the HP-compressor. But again, more realistic compressor efficiencies might have had a larger negative effect for the discharge temperature with high water concentration in the vapour due to larger pressure ratios.

Compressor volume Table 5.2 shows that there is a large difference vapour density at the compressor. With a 99 weight-% ammonia concentration in the vapour, the

density before the LP-compressor is four times higher, than with a 93 weight-% ammonia concentration. However, the vapour mass flow rate to the compressor increases for a fixed absorber capacity due to larger circulation ratio. If one disregards the volumetric losses in the compressor, the volumetric flow required to the LP compressor for a 99 weight-% ammonia concentration is 90 m^3/h, while for a 93 weight-% ammonia concentration it is 259 m^3/h, reducing the difference to three times as high. For the HP compressor, the difference in vapour density is three times higher for 99 weight-% than 93 weight-%, while the volumetric flow rates are 29 m^3/h and 64 m^3/h. The vapour density to the LP compressor remains unchanged regardless of the limitation to the discharge temperature, however, the circulation ratio increases, thus reducing the vapour mass flow rate. The reduced vapour mass flow rate results in a reduction of the volumetric flow rate between 20 - 25 % in all scenarios comparing the simulations with a 180 °C limitation the the discharge temperature and simulations with no limitation to the discharge temperature. Vapour densities before the HP-compressor decreases as the limitation to the discharge temperature increased due to lower pressures, and it counteracts the effect of a larger circulation ratio. For the HP compressor, the volumetric flow rate is reduced by 8 - 10 % in all scenarios comparing simulations with discharge temperatures limited to 180 °C and simulations with no limitations to discharge temperatures.

Desorber Table 5.2 shows that there are only small variations in the desorber capacity and total mixture mass flow rates only have small variations between simulations scenarios. However, the increasing non-linearity of temperature curves as the overall ammonia concentration increases, forces the mixture temperature at the absorber outlet to be higher when the heat sink inlet temperature is 100 °C. Combined with a smaller circulation ratio, the temperature of the mixture after solution heat exchanger #1 increases. It results in a higher expansion loss and a higher vapour mass fraction after expansion. It is worth mentioning that heat source temperatures out of the desorber was below 0 °C for some simulation scenarios, when this can be a limitation for pure water as heat source fluid.

Vapour fraction at absorber inlet For the thermodynamic approach with adiabatic mixing before the absorber, it is beneficial with a high vapour fraction at the absorber inlet since it provides a larger mixture temperature difference between absorber inlet and outlet and more vapour must condense, hence more heat (section 3.3). Comparing the scenarios, the vapour fraction at the absorber inlet increases. It can mainly be explained by smaller circulations ratios. It is worth noticing that the heat transfer in solution heat exchanger #2 is larger for the first simulation scenarios while the circulation ratio is larger which contributes to bring the liquid solution closer to the saturation temperature. With higher limitations to discharge temperatures, circulation ratios increase, thus the vapour fraction at the absorber inlet decreases. However, the reductions is only minor, but referring to figure 3.8, it could have a larger impact for high overall ammonia concentrations.

Desuperheater Figure 5.9 shows that the minimum temperature difference between the mixture temperature curve and the blue heat sink temperature curve occur at the exact same place in the heat exchange, regardless if the process is with or without a desuperheater. Because the total heat available is the same with and without the desuperheater, and the mixture is in thermodynamic equilibrium before the absorber, the temperature curve for the mixture will be unchanged except were the heat is delivered through the desuperheater. Since the total heat available and the heat sink inlet temperature is unchanged, the minimum heat sink mass flow rate to maintain the minimum temperature differences, will be exactly the same, hence the water outlet temperature will be the unchanged. The minimum temperature difference between the mixture temperature curve and the green heat sink temperature curve, occur at the absorber inlet. It means that the minimum heat sink flow rate to maintain the minimum temperature difference can be lower. With the same inlet temperature, the outlet temperature is higher. However, the temperature increase is only 1.2 °C in the simulation scenario in figure 5.9, due to the steepness of the vapour temperature curve. Even with a temperature drop from 220 °C to 160 °C, the heat available in the desuperheater is only 11 % of the total heat delivery. In the absorber the heat delivery is 2.02 kW/K, while it is only 0.18 kW/K in the desuperheater. One of the reasons is that the mixture mass flow through the absorber is larger than the vapour mass flow rate, thus when the water mass flow rate is dimensioned for the absorber process, the effect of the desuperheater is small and the effect will decrease when circulation ratios increase. Temperature curves for simulations with desuperheater when the discharge temperature is limited to 220 °C and without limitations is shown in figure C.1.

5.2 Absorber

Spray drying is one of the most important methods of drying liquid foods. It is a technique that utilizes liquid atomization to create droplets that are dried when in contact with a hot gas, typically air (Mujumdar, 2007). Drying processes often need air at high temperatures, and as air is drawn from the ambient, it requires a large temperature lift. Compression/absorption heat pumps can be a suitable measure in order to reduce primary energy demands in such processes. Figure 5.10 shows a schematic diagram where the hybrid compression/absorption process is integrated in a spray drying process. Air is heated in three steps. First, heat is recovered from the hot air exiting the dryer, before it is heated by the absorber. The remaining temperature lift is conducted by an additional heating device. The heat source for the desorber is the hot air exiting the air-to-air heat exchanger.

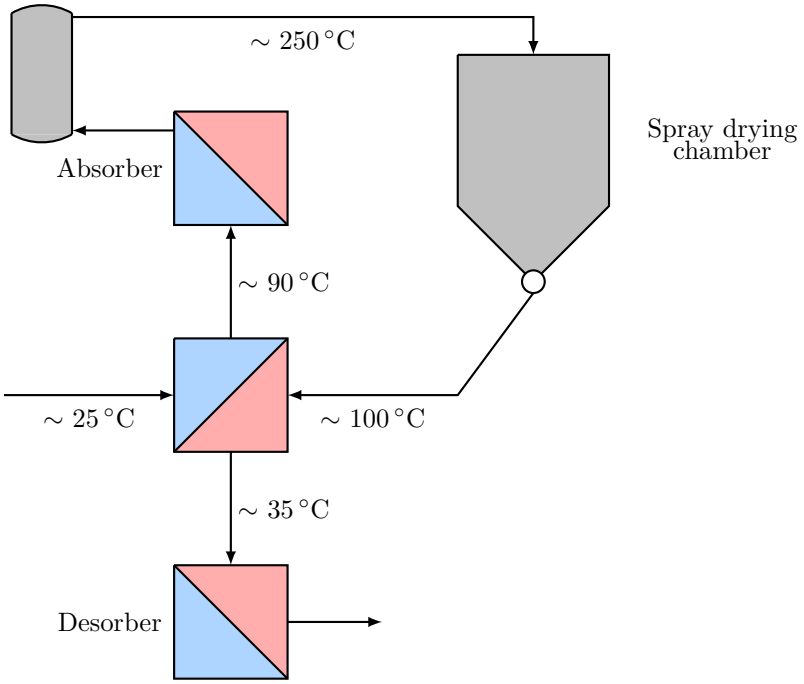

FIGURE 5.10: Schematic diagram of a spray drying process with desorber and absorber

The aim for the simulations is to assess the dimensioning of a finned, annular tube cross-flow absorber for the process of heating air. The mixture inlet temperature is set to 150 °C, and the overall ammonia is found so that complete absorption at the given pressure and overall ammonia concentration occur at 100 °C. Table 5.3 shows the simulation inputs. One of the great difficulties when simulating an absorption process with air as the cooling medium, is the large difference in mass flow of mixture and air. When the heat capacity of the absorber is set to 100 kW and the temperatures on the mixture side is 150 °C to 100 °C, it results in a mixture mass flow of 0.13 kg/s. In comparison, the air mass flow when heated from 90 °C to 140 °C, is 1.98 kg/s, 15 times larger than the mixture mass flow rate. Moreover, the frontal velocity of air is limited to 3.5 m/s in the simulations, which limits the possible air mass flow. An increasing number of tubes will allow more tube rows, hence larger frontal area of each segment and a larger air mass flow while maintaining the maximum air velocity. At the same time will to many tubes limit the mixture mass flow rate in each tube, reducing the mixture heat transfer coefficient. The EES procedure for external flow over a staggered bank used in the simulations is limited. The ratio between tube spacing perpendicular on the air flow and the outer tube diameter must be between 1.25 and 2.5. With a outer tube diameter of 25 mm, the minimum spacing is 31.25 mm and the maximum spacing is 62.5 mm.

Table 5.3: Parameters for the simulations of the finned, annular tube cross-flow absorber

Absorber duty	100 kW
Absorber pressure	25 bar
Mixture inlet temperature	150 °C
Air inlet temperature	90 °C
Maximum frontal air velocity	3.5 m/s
Tube inner diameter	22 mm
Tube outer diameter	25 mm
Fin thickness	0.25 mm
Mixture mass flow	0.13 kg/s
Overall ammonia concentration	0.5238
Material	Stainless steel

5.2.1 Simulation results

In order to maintain an relatively large mixture heat transfer coefficient, the number of tubes were limited to 24. Table 5.4 shows the simulation results for different number of tube rows and columns, with a staggered arrangement and vertical/horizontal tube spacing of 60 mm. The number of tube rows determines the width of each segment, while the number of columns determine the length of each segment. Temperature of the mixture and air versus the relative height of all four scenarios are shown in figure 5.11. Table 5.5 shows simulations results when the altering segment width and fin pitch for scenario #3. Table 5.6 shows the simulation results when the tube spacing is 40 mm.

Table 5.4: Heat exchanger geometries and simulation results with 60 mm tube spacing

Scenario	#1	#2	#3	#4
Number of tube rows [-]	4	6	8	12
Number of tube columns [-]	6	4	3	2
Width of segment [m]	0.30	0.42	0.54	0.78
Height of segment [m]	2.00	1.45	1.30	1.05
Length of segment [m]	0.42	0.30	0.24	0.18
Total height of absorber [m]	20.0	14.5	13.0	10.5
Fin pitch [mm]	7.5	4.0	3.0	2.0
Total heat transfer surface [m^2]	646	854	1044	1368
Volumetric flow rate of air [m^3/s]	2.10	2.13	2.46	2.87
Average mixture heat transfer coefficient [W/m^2-K]	1208	1205	1173	1145
Average air heat transfer coefficient [W/m^2-K]	69	66	62	56
U_y [W/m^2-K]	8.9	6.7	5.7	4.2
Pressure drop [Pa]	371	248	187	125
Fan work [kW]	3.1	2.1	1.8	1.4
Mixture outlet temperature [°C]	101.2	100.7	100.2	101.0
Air outlet temperature [°C]	139.7	139.6	133.4	126.3

TABLE 5.5: Heat exchanger geometries and simulation results with 8 tube rows and 3 tube columns and 60 mm tube spacing.

Scenario	# 2	#5	#6
Width of segment [m]	0.54	0.54	0.54
Height of segment [m]	1.30	0.80	0.80
Length of segment [m]	0.24	0.24	0.24
Total height of absorber [m]	13.0	8.0	8.0
Fin pitch [mm]	3.0	3.0	2.0
Total heat transfer surface [m^2]	1044	642	956
Volumetric flow rate of air [m^3/s]	2.46	1.51	1.51
Average mixture heat transfer coefficient [W/m^2-K]	1188	1260	1258
Average air heat transfer coefficient [W/m^2-K]	62	62	62
U_y [W/m^2-K]	5.7	6.1	5.2
Pressure drop [Pa]	187	184	183
Fan work [kW]	1.8	1.1	1.1
Mixture outlet temperature [°C]	100.2	115.0	109.2
Air outlet temperature [°C]	133.4	138.4	147.0

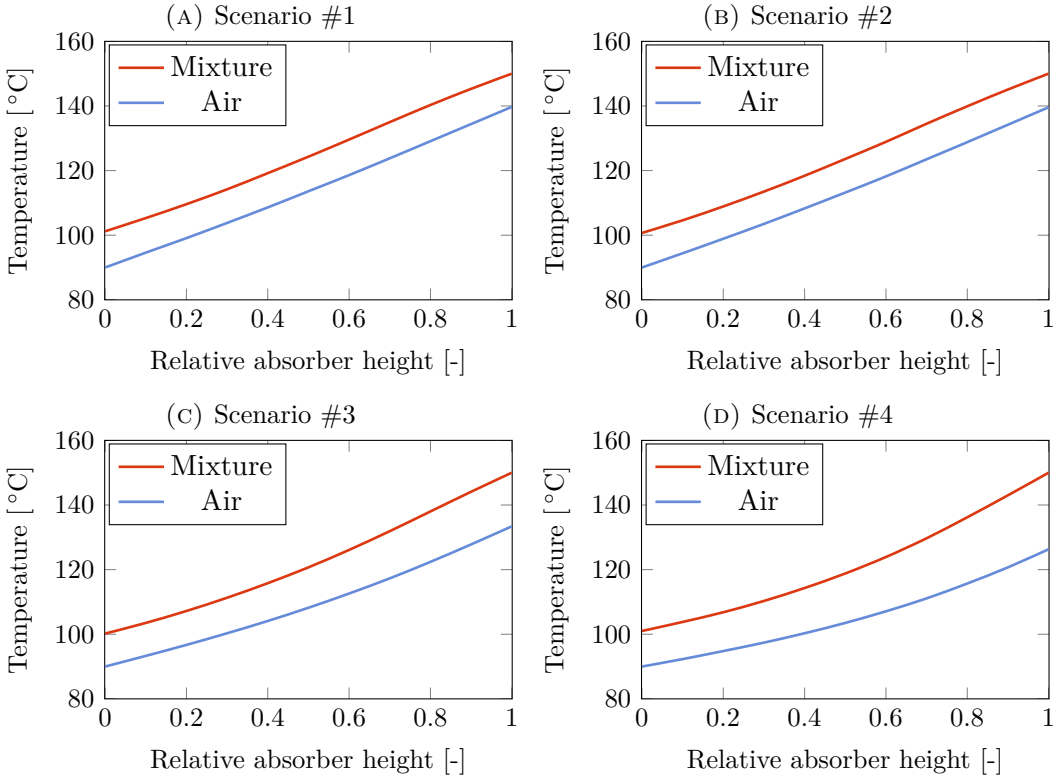

FIGURE 5.11: Temperature versus relative absorber height

TABLE 5.6: Heat exchanger geometries and simulation results with 12 tube rows and 2 tube columns and 40 mm tube spacing.

Scenario	# 7	# 8	#9
Width of segment [m]	0.52	0.52	0.52
Height of segment [m]	1.19	0.60	0.60
Length of segment [m]	0.12	0.12	0.12
Total height of absorber [m]	11.9	6.0	6.0
Fin pitch [mm]	3.0	3.0	2.0
Total heat transfer surface [m^2]	419	213	314
Volumetric flow rate of air [m^3/s]	2.15	1.09	1.09
Average mixture heat transfer coefficient [W/m^2-K]	1211	1298	1295
Average air heat transfer coefficient [W/m^2-K]	73	73	73
U_y [W/m^2-K]	13.8	15.0	12.9
Pressure drop [Pa]	337	331	329
Fan work [kW]	2.9	1.4	1.4
Mixture outlet temperature [°C]	100.4	122.5	120.6
Air outlet temperature [°C]	139.6	142.9	146.8

Figure 5.7 shows temperature versus cumulative heat load for the absorber. Mixture temperature curves for scenario #1 and #4 is plotted against the mixture temperature in figure 5.5 (B). In figure 5.5 (B) the temperature curves displays the simulation results for 25 bar, an overall ammonia concentration of 0.49 and the mixture inlet and outlet temperatures are a little higher than in the absorber simulation. However, there are only minor differences.

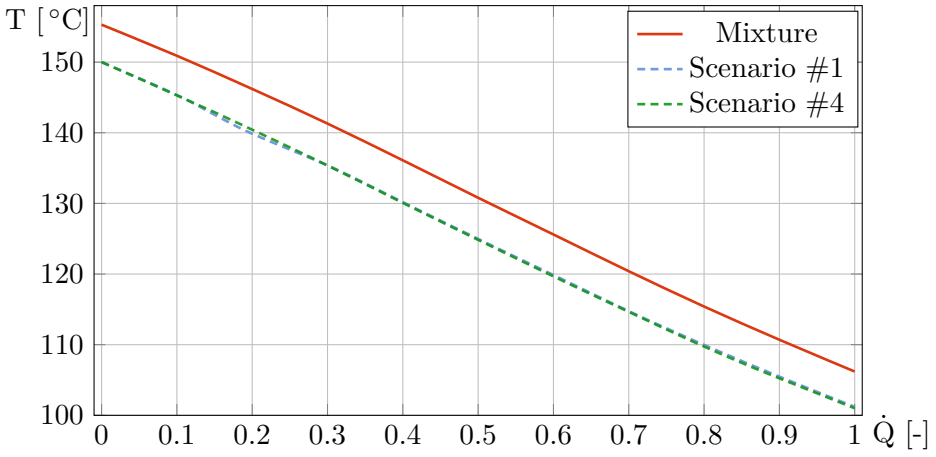

TABLE 5.7: Temperature versus the cumulative heat load in the absorber for scenario #1 and #4 and the temperature from the two-stage simulation scenario with absorber pressure at 25 bar and an overall ammonia concentration of 0.49.

5.2.2 Summary and discussion

Simulation results showed that dividing the mixture mass flow into 24 tubes results in an average heat transfer coefficient between 1100 and 1300 W/m^2-K. The construction

of the model does not consider the length of the tubes when calculating the mixture heat transfer coefficient, only in how many tubes the total mixture mass flow is divided into. Hence, increasing the number of tubes will result in a lower mixture heat transfer coefficient. Summarizing the results in table 5.4, 5.5 and 5.6 shows that by increasing the number of tube rows:

- pressure drop and fan work decreases
- fin pitch can be smaller
- total air-side surface increases
- volumetric air flow rate can be increases, however, lowering the air outlet temperature
- height of the absorber decreases, while the width and length increases

The air outlet temperature of air decreases due to a larger volumetric air flow rate. The frontal area of each segment increases with the increasing tube rows and when the frontal air velocity is constant at 3.5 m/s, the volumetric air flow rate must increase. If the fin pitch presented in table 5.4 is increased in any of the scenarios, the mixture will not be fully absorber and the air outlet temperature will be lower. If the fin pitch is smaller, the mixture will be subcooled and the air outlet temperature becomes higher. The fin pitches in the result tables are the smallest possible fin pitch before mixture reaches a temperature below 100 °C or the air outlet temperature exceeds the mixture inlet temperature. Evaluating the results in table 5.5 vindicates that the simulation model has a strict limitation regarding air flow, fin pitch and absorber height. In order to maintain the maximum frontal air velocity and a sufficient volumetric air flow for a specific absorber geometry, limits the possible fin pitch. In scenario #5 and #6 were the height of each segment is reduced and a smaller fin pitch in scenario #6, volumetric air flow rates are smaller than in scenario #2. If the width of the segment is increased from the width in scenario #6, the volumetric air flow rate increases. However, the air flow rate is still to small and simulations show that the air outlet temperature is higher than the mixture inlet temperature. When the tube spacing is 40 mm, width of each segment is smaller. The frontal area of each segment is limited, hence the volumetric air flow is limited. Although the total air surface area is lower than with 60 mm tube spacing, the pressure drop and fan work is twice as high than for scenario #3. Figure 5.7 shows temperature versus cumulative heat load for the mixture in scenario #1 and #4, and the mixture temperature curve from figure 5.5 (B). Although the temperature curves for scenario #1 and #4 is plotted for a slightly lower temperature, resulting curves appear quite similar to curves obtain from the two-stage model where the approach was a linear enthalpy decrease. However, this is only shown for an overall ammonia concentration of approximately 0.52, and not for higher concentrations.

The geometries of the absorber listed in table 5.4 are not entirely realistic due to the extreme ratio between absorber height and width/length. It is difficult to determine if the somewhat strange simulation results is due to the large difference in mixture

and air mass flow rates and that is impossible to accomplish a notable result, or if the problem is with the simulation model. However, it is worth repeating that with the simulation inputs, the air mass flow rate is 15 times higher than the mixture mass flow rate. This major mismatch and a maximum limitation of the air velocity, will result in a large required frontal area and the number of possible tube rows are limited. There are two factors that could limit the large difference between the absorber height and width/length. First, the air inlet temperature could be lowered which allows a smaller air mass flow rate and increases the driving forces, although it ultimately increases the temperature loss in the absorber. Second, the tube spacing could be increased. It would increase the frontal area of each segment without increasing the number of tube rows. However, it would cause a significant increase in air-side heat transfer area without increasing the total heat transfer. Table 5.4 shows that the total air-side heat transfer area is considerably higher when tube spacing is 60 mm compared to 40 mm. Another factor that may contribute to the results, is the absorber material. Since one of the working fluid components is ammonia, stainless steel was used to conduct a realistic simulation scenario. When calculating the overall fin efficiency, the EES function requires geometry of the fins, air-side heat transfer coefficient and the thermal conductivity of the absorber material. In scenario #1 to #4, the average overall fin efficiency is approximately 0.12, which could partially be explained by the high thermal resistance in the absorber material. Early tests of the simulation model with aluminium as absorber material resulted in higher fin efficiencies and overall heat transfer coefficients.

It would have beneficial to conduct simulations with other tube diameters to assess if the optimal solution for the process could have either larger or smaller tube diameters. Section 3.4 presented the work of Fernández-Seara et al. (2005) which emphasized that smaller tube diameters will have a significant effect on the absorption length. It is highly questionable if that is a factor in the simulation scenarios due to the simplicity of the absorption process model. It could however be a factor. Further, it would have been beneficial to conduct more simulations with different overall ammonia concentrations, since the mass ratio between components will affect the volume of the mixture stream in the tubes. In conclusion, the decision of dividing the absorber into 10 segments may not have been the best solution. However, with the simplicity of the model it probably would not have been beneficial to reduce the number of segments and increase the number of tube columns. The absorption process is approximated as equal in all tubes in the individual segment and the actual absorption process will evolve more rapidly at the first tube rows (section 3.4). It means that larger air temperature increases in each segment would have given a more inaccurate result since the variation in the absorption process in each tube would have been larger.

5.2.3 Spray drying case

In order to evaluate the compression/absorption heat pump for a spray drying process, it was conducted a simulation in the two-stage model with air as heat source and heat sink. Air temperature at the desorber inlet was set to 35 °C, and to avoid sub-atmospheric

desorber pressure, the vapour ammonia concentration had to be minimum 97.5 weight-%. It resulted in desorber pressure of 1.03 bar. Table 5.8 shows the inputs and simulation results. One advantages is that the required air mass flow in the absorber and desorber are fairly equal, which is convenient since the air flow through the absorber eventually runs through the desorber. It could be problematic if the necessary air flow through the absorber is significantly smaller, for the temperature lift, than the required air mass flow rate in the desorber. In order to remove the heat from the mixture and maintaining an equally air flow through absorber and desorber, the air mass flow rate in the absorber the must be increased. It will lower the outlet temperature, thus a large temperature lift after the absorber, which ultimately reduces the effect of the heat pump. Simulation results indicate that the performance of the compression/absorption heat pump is not convincing for this scenario. The simulation was conducted with no limitation to the discharge temperature, and if the COP is approximated to be 40 % lower with the discharge temperature limited to 180 °C (table 5.1), it is reduced to 0.87. It may have been more beneficial with a smaller temperature lift in the air-to-air heat exchanger. It would have decreased the air temperature at the absorber inlet, and the mixture temperature out of the absorber could be lower. System performance would be higher due to lower pressure ratios and compressor work, and the absorber pressure could be lowered. Although the heat pump performance would be higher, required air temperature after the additional heat device would be the same, hence more of the temperature lift would be conducted after the absorber. It is questionable if it would improve the total efficiency.

Table 5.8: Simulation results from spray drying case

Desorber pressure	1.03 bar
Absorber pressure	45.0 bar
Ammonia concentration in vapour	0.975
Overall ammonia concentration	0.75
Total mixture mass flow	0.11 kg/s
Air mass flow rate in desorber	1.57 kg/s
Air mass flow rate in absorber	1.82 kg/s
Circulation ratio	0.50
Absorber capacity	100.0 kW
$W_{\text{LP-compressor}}$	31.2 kW
$W_{\text{HP-compressor}}$	37.8 kW
W_{pump}	0.2 kW
W_{fan}	2.0 kW
COP	1.45
COP with fan work	1.40

Conclusion and suggestions for future work

6.1 Conclusion

The most important results obtained from the two-stage model simulations are:

- The overall ammonia concentration has a more significant impact on mixture temperature curves than the pressure.
- The highest COP obtained from simulations with discharge temperatures limited to 180 °C was 1.81, and the highest COP obtained from simulations with no limitations to discharge temperatures 2.53. Both results was from simulation with an ammonia concentration of 93 weight-% in the vapour at the compressor inlet.
- Simulations with higher ammonia concentration than 93 weight-% in the vapour at the compressor inlet, resulted lower in pressure ratios although the absorber pressures was significantly higher. Smaller circulations ratios, hence higher vapour mass flow rates, resulted in larger compressor work and smaller performances, however, differences between scenarios are only minor.
- Removing the limitation to the discharge temperature of 180 °C resulted in a 40 % increase in COP for most scenarios, while absorber pressures was reduced by 23 - 25 % and pressure ratios reduced by 12 - 13 %. Discharge temperatures for these simulations was in the range from 250 °C to 310 °C.
- Vapour densities at the compressor inlet was significantly higher when the ammonia concentration in the vapour was high. Although circulation ratios was higher, hence vapour mass flows higher, volumetric flow rates was significantly lower for high ammonia concentrations in the vapour.
- With the assumptions made in the model, simulations with a desuperheater showed that if the minimum temperature difference between mixture and heat sink temperature curves does not occur at the absorber inlet, employing a desuperheater will not increase the heat sink outlet temperature. If the heat sink inlet temperature is sufficiently low, the minimum temperature difference will occur at the absorber inlet. However, the effect of a desuperheater is small due to the large difference between heat rejection from the absorption process and from the vapour. This difference will increase when the circulation ratio increases.

Simulations with the absorber model and the spray drying case:

- The dimensioning of the finned cross-flow absorber gave some unrealistic results due to the extreme ratio between absorber height and absorber width/length. It is difficult to determine whether the problem was with the simulation model or if selection of inputs were unsuitable. It is noteworthy that the air mass flow rate was approximately 15 times larger than the mixture mass flow rate. Limitations to the air velocity and the width of the absorber made it difficult to acquire a good result
- Simulations resulted in total air-side surface areas between 600 and 1400 m^2 for an absorber duty of 100 kW.
- For a constant number of tubes, increasing the number of tube rows resulted in larger air mass flow rates, lower air outlet temperatures, larger air-side surface areas, smaller absorber heights and smaller air pressure drops.
- The simulation case were a compression/absorption heat pump was used in a spray drying process, indicated that it may not have been a suitable measure, at least for the case scenario. Due to the large temperature lift, the system performance was low, although the there was no limitation to the discharge temperature. With the discharge temperature limited to 180 °C, the performance is approximated to 0.87.

6.2 Suggestions for future work

Based on the tasks in the original thesis description that were not considered, suggestions for further work are:

- Evaluate different system designs to utilize the absorption heat to achieve higher temperature than the discharge gas temperature from the compressor
- Evaluate other heat exchanger types for optimizing the process

Based on the work performed in this thesis, the following are suggested as further development of the simulation models and case scenarios:

- Implement functions for the compressor efficiencies, investigation of a more suited intermediate pressure and calculation of compressor cooling in the two-stage model.
- A more suited procedure for calculating the desuperheater process in the two-stage model.
- Investigation of compressor limitations regarding the maximum allowable water content and maximum discharge temperatures.

- A more detailed investigation of the absorption process. The calculations of thermophysical properties and heat transfer coefficients can be further developed or changed in order to acquire a more realistic model. Moreover can newer equations for the ammonia/water mixture be more appropriate.
- Further optimization of the finned, annular tube cross-flow absorber. Different tube diameters and a different approach to the absorber design can contribute in optimizing the process.

Bibliography

Alefeld, G. and R. Radermacher (1993). *Heat Conversion Systems*. CRC Press.

Atkins, P. and J. de Paula (2010). *Physical Chemistry*. W.H Freeman and Company.

Bolaji, B. O. and Z. Huan (2013). "Ozone depletion and global warming: Case for the use of natural refrigerant - A review". In: *Renewable and Sustainable Energy Reviews* 18, pp. 49–54.

Brunin, O et al. (1997). "Comparison of the working domains of some compression heat pumps and a compression-absorption heat pump". In: *International Journal of Refrigeration* 20.5, pp. 308 –318.

Cerezo, J. et al. (2009). "Experimental study of an ammonia-water bubble absorber using a plate heat exchanger for absorption refrigeration machines". In: *Applied Thermal Engineering* 29, pp. 1005 –1011.

Chua, K. et al. (2010). "Advances in heat pump systems: A review". In: *Applied Energy* 87, pp. 3611 –3624.

Conde-Petit, D. M. R. (2004). "Thermophysical Properties of NH_3 + H_2O solution for the industrial design of absorption refrigeration equipment". In:

Dinçer, İbrahim and M. Kanoğlu (2010). *Refrigeration Systems and Applications*. John Wiley & Sons, Ltd.

Fernández-Seara, J. et al. (2005). "Ammonia–water absorption in vertical tubular absorbers". In: *International Journal of Thermal Sciences* 44.3, pp. 277 –288.

Fernández-Seara, J. et al. (2007). "Analysis of an air cooled ammonia–water vertical tubular absorber". In: *International Journal of Thermal Sciences* 46, pp. 93 –103.

Fornasieri, E. et al. (2009). "Natural Refrigerant CO_2". In: *Leonardo Project "NARECO2"*.

Granryd, E. et al. (2009). *Refrigerant Engineering*. Royal Institute of Technology, KTH.

Hultén, M. and T. Berntsson (1999). "The compression/absorption cycle - influence of some major parameters on COP and a comparison with the compression cycle". In: *International Journal of Refrigeration* 22, pp. 91–106.

– (2002). "The compression/absorption heat pump cycle - conceptual design improvments and ccomparison with the compression cycle". In: *International Journal of Refrigeration* 25, pp. 487–497.

Ibrahim, O. M. and S. A. Klein (1993). "Thermodynamic Properties of Ammonia-Water Mixtures". In: *ASHRAE Trans.: Symposia* 21,2, p. 1495.

IEA-HPC (2014). *Heat Pumps in Industry*. International Energy Agency - Heat Pump Centre. URL: `http://www.heatpumpcentre.org/en/Sidor/default.aspx`.

Incropera, F. P. et al. (2006). *Fundamentals of Heat and Mass Transfer*. 6th ed. John Wiley & Sons, Ltd.

Itard, L. and C. Machielsen (1994). "Considerations when modelling compression/resorption heat pumps". In: *International Journal of Refrigeration* 17, pp. 453 –460.

Jakobs, R. et al. (2010). "Status And Outlook: Industrial Heat Pumps". In: *International Refrigeration and Air Conditioning Conference*.

Kang, Y. T. et al. (2000). "Analytical investigation of two different absorption modes: falling film and bubble types". In: *International Journal of Refrigeration* 23, pp. 430 –443.

Killion, J. D. and S. Garimella (2001). "A critical review of models of coupled heat and mass transfer in falling-film absorption". In: *International Journal of Refrigeration* 24, pp. 755 –797.

Kim, J. et al. (2013). "Experimental study of operating characteristics of compression/absorption high-temperature hybrid heat pump using waste heat". In: *Renewable Energy* 54, pp. 13 –19.

Kim, M. H. et al. (2004). "Fundamental process and system design issues in CO_2 vapor compression systems". In: *Progress in Energy and Combustion Science* 30, pp. 119–174.

Laue, H. (2006). "Heat Pumps". In: Energy Technologies. Chap. 9, pp. 605–626.

Lee, K. B. et al. (2002a). "Comparison of heat and mass transfer in falling film and bubble absorbers of ammonia-water". In: *Experimental Heat Transfer* 15, pp. 191–205.

Lee, K. B. et al. (2002b). "Experimental analysis of bubble mode in a plate-type absorber". In: *Chemical Engineering Science* 57, pp. 1923 –1929.

Lee, S. et al. (2012). "Measurement of absorption rates in horizontal-tube falling-film ammonia-water absorbers". In: *International Journal of Refrigeration* 35.3. Refrigeration and Heat Pumping with Sorption Processes, pp. 613 –632.

LeonardoEnergy (2007). "Industrial Heat Pumps". In: *Power Quality and Utilization guide*.

Lorentzen, G. (1995). "The use of natural refrigerants: a complete solution to the CFC/HCFC predicament". In: *International Journal of Refrigeration* 18, pp. 190–197.

McMullan, A. (2003). "Industrial Heat Pumps for Steam and Fuel Savings". In: *U.S. Department of Energy: Energy Efficiency and Renewable Energy*.

Morawetz, E. (1989). "Sorption-compression heat pumps". In: *International Journal of Energy Research* 13, pp. 83–102.

Mujumdar, A. S. (2007). "Handbook of Industrial Drying". In: ed. by A. S. Mujumdar. Taylor & Francis Group. Chap. 2, pp. 137–520.

Nellis, G. and S. Klein (2009). *Heat Transfer*. Cambridge University Press.

Nordtvedt, S. (2013). "Norsk deltagelse i IEA Heat Pump Programme Annex 34 - sluttrapport". In: *Institutt for energiteknikk*.

Nordtvedt, S. R. (2005). "Experimental and theoretical study of a compression/absorption heat pump with ammonia/water as working fluid". PhD thesis. Norwegian University of Science and Technology.

Pearson, A. (2012). "High Temperature Heat Pumps with Natural Refrigerants". In: *IEA Heat Pump Centre Newsletter* 30, pp. 33–35.

Rane, M. V. and R. Radermacher (1993). "Feasibility study of a two-stage vapour compression heat pump with ammonia-water solution circuits: experimental results".

In: *International Journal of Refrigeration* 16. Special Issue on Absorption Systems, pp. 258 –264.

Rane, M. V. et al. (1993). "Performance enhancement of a two-stage vapour compression heat pump with solution circuits by eliminating the rectifier". In: *International Journal of Refrigeration* 16.4. Special Issue on Absorption Systems, pp. 247 –257.

Stene, J. (1993). *Varmepumper - Industrielle anvendelser*. NTH-SINTEF Kuldeteknikk.

– (1997). *Varmepumper - Grunnleggende varmepumpeteknikk*. SINTEF Energiforsk AS.

Stokar, M and C. Trepp (1987). "Compression heat pump with solution circuit Part 1: design and experimental results". In: *International Journal of Refrigeration* 10, pp. 87 –96.

Sveine, T. et al. (1998). "Design of high temperature absorption/compression heat pump". In: *Natural Working Fluids, IIR - Gustav Lorentzen conference*.

Thorin, E. (2001). "Thermophysical Properties of Ammonia/Water Mixtures for Prediction of Heat Transfer Areas in Power Cycles". English. In: *International Journal of Thermophysics* 22, pp. 201–214.

Vuddagiri, S. R. and P. T. Eubank (1998). "Condensation of mixed vapors and thermodynamics". In: *AIChE Journal* 44, pp. 2526–2541.

Watanabe, C. (2012). "Trends in Industrial Heat Pump Technology in Japan". In: *IEA Heat Pump Centre Newsletter* 30, pp. 36–38.

Yuan, Q. and J. Blaise (1988). "Water - A working fluid for CFC replacement". In: *International Journal of Refrigeration* 11, pp. 243–247.

Zhou, G. et al. (2012). "Review Status on High Temperature Heat Pumps". In: *Applied Mechanics and Materials* 170-173, pp. 2550–2553.

Zhou, Q. and R. Radermacher (1997). "Development of a vapor compression cycle with a solution circuit and desorber/absorber heat exchange". In: *International Journal of Refrigeration* 20, pp. 85 –95.

EES Procedure for the Two-Stage Compression/Absorption Heat Pump Model

Calculation procedure of each thermodynamic state point in the two-stage compression/absorption heat pump model is shown in table A.1. When using the EES function NH3H20, the call function needs a 3 digit code which determines the three thermodynamic properties used as inputs. There are 8 different properties available in the NH3H2O function:

1) T = [K]
2) P = [bar]
3) x = [ammonia mass fraction]
4) h = [kJ/kg]
5) s = [kJ/kg-K]
6) u = [kJ/kg]
7) v = [m^3/kg]
8) q = [vapour mass fraction]

TABLE A.1: EES calculation procedure of each thermodynamic state point for the two-stage compression/absorption heat pump model.

State	Code	Explanation
1	138	T_1 and x_1 is determined by the model inputs. Requiring saturated vapour, thus $q_1 = 1$. After the model has run this call, the desorber pressure is set to P_1.
2	234	After the desorber pressure is determined for state 1, the intermediate pressure is calculated: $P_{MP} = \sqrt{P_{LP} \cdot P_{HP}}$. P_2 is set to the intermediate pressure. The ammonia concentration in the vapour through the compressor circuit is constant and $x_2 = x_1$. First h_{2s} is found using P_2, x_2 and s_1, then $h_2 = h_1 + (h_{2s} - h_1)/\eta_{is}$. If the simulation is conducted with compressor cooling, T_2 is set to the maximum allowable temperature, while the compressor work is still calculated with the original T_2.
3	234	$x_3 = x_1$ and $P_3 = P_2$. h_3 is calculated using the function for solution heat exchanger #2.

4	234	$x_4 = x_1$ and P_4 is set to the absorber pressure from the inputs. First h_{4s} is found using P_4, x_4 and s_3, then $h_4 = h_3 + (h_{4s} - h_3)/\eta_{is}$. If the simulation is conducted with compressor cooling, T_4 is set to the maximum allowable temperature, while the compressor work is still calculated with the original T_4.
5	123	$x_5 = x_1$ and $P_4 = P_{HP}$. T_5 needs to be specified in the model. Heat delivery in the desuperheater is calculated as the enthalpy difference between state 4 and 5.
6	234	$P_6 = P_{HP}$ and $x_6 = ZZ$. Assuming adiabatic mixing between vapour and liquid solution, $h_6 = (h_5 \cdot \dot{m}_{vap} + h_{14} \cdot \dot{m}_{liq})/\dot{m}_{tot}$.
7	238	$P_7 = P_{HP}$ and $x_7 = ZZ$. Requiring saturated liquid solution at the absorber outlet, $q_7 = 0$.
8	234	$P_8 = P_{HP}$ and $x_7 = ZZ$. h_8 is calculated using the function for solution heat exchanger #2.
9	234	$x_9 = ZZ$. Assuming isenthalpic expansion before the desorber, $P_9 = P_{LP}$ and $h_9 = h_8$
10	123	$P_{10} = P_{LP}$ and $x_{10} = ZZ$. Mixture temperature at the desorber outlet is required to be the heat source inlet temperature minus the minimum temperature difference. $T_{10} = T_1 = T_{11} = T_{heat\ source\ in} - \Delta T_{min}$
11	128	$T_{11} = T_1$ and $P_{11} = P_1$. Requiring saturated liquid, thus $q_{11} = 0$. After the model runs this call, $x_{liq} = x_{11}$
12	235	$x_{12} = x_{11}$. Assuming isentropic pump work to the high-pressure side, $P_{12} = P_{HP}$ and $s_{12} = s_{11}$
13	234	$P_{13} = P_{HP}$ and $x_{13} = x_{11}$. h_{13} is calculated using the function for solution heat exchanger #1.
14	234	$P_{14} = P_{HP}$ and $x_{14} = x_{11}$. h_{14} is calculated using the function for solution heat exchanger #2.

Thermophysical Properties for the Ammonia/Water Mixture

Thermal conductivity and viscosity of the ammonia/water mixture is calculated using the thermodynamic properties of the mixture given by Ibrahim and Klein (1993) and correlations for predicting the thermophysical properties of the mixture given by Thorin (2001) and Conde-Petit (2004). The mixture critical temperature and pressure is found by using equation (B.1) and (B.2). The constants of the equation is given in table B.1.

$$T_{crit,mix} = \Sigma_{i=0}^{4}\ a_i x^i \tag{B.1}$$

$$P_{crit,mix} = \Sigma_{i=0}^{4}\ b_i x^i \tag{B.2}$$

TABLE B.1: Constant for equations calculating critical temperature and pressure for ammonia/water mixture (Conde-Petit, 2004).

i	a_i	b_i
0	647.14	220.64
1	-199.822 371	-37.923 795
2	109.035 522	36.424 739
3	-239.626 271	-41.851 597
4	88.689 691	-63.805 617

Thermal conductivity Saturation pressure of each component is found for the temperature of each component obtained from equation (B.3), (B.4) and (B.5). The thermal conductivity of the liquid mixture is found using equation (B.6), where the thermal conductivity of each component is found for the given temperature and pressure.

$$\theta_{mix} = \frac{T}{T_{crit,mix}} \tag{B.3}$$

$$T_{x,\mathrm{NH_3}} = \theta \cdot 405.4 \tag{B.4}$$

$$T_{x,\mathrm{H_2O}} = \theta \cdot 674.14 \tag{B.5}$$

$$\lambda_{sol} = x \cdot \lambda_{\mathrm{NH_3}} + (1 - x) \cdot \lambda_{\mathrm{H_2O}} \tag{B.6}$$

Viscosity Viscosity for each component is found using the same temperature and pressure as for thermal conductivity. The viscosity of the liquid mixture is found using equation (B.7), (B.8) and (B.9).

$$\mu_{mix} = exp[x \cdot ln(\mu_{\mathrm{NH_3}}) + (1 - x) \cdot ln(\mu_{\mathrm{H_2O}}) + \Delta\mu_{T,x}] \tag{B.7}$$

$$\Delta\mu_{T,x} = \left[0.534 - 0.815 \cdot \frac{T}{674.14}\right] \cdot F \tag{B.8}$$

$$F = 6.38(1 - x)^{1.125x}(1 - e^{-0.585x(1-x)^{0.18}})ln\left(\mu_{\mathrm{NH_3}}^{0.5} \cdot \mu_{\mathrm{H_2O}}^{0.5}\right) \tag{B.9}$$

Simulation Results

- Mixture temperature out of the desorber is 45 °C in all simulations
- In simulation # 1 - 6, $x_{vap} = 0.93$
- In simulation # 7 - 12, $x_{vap} = 0.95$
- In simulation # 13 - 18, $x_{vap} = 0.97$
- In simulation # 19 - 24, $x_{vap} = 0.99$
- Odd number simulations are without desuperheater
- Even number simulations are with desuperheater

TABLE C.1: Summary of simulation results for the two-stage model

Simulation #	1	2	3	4	5	6	7	8	9	10	11	12
P_{HP} [bar]	33.0	33.0	29.0	29.0	25.0	25.0	38.5	38.5	33.5	33.5	29.5	29.5
PR [-]	5.651	5.651	5.297	5.297	4.918	4.918	5.367	5.367	5.007	5.007	4.698	4.698
x_{liq} [-]	0.222	0.222	0.222	0.222	0.222	0.222	0.256	0.256	0.256	0.256	0.256	0.256
ZZ [-]	0.565	0.565	0.530	0.530	0.490	0.490	0.615	0.615	0.570	0.570	0.535	0.535
CR [-]	1.064	1.064	1.299	1.299	1.642	1.642	0.934	0.934	1.212	1.212	1.490	1.490
$\dot{m}_{tot}$ [kg/s]	0.129	0.129	0.127	0.127	0.129	0.129	0.128	0.128	0.128	0.128	0.128	0.128
$Q_{absorber}$ [kW]	100.0	96.28	100.0	90.84	100.0	81.14	100.0	96.05	100.0	90.16	100.0	80.89
Q_{dsh} [kW]	0	3.62	0	9.16	0	18.86	0	3.95	0	9.84	0	19.11
$Q_{desorber}$ [kW]	74.85	74.85	67.22	67.22	60.50	60.5	73.89	73.89	66.43	66.43	59.98	59.98
$Q_{ihx\ \#\ 1}$ [kW]	14.28	14.28	15.15	15.15	16.87	16.87	13.46	13.46	15.18	15.18	16.25	16.25
$Q_{ihx\ \#\ 2}$ [kW]	17.02	17.02	13.02	13.02	10.71	10.71	16.98	16.98	12.92	12.92	10.77	10.77
COP [-]	1.81	1.81	2.13	2.13	2.53	2.53	1.79	1.79	2.11	2.11	2.50	2.50
$W_{LP\ compressor}$ [kW]	25.29	25.29	21.30	21.30	17.89	17.89	25.65	25.65	21.44	21.44	18.15	18.15
$W_{HP\ compressor}$ [kW]	29.68	29.68	25.55	25.55	21.40	21.40	30.07	30.07	25.62	25.62	21.63	21.63
W_{pump} [kW]	0.235	0.235	0.221	0.221	0.212	0.212	0.256	0.256	0.252	0.252	0.241	0.241
ΔW_{thr} [kW]	9.59	9.59	7.63	7.63	6.00	6.00	10.32	10.32	8.10	8.10	6.48	6.48
q_6 [-]	0.443	0.429	0.429	0.394	0.402	0.331	0.482	0.466	0.449	0.410	0.428	0.354
v_1 [m^3/kg]	1.481	1.481	1.481	1.481	1.481	1.481	1.143	1.143	1.143	1.143	1.143	1.143
v_3 [m^3/kg]	0.312	0.312	0.340	0.340	0.365	0.365	0.254	0.253	0.277	0.277	0.294	0.294
T_4 [°C]	313.4	313.4	314.5	314.5	302.6	302.6	306.7	306.7	305.5	305.5	295.0	295.0
T_6 [°C]	157.2	155.4	157.1	152.7	155.3	146.8	158	156	157.5	152.7	156.6	147.4
T_7 [°C]	107.5	107.5	106.6	106.6	106.2	106.2	108.1	108.1	107.5	107.5	106.6	106.6
T_9 [°C]	7.4	7.4	11.3	11.3	15.8	15.8	6.1	6.1	11.2	11.2	15	15
T_{14} [°C]	129.6	129.6	135.2	135.2	124.3	124.3	134.5	134.5	135.9	135.9	125.8	125.8
$\dot{m}_{heat\ sink\ \#\ 1}$ [kg/s]	0.472	0.472	0.465	0.462	0.477	0.470	0.470	0.471	0.469	0.469	0.469	0.467
$T_{heat\ sink\ \#\ 1,\ in}$ [°C]	100.6	100.6	100.3	100.2	100.5	100.3	100.2	100.2	100.4	100.4	100.2	100.1
$T_{heat\ sink\ \#\ 1,\ out}$ [°C]	150.2	148.5	150.8	146.3	149.6	140.9	150.1	148.1	150.5	145.7	150.2	140.9
$\dot{m}_{heat\ sink\ \#\ 2}$ [kg/s]	0.440	0.442	0.445	0.432	0.467	0.450	0.420	0.421	0.439	0.429	0.499	0.437
$T_{heat\ sink\ \#\ 2,\ in}$ [°C]	99.1	99.2	99.3	98.4	101.1	99.4	97.1	97.4	99.0	98.2	99.4	98.8
$T_{heat\ sink\ \#\ 2,\ out}$ [°C]	152.2	150.4	152.1	147.7	150.3	141.8	153	151	152.5	147.7	151.6	142.4
$\dot{m}_{heat\ source}$ [kg/s]	0.476	0.476	0.477	0.477	0.496	0.496	0.454	0.454	0.470	0.470	0.479	0.479
$T_{heat\ source,\ out}$ [°C]	12.4	12.4	16.2	16.2	20.8	20.8	11.1	11.1	16.2	16.2	20.4	20.4

TABLE C.2: Summary of simulation results for the two-stage model

Simulation #	13	14	15	16	17	18	19	20	21	22	23	24
P_{HP} [bar]	45.0	45.0	41.0	41.0	36.5	36.5	70.0	70.0	58.0	58.0	53.5	53.5
PR [-]	4.951	4.951	4.600	4.600	4.340	4.340	4.182	4.182	3.807	3.807	3.656	3.656
x_{liq} [-]	0.309	0.309	0.309	0.309	0.309	0.309	0.426	0.426	0.426	0.426	0.426	0.456
ZZ [-]	0.690	0.690	0.635	0.635	0.595	0.595	0.850	0.850	0.770	0.770	0.735	0.735
CR [-]	0.735	0.735	1.027	1.027	1.311	1.311	0.330	0.330	0.639	0.639	0.824	0.824
$\dot{m}_{tot}$ [kg/s]	0.124	0.124	0.127	0.127	0.129	0.129	0.120	0.120	0.120	0.120	0.122	0.122
$Q_{absorber}$ [kW]	100	95.44	100	88.98	100	80.56	100	93.03	100	85.75	100	79.78
Q_{dsh} [kW]	0	4.56	0	11.02	0	19.44	0	6.97	0	14.25	0	20.22
$Q_{desorber}$ [kW]	72.53	72.53	69.97	69.97	59.49	59.49	74.21	74.21	63.48	63.48	59.04	59.04
$Q_{ihx\ \#\ 1}$ [kW]	11.96	11.96	14.33	14.33	16.12	16.12	7.67	7.67	11.42	11.42	13.24	13.24
$Q_{ihx\ \#\ 2}$ [kW]	16.77	16.77	12.76	12.76	10.68	10.68	11.38	11.38	11.80	11.80	10.16	10.16
COP [-]	1.75	1.75	2.11	2.11	2.47	2.47	1.56	1.56	2.16	2.16	2.44	2.44
$W_{LP\ compressor}$ [kW]	26.16	26.16	21.58	21.58	18.43	18.43	28.46	28.46	21.27	21.27	18.75	18.75
$W_{HP\ compressor}$ [kW]	30.59	30.59	25.60	25.60	21.83	21.83	35.47	35.47	24.83	24.83	21.85	21.85
W_{pump} [kW]	0.27	0.27	0.29	0.29	0.29	0.29	0.23	0.23	0.30	0.30	0.32	0.32
ΔW_{thr} [kW]	11.35	11.35	8.72	8.72	7.04	7.04	13.84	13.84	9.42	9.42	7.96	7.96
q_6 [-]	0.557	0.537	0.501	0.455	0.463	0.386	0.774	0.741	0.662	0.595	0.614	0.520
v_1 [m^3/kg]	0.786	0.786	0.786	0.786	0.786	0.786	0.375	0.375	0.375	0.375	0.375	0.375
v_3 [m^3/kg]	0.189	0.189	0.206	0.206	0.217	0.217	0.114	0.114	0.117	0.117	0.121	0.121
T_4 [°C]	297.3	297.3	292.4	292.4	283.2	283.2	307.7	307.7	265.6	265.6	258.8	258.8
T_6 [°C]	159.6	157.0	158.7	152.8	157.8	147.7	161.8	157.0	161.9	152.8	161.2	148.7
T_7 [°C]	109.9	109.9	108.8	108.8	108.2	108.2	116.6	116.6	112.8	112.8	111.7	111.7
T_9 [°C]	4.8	4.8	10.8	10.8	15.1	15.1	6.3	6.3	12.8	12.8	16.0	16.0
T_{14} [°C]	145.1	145.1	139.2	139.2	127.7	127.7	165.8	165.8	150.9	150.9	137.2	137.2
$\dot{m}_{heat\ sink\ \#\ 1}$ [kg/s]	0.472	0.475	0.469	0.474	0.473	0.479	0.518	0.540	0.477	0.503	0.473	0.505
$T_{heat\ sink\ \#\ 1,\ in}$ [°C]	100.2	100.3	100.4	100.6	100.6	100.9	102.6	103.4	100.8	101.9	100.7	102.0
$T_{heat\ sink\ \#\ 1,\ out}$ [°C]	150.0	147.5	150.4	144.7	150.3	140.4	147.9	143.9	150.1	142.0	150.4	139.1
$\dot{m}_{heat\ sink\ \#\ 2}$ [kg/s]	0.392	0.385	0.409	0.404	0.433	0.419	0.338	0.330	0.357	0.353	0.373	0.365
$T_{heat\ sink\ \#\ 2,\ in}$ [°C]	94.6	93.8	96.4	96.1	98.6	97.5	87.3	85.6	91.1	90.6	93.2	92.3
$T_{heat\ sink\ \#\ 2,\ out}$ [°C]	154.6	152	153.7	147.8	152.8	142.7	156.6	152	156.9	147.8	156.2	143.7
$\dot{m}_{heat\ source}$ [kg/s]	0.432	0.432	0.456	0.456	0.476	0.476	0.459	0.459	0.471	0.471	0.487	0.487
$T_{heat\ source,\ out}$ [°C]	9.8	9.8	15.8	15.8	20.1	20.1	11.3	11.3	17.8	17.8	21.0	21.0

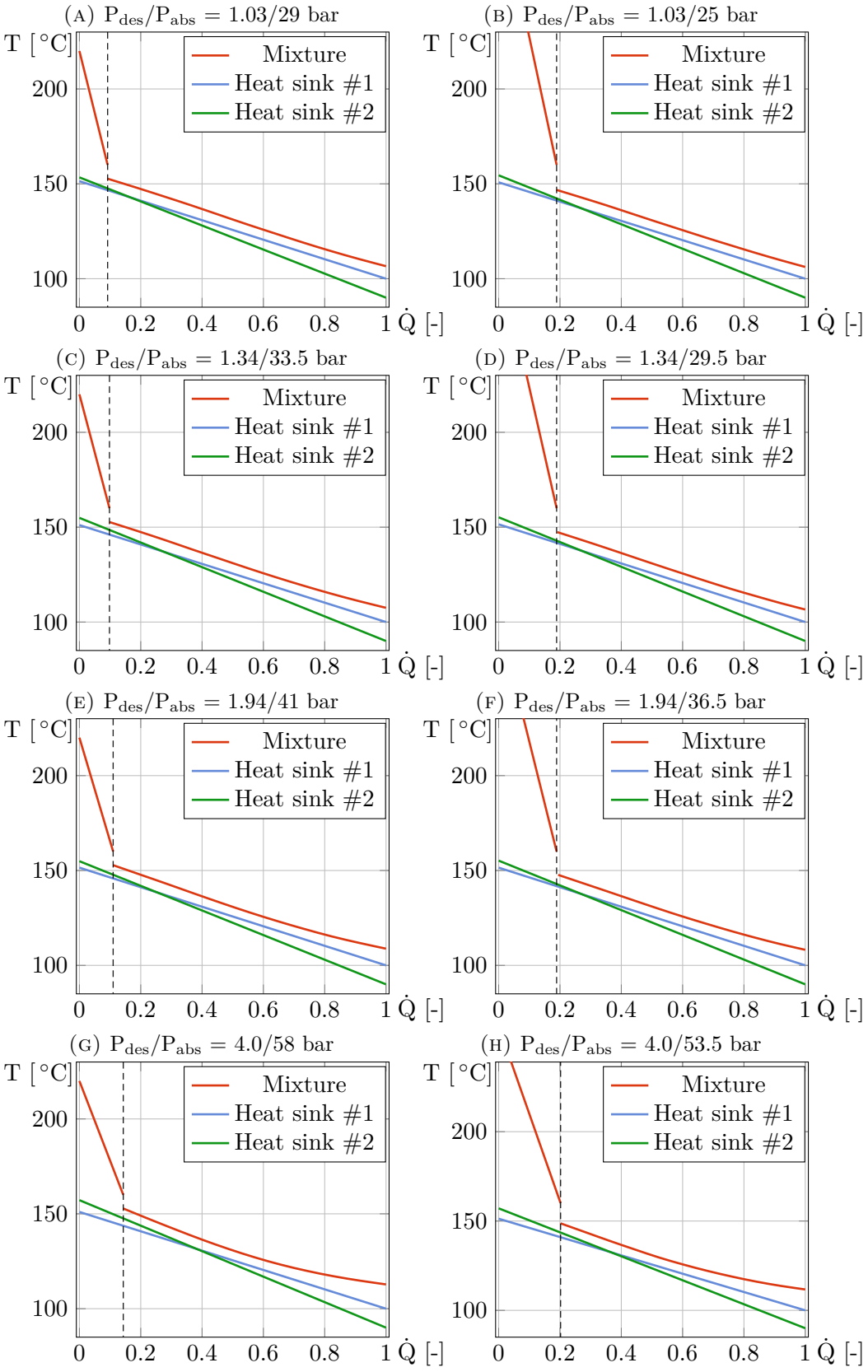

FIGURE C.1: Temperature versus cumulative heat load for a two-stage compression/absorption cycle with $P_{desorber}$ = 1.03 bar and $P_{absorber}$ = 33 bar.

EES Source Code for Simulation Models

Two-stage compression/absorption heat pump model

```
$UnitSystem SI C bar kJ mass rad
$TabStops 0,1 0,4 0,6 0,8 cm

"FUNCTIONS"

function tk(T)  "converting temperaure from K to C"
        tk:= T - 273,15
end

function tc(T)  "converting temperaure from C to K"
        tc:= T + 273,15
end

procedure ihx1(T;K;P;O;Z;X;M;N;E:C1;C2)
        qihx:= 0
        if(T<K) then goto 10
        i:= 1
        CALL NH3H2O(123;T+273,15;P;Z:T[i];P[i];x[i];h[i];s[i];u[i];v[i];q[i])
        i:= i + 1
        CALL NH3H2O(123;K+273,15;P;Z:T[i];P[i];x[i];h[i];s[i];u[i];v[i];q[i])
        qh:= (h[1] - h[2]) * M
```

```
    i:= i + 1
    CALL NH3H2O(123;T+273,15;0;X:T[i];P[i];x[i];h[i];s[i];u[i];v[i];q[i])
    i:= i + 1
    CALL NH3H2O(123;K+273,15;0;X:T[i];P[i];x[i];h[i];s[i];u[i];v[i];q[i])
    qc:= (h[3] - h[4]) * N
    qmax:= min(qh;qc)
    qihx = qmax * E
10: C1:= h[1] - (qihx / M)
    C2:= h[4] + (qihx / N)
end

"calculating the heat duty for internal heat exchanger #1"

procedure ihx2(T;K;P;0;Z;X;M;N;E:C1;C2)
    E:= E + 0,01
10: E:= E - 0,01
    i:= 1
    CALL NH3H2O(123;tc(T);P;Z:T[i];P[i];x[i];h[i];s[i];u[i];v[i];q[i])
    i:= i + 1
    CALL NH3H2O(123;tc(K);P;Z:T[i];P[i];x[i];h[i];s[i];u[i];v[i];q[i])
    qh:= (h[1] - h[2]) * M
    i:= i + 1
    CALL NH3H2O(123;tc(T);0;X:T[i];P[i];x[i];h[i];s[i];u[i];v[i];q[i])
    i:= i + 1
    CALL NH3H2O(123;tc(K);0;X:T[i];P[i];x[i];h[i];s[i];u[i];v[i];q[i])
    qc:= (h[3] - h[4]) * N
    qmax:= min(qh;qc)
    qihx = qmax * E
    i:= i + 1
    h_a = h[1] - (qihx / M)
    CALL NH3H2O(234;P;Z;h_a:T[i];P[i];x[i];h[i];s[i];u[i];v[i];q[i])
    if(q[i]<1) then goto 10
    i:= i + 1
    h_b = h[4] + (qihx / N)
    CALL NH3H2O(234;0;X;h_b:T[i];P[i];x[i];h[i];s[i];u[i];v[i];q[i])
    if(q[i] > 0) then goto 10
    C1:= h[1] - (qihx / M)
    C2:= h[4] + (qihx / N)
end
```

```
"calculating the heat duty for internal heat exchanger #2"

procedure absorber1(Z[200..250];A[200..250];O;M;N;DELTAT:C1;C2;C3)
        B:= DELTAT
        B:= B - 0,1
    10: i:= 200
        B:= B + 0,1
        W[i]:= Z[i] - B
        r:= enthalpy('Water';P=O;T=W[i])
        e[i]:= r
        D[i] = B
        repeat
        i = i + 1
        q[i]:= (A[i-1] - A[i]) * M
        e[i]:= e[i-1] - (q[i] / N)
        N:= (((A[200] - A[i]) * M) / (r - e[i]))
        K:= temperature('Water';P=O;h=e[i])
        D[i]:= Z[i] - K
        if(D[i]<DELTAT) then goto 10
        W[i]:=K
        until(i=250)
        C1:= D[200]
        C2:= D[250]
        C3:= N
end

"calculates the temperature curve in the absorber"

procedure absorber2(Z[200...250];A[200...250];O;M;N;DELTAT:C1;C2;C3)
        B:= DELTAT
        N:= N + 0,001
    10: i = 200
        N:= N - 0,001
        W[i]:= Z[i] - DELTAT
        r:= enthalpy('Water';P=O;T=W[i])
        e[i]:=r
        D[i]:= DELTAT
        repeat
```

```
    i:= i + 1
    q[i]:= (A[i-1] - A[i]) * M
    e[i]:= e[i-1] - (q[i] / N)
    K:=temperature('Water';P=0;h=e[i])
    D[i]:=Z[i] - K
    if(D[i]<5) then goto 10
    W[i]:=K
    until(i=250)
    C1:=D[200]
    C2:=Z[250] - W[250]
    C3:=N
end

"calculates the temperature curve in the absorber"

function dsh(T;K;F;P;Z;M)
      i:= 1
      CALL NH3H2O(123;T;P;Z:T[i];P[i];x[i];h[i];s[i];u[i];v[i];q[i])
      i:= i + 1
      CALL NH3H2O(123;K;P;Z:T[i];P[i];x[i];h[i];s[i];u[i];v[i];q[i])
      i:= i + 1
      CALL NH3H2O(123;F;P;Z:T[i];P[i];x[i];h[i];s[i];u[i];v[i];q[i])
      q:= (h[1] - h[2]) * M
      qmax:= (h[1] - h[3]) * M
      epsilon:= q / qmax
      dsh:= epsilon
end

"function for desuperheater"

"INPUTS"

T_wd1 = 50 [C]              "heat source inlet temperature"
DELTAT_min = 5 [K]          "minimum temperature difference"
Q_absorber = 100 [kW] {- Q_desuperheater}      "absorber heat capacity"
P_HP = 25 [bar]             "absorber pressure"
ZZ = 0,52 [-]               "overall ammonia concentration"
x_vap = 0,93 [-]            "ammonia concentration in the vapour to the compressor"
eta_LP = 0,8 [-]            "isentropic efficiency LP compressor"
```

```
eta_HP = 0,8 [-]         "isentropic efficiency HP compressor"
epsilon_ihx1 = 0,8 [-]   "thermal efficiency IHX 1"
epsilon_ihx2 = 0,8 [-]   "thermal efficiency IHX 2"
F$ = 'Water'

"VARIABLES"

T_1 = T_wd1 - DELTAT_min         "desorber outlet temperature"
P_LP  = P[1]                     "desorber pressure"
P_MP = sqrt(P_LP * P_HP)         "intermediate pressure"
PR_LP = P_MP / P_LP              "LP pressure ratio"
PR_HP = P_HP / P_MP              "HP pressure ratio"
x_liq = x[11]                    "ammonia concentration in the weak solution"
CR = (x_vap - ZZ) / (ZZ - x_liq)         "circulation ratio"
m_dot = Q_absorber / DELTAh_absorber     "total mass flow"
m_dot_vap = m_dot / (1 + CR)             "vapour mass flow"
m_dot_liq = m_dot - m_dot_vap            "solution mass flow"
Q_desorber = DELTAh_desorber * m_dot     "desorber capacity"
{Q_desuperheater = DELTAh_desuperheater * m_dot_vap     "desuperheater capacity"}
Q_ihx1 = (h[7] - h[8]) * m_dot           "heat transfer in IHX 1"
Q_ihx2 = (h[2] - h[3]) * m_dot_vap       "heat transfer in IHX 2"

"CYCLE DATA (Array [1]-[14])"

"calculates all the thermodynamic state points"

CALL NH3H2O(138;T_1+273,15;x_vap;1:tc(T[1]);P[1];x[1];h[1];s[1];u[1];v[1];q[1])
CALL NH3H2O(235;P_MP;x_vap;s[1]:tc(T_2s);P_2s;x_2s;h_2s;s_2s;u_2s;v_2s;q_2s)
h_2 = h[1] + ((h_2s - h[1]) / eta_LP)
CALL NH3H2O(234;P_MP;x_vap;h_2:tc(T[2]);P[2];x[2];h[2];s[2];u[2];v[2];q[2])
T_2cooling =180 "if no compressor cooling, T_2cooling = T[2]"
CALL ihx2(T_2cooling;T[13];P_MP;P_HP;x_vap;x_liq;m_vr;m_lr;epsilon_ihx2:h_3;h_14)
CALL NH3H2O(234;P_MP;x_vap;h_3:tc(T[3]);P[3];x[3];h[3];s[3];u[3];v[3];q[3])
CALL NH3H2O(235;P_HP;x_vap;s[3]:tc(T_4s);P_4s;x_4s;h_4s;s_4s;u_4s;v_4s;q_4s)
h_4 = h[3] + ((h_4s - h[3])/eta_HP)
CALL NH3H2O(234;P_HP;x_vap;h_4:tc(T[4]);P[4];x[4];h[4];s[4];u[4];v[4];q[4])
T_5 = 160 "if no desuperheater, T_5 = T[4]"
CALL NH3H2O(123;tc(T_5);P_HP;x_vap:tc(T[5]);P[5];x[5];h[5];s[5];u[5];v[5];q[5])
h_6 = ((h[5] * m_vr) + (h[14] * m_lr)) / m_ar
```

```
CALL NH3H2O(234;P_HP;ZZ;h_6:tc(T[6]);P[6];x[6];h[6];s[6];u[6];v[6];q[6])
CALL NH3H2O(238;P_HP;ZZ;0:tc(T[7]);P[7];x[7];h[7];s[7];u[7];v[7];q[7])
CALL ihx1(T[7];T[12];P_HP;P_HP;ZZ;x_liq;m_ar;m_lr;epsilon_ihx1:h_8;h_13)
CALL NH3H2O(234;P_HP;ZZ;h_8:tc(T[8]);P[8];x[8];h[8];s[8];u[8];v[8];q[8])
CALL NH3H2O(234;P_LP;ZZ;h[8]:tc(T[9]);P[9];x[9];h[9];s[9];u[9];v[9];q[9])
CALL NH3H2O(123;T_1+273,15;P_LP;ZZ:tc(T[10]);P[10];x[10];h[10];s[10];u[10];v[10];q[10])
CALL NH3H2O(128;T_1+273,15;P_LP;0:tc(T[11]);P[11];x[11];h[11];s[11];u[11];v[11];q[11])
CALL NH3H2O(235;P_HP;x_liq;s[11]:tc(T[12]);P[12];x[12];h[12];s[12];u[12];v[12];q[12])
CALL NH3H2O(234;P_HP;x_liq;h_13:tc(T[13]);P[13];x[13];h[13];s[13];u[13];v[13];q[13])
CALL NH3H2O(234;P_HP;x_liq;h_14:tc(T[14]);P[14];x[14];h[14];s[14];u[14];v[14];q[14])

"DESORBER (Array [100]-[150])"

P_dwater = 1 [bar]                      "pressure of heat source"
DELTAh_desorber = h[10] - h[9]          "mixture enthalpy difference in desorber"
T_dwater1 = T_wd1                       "heat source inlet temperature"
T_dwater2 = T[9] + DELTAT_min           "heat source outlet temperature"
h_dwater1 = enthalpy(F$;T=T_dwater1;P=P_dwater)         "heat source inlet temperature"
h_dwater2 = enthalpy(F$;T=T_dwater2;P=P_dwater)         "heat source outlet temperature"
m_dot_dwater = Q_desorber / (h_dwater1 - h_dwater2)     "heat source mass flow"

"calculates the temperature of the mixture at 51 segments"

step_da = (h[10] - h[9]) / 50
A[100] = h[9]
duplicate i =101;150
        A[i] = A[i-1] + step_da
end
duplicate i =100;150
        CALL NH3H2O(234;P_LP;ZZ;A[i]:tc(T[i]);P[i];x[i];h[i];s[i];u[i];v[i];q[i])
end

"calculates the heat source temperature curve"

step_dw  = (T_dwater1 - T_dwater2) / 50
T_water[150] = T_dwater1
duplicate i = 100;149
        T_water[i] = T_water[i+1] - step_dw
end
```

```
"the temperature of mixture temperature and heat source"
"temperature is plotted with the corresponding Q_dot"

duplicate i = 100;150
      Q_dot[i] = (h[i] - h[100]) / (h[150] - h[100])
end

"ABSORBER (Array [200]-[250])"

P_awater = 7 [bar]                    "pressure of heat sink"
DELTAh_absorber = h[6] - h[7]    "enthalpy difference for the mixture in the absorber"

"calculates the temperature of the mixture at 51 segments"

step_aa = (h[6] - h[7]) / 50
A[200] = h[6]
duplicate i = 201;250
      A[i] = A[i-1] - step_aa
end
duplicate i =200;250
      CALL NH3H2O(234;P_HP;ZZ;A[i]:tc(T[i]);P[i];x[i];h[i];s[i];u[i];v[i];q[i])
end

h_waterapprox1 = enthalpy(F$;T=T[250] - DELTAT_min;P=P_awater)
h_waterapprox2 = enthalpy(F$;T=T[200] - DELTAT_min;P=P_awater)
m_waterapprox = Q_absorber / (h_waterapprox2 - h_waterapprox1)

"an approximation of the water (heat sink) mass flow with the"
"assumption that the temperature difference between mixture"
"and water at absorber inlet and outlet is DELTAT_min"

CALL absorber1(T[200..250];h[200..250];P_awater;
m_dot;m_waterapprox;DELTAT_min:DELTAT1;DELTAT2;m_dot_water)
CALL absorber2(T[200..250];h[200..250];P_awater;
m_dot;m_waterapprox;DELTAT_min:DELTAT3;DELTAT4;m_dot_water2)

"output of absorber1 is temperature difference at outlet and inlet"
"and water mass flow, assuming the same temperature difference."
```

```
"absorber2 has the same outputs as absorber1, the temperature difference"
"at the absorber inlet is fixed and the water mass flow is adjusted"

duplicate i = 200;250
        Q_dot[i] = (h[i] - h[200]) / (h[250] - h[200])
end

"the temperature of mixture temperature and heat source"
"temperature is plotted with the corresponding Q_dot"

"sets the water temperature at the absorber inlet and outlet,"
"and calculates the temperature curves for heat sink"

T_water[200] = T[200] - DELTAT1
T_water[250] = T[250] - DELTAT2
T_water_2[200] = T[200] - DELTAT3
T_water_2[250] = T[250] - DELTAT4
step_aw1 = (T_water[200] - T_water[250]) / 50
step_aw2 = (T_water_2[200] - T_water_2[250]) / 50
duplicate i = 201;249
        T_water[i] = T_water[i-1] - step_aw1
        T_water_2[i] = T_water_2[i-1] - step_aw2
end
duplicate i = 200;250
        DELTAT_absorber[i] = T[i] - T_water[i]
        DELTAT_absorber_2[i] = T[i] - T_water_2[i]
end

T_water2o = T[6] - DELTAT3
T_water2i = T[7] - DELTAT4
h_water2o = enthalpy(F$;T=T_water2o;P=P_awater)
h_water2i = enthalpy(F$;T=T_water2i;P=P_awater)

T_water2[6] = T_water2[200]
T_water2[7] = T_water2[250]

{DESUPERHEATER}

DELTAh_desuperheater = h[16] - h[5]
```

```
T_hid =  180
CALL NH3H2O(123;T_hid+273,15;P_HP;x_vap:T[16];P[16];x[16];h[16];s[16];u[16];v[16];q[16])
T_hod = T[5]
T_cid = T_water[6] + 273,15
epsilon_dsh = dsh(T[16];T[5];T_cid;P_HP;x_vap;m_dot_vap)
h_cid = enthalpy(F$;T=T_cid;P=P_awater)
h_cod = h_cid + (Q_desuperheater / m_dot_water)
T_cod = temperature(F$;P=P_awater;h=h_cod)

T_celsius[30] = T_hid           {Hot stream inlet temperature}
T_celsius[31] = T_hod - 273,15  {Hot stream outlet temperature}
T_celsius[32] = T_water[6]      {Cold stream inlet temperature}
T_celsius[33] = T_cod - 273,15  {Cold stream outlet temperature}

x[30] = 0
x[31] = 1
x[32] = 1
x[33] = 0

T_water[5] = T_celsius[33]

h_water2d = (Q_desuperheater / m_dot_water2) + h_water2o
T_water2[5] = temperature(F$;P=P_awater;h=h_water2d) - 273,15

T_celsius[34] = T_hid   {Hot stream inlet temperature}
T_celsius[35] = T_hod - 273,15  {Hot stream outlet temperature}
T_celsius[36] = T_water2[6]     {Cold stream inlet temperature}
T_celsius[37] = T_water2[5]     {Cold stream outlet temperature}

x[34] = 0
x[35] = 1
x[36] = 1
x[37] = 0

{IHX 1}

T_celsius[20] = T_celsius[7]    {Hot stream inlet temperature}
T_celsius[21] = T_celsius[8]    {Hot stream outlet temperature}
T_celsius[22] = T_celsius[12]   {Cold stream inlet temperature}
```

```
T_celsius[23] = T_celsius[13]   {Cold stream outlet temperature}

x[20] = 0
x[21] = 1
x[22] = 1
x[23] = 0

{IHX 1}

T_celsius[25] = T_celsius[2]    {Hot stream inlet temperature}
T_celsius[26] = T_celsius[3]    {Hot stream outlet temperature}
T_celsius[27] = T_celsius[13]   {Cold stream inlet temperature}
T_celsius[28] = T_celsius[14]   {Cold stream outlet temperature}

x[25] = 0
x[26] = 1
x[27] = 1
x[28] = 0

{ENERGY}

W_comp_1 = (h[2] - h[1]) * m_dot_vap
W_comp_2 = (h[4] - h[3]) * m_dot_vap
W_pump = (h[12] - h[11]) * m_dot_liq
COP = (Q_absorber {+ Q_desuperheater} ) / (W_comp_1 + W_comp_2 + W_pump)

{MISCELLANEOUS}

m_ar = 1
m_vr = m_ar / (1 + CR)
m_lr = m_ar - m_vr

duplicate i = 1;5
        m_dot[i] = m_dot_vap
end
duplicate i = 6;10
        m_dot[i] = m_dot
end
duplicate i = 11;14
```

```
        m_dot[i] = m_dot_liq
end

DELTAW_throttling = m_dot * T[8] * (s[9] - s[8]
```

Absorber model

```
$UnitSystem SI MASS RAD PA K J
$TabStops 0,1 0,4 0,6 0,8 cm

"FUNCTIONS"

"procedure with mixture thermophysical properties as outputs"

procedure thermophysical_properties(x;T:T_c_sol;P_c_sol;lambda_sol;mu_sol)
        a_0:=647,14
        a_1:=-199,822371
        a_2:=109,035522
        a_3:=-239,626217
        a_4:=88,689691
        b_0:=220,64
        b_1:=-37,923795
        b_2:=36,424739
        b_3:=-41,851597
        b_4:=-65,805617
        T_c_sol:= (a_0) + (a_1*x) + (a_2*x^2) + (a_3*x^3) +(a_4*x^4)
        P_c_sol:= (b_0) + (b_1*x) + (b_2*x^2) + (b_3*x^3) +(b_4*x^4)
        Theta:= T/ T_c_sol
        T_x_NH3:= Theta * 405,4
        T_x_H2O:= Theta * 674,14
        c_0:= 8,902275 * 10^(2)
        c_1:= -0,69235
        c_2:= -2,4010 * 10^(-3)
        c_3:= 0
        P_sat_NH3:= p_sat('Ammonia';T=T_x_NH3)
        P_sat_H2O:= p_sat('Water';T=T_x_H2O)
        lambda_NH3:= conductivity('Ammonia';T=T_x_NH3-1;P=P_sat_NH3)
```

```
    lambda_H2O:= conductivity('Water';T=T_x_H2O-1;P=P_sat_H2O)
    lambda_sol:=(x * lambda_NH3) + ((1-x) * lambda_H2O)
    mu_NH3:= viscosity('Ammonia';T=T_x_NH3-1;P=P_sat_NH3)
    mu_H2O:= viscosity('Water';T=T_x_H2O-1;P=P_sat_H2O)
    F:= 6,38 * (1-x)^(1,125*x) * (1- exp(-0,585*x*(1-x)^(0,18))) * ln((mu_NH3)^0,5 * (mu_H2O)^0,5)
    DELTAmu_T_x:= (0,534-0,815 *(T / 674,14))*F
    mu_sol:= exp((x* ln(mu_NH3)) + ((1-x) * ln(mu_H2O)) + DELTAmu_T_x)
end

"procedure mixture heat transfer coefficient as output"

procedure tube_flow(m_dot;mu;T_1;T_2;P;D_in;lambda;P_c;L;x:A;B;C;D)
    CALL NH3H2O(128;T_1;P;0:T[1];P[1];x[1];h[1];s[1];u[1];v[1];q[1])
    CALL NH3H2O(128;T_2;P;0:T[2];P[2];x[2];h[2];s[2];u[2];v[2];q[2])
    CALL NH3H2O(128;T_1;P;1:T[3];P[3];x[3];h[3];s[3];u[3];v[3];q[3])
    CALL NH3H2O(128;T_2;P;1:T[4];P[4];x[4];h[4];s[4];u[4];v[4];q[4])
    CALL NH3H2O(123;T_1;P;x:T[5];P[5];x[5];h[5];s[5];u[5];v[5];q[5])
    CALL NH3H2O(123;T_2;P;x:T[6];P[6];x[6];h[6];s[6];u[6];v[6];q[6])
    v_l_avg:=(v[1]+v[2])/2
    rho_l_avg:=1/v_l_avg
    v_g_avg:=(v[3]+v[4])/2
    rho_g_avg:=1/v_g_avg
    q_avg:=(q[5]+q[6])/2
    rho_avg:=(rho_l_avg*(1-q_avg))+(rho_g_avg*q_avg)
    u_m:=(4*m_dot)/(rho_avg*D_in^2)
    Re_D:= (rho_l_avg*u_m*D_in)/(mu)
    cp:= ((h[1]-h[2])*1000)/(T_1-T_2)
    Pr:=(cp*mu)/lambda
    alpha:=0,023 * (Re_D)^0,8 * Pr^0,4 * (lambda/D_in)
    R_in:= 1 / (alpha * pi * D_in * L)
    A:=alpha
    B:=R_in
    C:=Re_d
    D:=u_m
end

"procedure with tube wall conductivity and conduction resistance as outputs"

procedure conduction_resistance(T_avg;D_o;D_i;L:A;B)
```

```
        A:=k_('Stainless_AISI304';T_avg)
        B:=ln(D_o / D_i) / (2 * pi * A * L)
end

"procedure with air side resistance as output"

procedure air_flow(T_C_in;T_C_out;T_avg;P;u_m ;N_t_col;D_out;s_v;s_h;A_s_fin_tot;p_fin;th_fin;L_tube;k_m;A_tot:A;B;C;D;E)
        call external_flow_staggered_bank('Air';T_C_in;T_C_out;T_avg;P;u_m;N_t_col;D_out;s_v;s_h:h_out;DELTAP;Nusselt;Re_out)
        r_fin_eff = sqrt((D_out / 2)^2 + ((A_s_fin_tot * p_fin) / (2 * pi * L_tube)))
        eta_fin:= eta_fin_annular_rect(th_fin;D_out/2;r_fin_eff;h_out;k_m)
        eta_o:= 1 - A_s_fin_tot * (1 - eta_fin) / A_tot
        air_side_resistance:= 1 / (eta_o * h_out * A_tot)
        A:=h_out
        B:=air_side_resistance
        C:=Re_out
        D:=eta_o
        E:=DELTAP
end

"procedure with capacitance rate of C,H,min;max and NTU as outputs"

procedure capacitance_rate(T_C_in;T_C_out;V_dot_C;m_dot_H;P;UA;c_H:A;B;C;D;E)
        rho_C:= density('Air';T=(T_C_in+T_C_out)/2;P=P)
        m_dot_C:= rho_C * V_dot_C
        A:= Cp('Air';T=(T_C_in+T_C_out)/2)
        B:= m_dot_C * A
        C:= m_dot_H * c_H
        D:= min(B;C)
        E:= max(B;C)
end

"INPUTS"

D_in = 22 [mm]*convert(mm;m)            "tube inner diameter"
D_out = 25 [mm]*convert(mm;m)           "outer diameter of tube"
th = (D_out - D_in) / 2                 "tube wall thickness"

N_t_row = 12 [-]                        "number of tube rows"
N_t_col = 2 [-]                         "number of tube columns"
```

```
N_tubes = N_t_row * N_t_col              "number of tubes"
L_tube = N_t_row * N_t_col * W * S       "total tube length"
H = (N_t_row + 1) * s_v                  "height of heat exchanger face"
L =  (N_t_col + 1) * s_h                 "length of heat exchanger in air flow direction"
W =  1,2 [m]                             "width of heat exchanger face"
s_v = 40 [mm]*convert(mm;m)              "vertical separation distance between tubes"
s_h = 40 [mm]*convert(mm;m)              "horizontal separation distance between tubes"
th_fin = 0,5 [mm]*convert(mm;m)          "fin thickness"
p_fin = 7,5 [mm]*convert(mm;m)           "fin pitch"
e = 1,0 [micron]*convert(micron;m)       "roughness of tube internal surface"

A_s_fin_tot = 2 * (W / p_fin) * (H * L - N_t_row * N_t_col * pi * D_out^2 / 4)  "total fin area"
A_s_unfin = pi * D_out * L_tube_S * (1- th_fin / p_fin)                         "total un-finned area"
A_tot = A_s_fin_tot + A_s_unfin                                                 "total air-side surface area"
A_c = (H - N_t_row * D_out) * W * (1 - th_fin / p_fin)                          "cross-sectional area available for flow"
u_m = V_dot_C / A_C                                                             "frontal velocity for external flow calculation"
A_c_2 = H * W
u_m_2 = V_dot_C / A_C_2
eta_fan = 0,5

P = 1 [atm]*convert(atm;Pa)              "atmospheric pressure"
T_C_in = convertTemp(C;K;90 [C])         "inlet air temperature"
T_H_in = convertTemp(C;K;150 [C])        "inlet water temperature"
V_dot_C = 3 *A_c_2                       "volumetric flow rate of air"
{V_dot_C = V_dot_air_approximately}
S = 10 [-]                               "number of heat schanger segments"
L_tube_S = L_tube / S                    "total tube length per segment"

T_C_out = convertTemp(C;K;125 [C])       "guess for the cold stream exit temperature"
T_H_out = convertTemp(C;K;100 [C])       "guess for the hot stream exit temperature"

step_C = (T_C_out - T_C_in) / S          "initial temperature step per segment for air"
step_H = (T_H_in - T_H_out) / S          "initial temperature step per segment for mixture"

Q_dot_absorber = 100 [kW]                                                       "absorber duty"
P_H = 25 [bar]                                                                  "mixture pressure"
Call NH3H2O(128;T_H_out;P_H;0:T_x_out;P_out;x_out;h_out;s_out;u_out;v_out;q_out) "mixture outlet properties for guess value"
Call NH3H2O(123;T_H_in;P_H;x_out:T_x_in;P_in;x_in;h_in;s_in;u_in;v_in;q_in)      "mixture inlet properties"
m_dot_H_tot = Q_dot_absorber / (h_in - h_out)                                    "mass flow rate of mixture"
```

```
m_dot_H = m_dot_H_tot / (N_t_col * N_t_row)                                    "mass flow rate of mixture per tube"

h_air_in = enthalpy('Air';T=T_C_in)
h_air_out = enthalpy('Air';T=T_C_out)
m_dot_air_approximately = (Q_dot_absorber * 1000) / (h_air_out - h_air_in)
rho_air_in = density('Air';T=T_C_in;P=P)
rho_air_out = density('Air';T=T_C_out;P=P)
rho_bar_air = (rho_air_in + rho_air_out) / 2
V_dot_air_approximately = m_dot_air_approximately / rho_bar_air

A_tube_in = pi * D_in * L_tube_S
A_tube_out = pi * D_out * L_tube_S
A_tube_m = pi * L_tube_S * ((D_out - D_in) / ln(D_out/D_in))

"- - - - - - - - - - - - - - - - - - - - - - - - - - - - - -"

T_C[1] = T_C_out
T_H[1] = T_H_in
DELTAT[1] = T_H[1] - T_C[1]
T_C_y[S+1] = T_C_in
T_H_y[1] = T_H_in
h_H_y[1] = h_in
DELTAT_C[1] = T_C[1] - T_C_in
DELTAT_H[1] = T_H_in - T_H[S+1]
CALL NH3H2O(123;T_H_in;P_H;x_out:T_x[1];P[1];x[1];h[1];s[1];u[1];v[1];q[1])
L_x[1] = 1

duplicate i=2;(S+1)
        T_C[i] = T_C[i-1] - step_C
        T_H[i] = T_H[i-1] - step_H
        T_avg[i] = (T_H[i-1] + T_C[i]) / 2
        T_bar_H[i] = (T_H[i-1] + T_H[i]) / 2
        T_bar_C[i] = (T_C[i-1] + T_C[i]) / 2
        CALL NH3H2O(128;T_bar_H[i];P_H;0:T_l[i];P_l[i];x_l[i];h_l[i];s_l[i];u_l[i];v_l[i];q_l[i])
        call thermophysical_properties(x_l[i];T_bar_H[i]:T_c_sol[i];P_c_sol[i];lambda_sol[i];mu_sol[i])
        call tube_flow(m_dot_H;mu_sol[i];T_H[i-1];T_H[i];P_H;D_in;lambda_sol[i];P_c_sol[i];L_tube_S;x_out:alpha_in[i];
                R_in[i];Re_D[i];u_m[i])
        call conduction_resistance(T_avg[i];D_out;D_in;L_tube_S:k_m[i];R_cond[i])
        call air_flow(T_C[i];T_C[i-1];T_avg[i];P;u_m;N_t_col;D_out;s_v;s_h;A_s_fin_tot;p_fin;th_fin;L_tube_S;k_m[i];A_tot:
```

```
            alpha_out[i];R_out[i];Re_out[i];eta_o[i];DELTAP[i])
        call CHX_h_finned_tube('fc_tubes_s80-38T';V_dot_c*rho_bar_air;W*H;'Air';T_bar_C[i];P:h_bar_out_CHX[i])
        R_tot[i] = R_in[i] + R_cond[i] + R_out[i]
        UA[i] = 1 / R_tot[i]
        CALL NH3H2O(123;T_H[i];P_H;x_out:T_x[i];P[i];x[i];h[i];s[i];u[i];v[i];q[i])
        c_H[i] = ((h[i-1] - h[i]) / (T_x[i-1] - T_x[i])) * 1000
        call capacitance_rate(T_C[i];T_C[i-1];V_dot_C;m_dot_H;P;UA[i];c_H[i]:c_C[i];C_dot_C[i];C_dot_H[i];C_dot_min[i];C_dot_max[i])
        DELTAT[i] = T_H[i] - T_C[i]
        DELTAT_lm_cf[i] = (DELTAT[i] - DELTAT[i-1]) / ln (DELTAT[i] / DELTAT[i-1])
        P_HX[i] = (T_C[i-1] - T_C[i]) / (T_H[i-1] - T_C[i])
        R_HX[i] = (T_H[i-1] - T_H[i]) / (T_C[i-1] - T_C[i])
        F_HX[i] = LMTD_CF('crossflow_both_unmixed';P_HX[i];R_HX[i])
        DELTAT_lm[i] = DELTAT_lm_cf[i] * F_HX[i]
        q_dot[i] = UA[i] * DELTAT_lm[i]
        T_C_y[i-1] = T_C_y[i] + (q_dot[i] / C_dot_C[i])
        h_H_y[i] = h_H_y[i-1] - (q_dot[i] / (m_dot_H_tot * 1000))
        CALL NH3H2O(234;P_H;x_out;h_H_y[i]:T_H_y[i];P_y[i];x_y[i];h_y[i];s_y[i];u_y[i];v_y[i];q_y[i])
        L_x[i] = L_x[i-1] - (L_tube_S / L_tube)
end

S_2 = S+2
T_C[S_2] = (T_C[1] + T_C_y[1]) / 2
T_H[S_2] = (T_H[1] + T_H_y[1]) / 2
DELTAT[S_2] = T_H[S_2] - T_C[S_2]
T_C_y[S_2+S] = T_C_in
T_H_y[S_2] = T_H_in
h_H_y[S_2] = h_in
DELTAT_C[S_2] = T_C[S_2] - T_C_in
DELTAT_H[S_2] = T_H_in - T_H[S_2+S]
Call NH3H2O(123;T_H_in;P_H;x_out:T_x[S_2];P[S_2];x[S_2];h[S_2];s[S_2];u[S_2];v[S_2];q[S_2])
L_x[S_2] = 1

duplicate i = (S_2+1);(S_2+S)
        T_C[i] = (T_C[i - 11] + T_C_y[i - 11]) / 2
        T_H[i] = (T_H[i - 11] + T_H_y[i - 11]) /2
        T_avg[i] = (T_H[i-1] + T_C[i]) / 2
        T_bar_H[i] = (T_H[i-1] + T_H[i]) / 2
        T_bar_C[i] = (T_C[i-1] + T_C[i]) / 2
        CALL NH3H2O(128;T_bar_H[i];P_H;0:T_l[i];P_l[i];x_l[i];h_l[i];s_l[i];u_l[i];v_l[i];q_l[i])
```

```
        call thermophysical_properties(x_l[i];T_bar_H[i]:T_c_sol[i];P_c_sol[i];lambda_sol[i];mu_sol[i])
        call tube_flow(m_dot_H;mu_sol[i];T_H[i-1];T_H[i];P_H;D_in;lambda_sol[i];P_c_sol[i];L_tube_S;x_out:alpha_in[i];
               R_in[i];Re_D[i];u_m[i])
        call conduction_resistance(T_avg[i];D_out;D_in;L_tube_S:k_m[i];R_cond[i])
        call air_flow(T_C[i];T_C[i-1];T_avg[i];P;u_m;N_t_col;D_out;s_v;s_h;A_s_fin_tot;p_fin;th_fin;L_tube_S;k_m[i];A_tot:
               alpha_out[i];R_out[i];Re_out[i];eta_o[i];DELTAP[i])
        R_tot[i] = R_in[i] + R_cond[i] + R_out[i]
        UA[i] = 1 / R_tot[i]
        CALL NH3H2O(123;T_H[i];P_H;x_out:T_x[i];P[i];x[i];h[i];s[i];u[i];v[i];q[i])
        c_H[i] = ((h[i-1] - h[i]) / (T_x[i-1] - T_x[i])) * 1000
        call capacitance_rate(T_C[i];T_C[i-1];V_dot_C;m_dot_H;P;UA[i];c_H[i]:c_C[i];C_dot_C[i];C_dot_H[i];C_dot_min[i];C_dot_max[i])
        DELTAT[i] = T_H[i] - T_C[i]
        DELTAT_lm_cf[i] = (DELTAT[i] - DELTAT[i-1]) / ln (DELTAT[i] / DELTAT[i-1])
        P_HX[i] = (T_C[i-1] - T_C[i]) / (T_H[i-1] - T_C[i])
        R_HX[i] = (T_H[i-1] - T_H[i]) / (T_C[i-1] - T_C[i])
        F_HX[i] = LMTD_CF('crossflow_both_unmixed';P_HX[i];R_HX[i])
        DELTAT_lm[i] = DELTAT_lm_cf[i] * F_HX[i]
        q_dot[i] = UA[i] * DELTAT_lm[i]
        T_C_y[i-1] = T_C_y[i] + (q_dot[i] / C_dot_C[i])
        h_H_y[i] = h_H_y[i-1] - (q_dot[i] / (m_dot_H_tot * 1000))
        CALL NH3H2O(234;P_H;x_out;h_H_y[i]:T_H_y[i];P_y[i];x_y[i];h_y[i];s_y[i];u_y[i];v_y[i];q_y[i])
        L_x[i] = L_x[i-1] - (L_tube_S / L_tube)
end

S_3 = 2*S+3
T_C[S_3] = (T_C[S_2] + T_C_y[S_2]) / 2
T_H[S_3] = (T_H[S_2] + T_H_y[S_2]) / 2
DELTAT[S_3] = T_H[S_3] - T_C[S_3]
T_C_y[S_3+S] = T_C_in
T_H_y[S_3] = T_H_in
h_H_y[S_3] = h_in
DELTAT_C[S_3] = T_C[S_3] - T_C_in
DELTAT_H[S_3] = T_H_in - T_H[S_3+S]
Call NH3H2O(123;T_H_in;P_H;x_out:T_x[S_3];P[S_3];x[S_3];h[S_3];s[S_3];u[S_3];v[S_3];q[S_3])
L_x[S_3] = 1

duplicate i = (S_3+1);(S_3+S)
        T_C[i] = (T_C[i - 11] + T_C_y[i - 11]) / 2
        T_H[i] = (T_H[i - 11] + T_H_y[i - 11]) /2
```

```
    T_avg[i] = (T_H[i-1] + T_C[i]) / 2
    T_bar_H[i] = (T_H[i-1] + T_H[i]) / 2
    T_bar_C[i] = (T_C[i-1] + T_C[i]) / 2
    CALL NH3H2O(128;T_bar_H[i];P_H;0:T_l[i];P_l[i];x_l[i];h_l[i];s_l[i];u_l[i];v_l[i];q_l[i])
    call thermophysical_properties(x_l[i];T_bar_H[i]:T_c_sol[i];P_c_sol[i];lambda_sol[i];mu_sol[i])
    call tube_flow(m_dot_H;mu_sol[i];T_H[i-1];T_H[i];P_H;D_in;lambda_sol[i];P_c_sol[i];L_tube_S;x_out:alpha_in[i];
          R_in[i];Re_D[i];u_m[i])
    call conduction_resistance(T_avg[i];D_out;D_in;L_tube_S:k_m[i];R_cond[i])
    call air_flow(T_C[i];T_C[i-1];T_avg[i];P;u_m;N_t_col;D_out;s_v;s_h;A_s_fin_tot;p_fin;th_fin;L_tube_S;k_m[i];A_tot:
          alpha_out[i];R_out[i];Re_out[i];eta_o[i];DELTAP[i])
    R_tot[i] = R_in[i] + R_cond[i] + R_out[i]
    UA[i] = 1 / R_tot[i]
    CALL NH3H2O(123;T_H[i];P_H;x_out:T_x[i];P[i];x[i];h[i];s[i];u[i];v[i];q[i])
    c_H[i] = ((h[i-1] - h[i]) / (T_x[i-1] - T_x[i])) * 1000
    call capacitance_rate(T_C[i];T_C[i-1];V_dot_C;m_dot_H;P;UA[i];c_H[i]:c_C[i];C_dot_C[i];C_dot_H[i];C_dot_min[i];C_dot_max[i])
    DELTAT[i] = T_H[i] - T_C[i]
    DELTAT_lm_cf[i] = (DELTAT[i] - DELTAT[i-1]) / ln (DELTAT[i] / DELTAT[i-1])
    P_HX[i] = (T_C[i-1] - T_C[i]) / (T_H[i-1] - T_C[i])
    R_HX[i] = (T_H[i-1] - T_H[i]) / (T_C[i-1] - T_C[i])
    F_HX[i] = LMTD_CF('crossflow_both_unmixed';P_HX[i];R_HX[i])
    DELTAT_lm[i] = DELTAT_lm_cf[i] * F_HX[i]
    q_dot[i] = UA[i] * DELTAT_lm[i]
    T_C_y[i-1] = T_C_y[i] + (q_dot[i] / C_dot_C[i])
    h_H_y[i] = h_H_y[i-1] - (q_dot[i] / (m_dot_H_tot * 1000))
    CALL NH3H2O(234;P_H;x_out;h_H_y[i]:T_H_y[i];P_y[i];x_y[i];h_y[i];s_y[i];u_y[i];v_y[i];q_y[i])
    L_x[i] = L_x[i-1] - (L_tube_S / L_tube)
end

S_4 = 3*S+4
T_C[S_4] = (T_C[S_3] + T_C_y[S_3]) / 2
T_H[S_4] = (T_H[S_3] + T_H_y[S_3]) / 2
DELTAT[S_4] = T_H[S_4] - T_C[S_4]
T_C_y[S_4+S] = T_C_in
T_H_y[S_4] = T_H_in
h_H_y[S_4] = h_in
DELTAT_C[S_4] = T_C[S_4] - T_C_in
DELTAT_H[S_4] = T_H_in - T_H[S_4+S]
Call NH3H2O(123;T_H_in;P_H;x_out:T_x[S_4];P[S_4];x[S_4];h[S_4];s[S_4];u[S_4];v[S_4];q[S_4])
L_x[S_4] = 1
```

```
duplicate i = (S_4+1);(S_4+S)
        T_C[i] = (T_C[i - 11] + T_C_y[i - 11]) / 2
        T_H[i] = (T_H[i - 11] + T_H_y[i - 11]) /2
        T_avg[i] = (T_H[i-1] + T_C[i]) / 2
        T_bar_H[i] = (T_H[i-1] + T_H[i]) / 2
        T_bar_C[i] = (T_C[i-1] + T_C[i]) / 2
        CALL NH3H2O(128;T_bar_H[i];P_H;0:T_l[i];P_l[i];x_l[i];h_l[i];s_l[i];u_l[i];v_l[i];q_l[i])
        call thermophysical_properties(x_l[i];T_bar_H[i]:T_c_sol[i];P_c_sol[i];lambda_sol[i];mu_sol[i])
        call tube_flow(m_dot_H;mu_sol[i];T_H[i-1];T_H[i];P_H;D_in;lambda_sol[i];P_c_sol[i];L_tube_S;x_out:alpha_in[i];
                R_in[i];Re_D[i];u_m[i])
        call conduction_resistance(T_avg[i];D_out;D_in;L_tube_S:k_m[i];R_cond[i])
        call air_flow(T_C[i];T_C[i-1];T_avg[i];P;u_m;N_t_col;D_out;s_v;s_h;A_s_fin_tot;p_fin;th_fin;L_tube_S;k_m[i];A_tot:
                alpha_out[i];R_out[i];Re_out[i];eta_o[i];DELTAP[i])
        R_tot[i] = R_in[i] + R_cond[i] + R_out[i]
        UA[i] = 1 / R_tot[i]
        CALL NH3H2O(123;T_H[i];P_H;x_out:T_x[i];P[i];x[i];h[i];s[i];u[i];v[i];q[i])
        c_H[i] = ((h[i-1] - h[i]) / (T_x[i-1] - T_x[i])) * 1000
        call capacitance_rate(T_C[i];T_C[i-1];V_dot_C;m_dot_H;P;UA[i];c_H[i]:c_C[i];C_dot_C[i];C_dot_H[i];C_dot_min[i];C_dot_max[i])
        DELTAT[i] = T_H[i] - T_C[i]
        DELTAT_lm_cf[i] = (DELTAT[i] - DELTAT[i-1]) / ln (DELTAT[i] / DELTAT[i-1])
        P_HX[i] = (T_C[i-1] - T_C[i]) / (T_H[i-1] - T_C[i])
        R_HX[i] = (T_H[i-1] - T_H[i]) / (T_C[i-1] - T_C[i])
        F_HX[i] = LMTD_CF('crossflow_both_unmixed';P_HX[i];R_HX[i])
        DELTAT_lm[i] = DELTAT_lm_cf[i] * F_HX[i]
        q_dot[i] = UA[i] * DELTAT_lm[i]
        T_C_y[i-1] = T_C_y[i] + (q_dot[i] / C_dot_C[i])
        h_H_y[i] = h_H_y[i-1] - (q_dot[i] / (m_dot_H_tot * 1000))
        CALL NH3H2O(234;P_H;x_out;h_H_y[i]:T_H_y[i];P_y[i];x_y[i];h_y[i];s_y[i];u_y[i];v_y[i];q_y[i])
        L_x[i] = L_x[i-1] - (L_tube_S / L_tube)
end

S_5 = 4*S+5
T_C[S_5] = (T_C[S_4] + T_C_y[S_4]) / 2
T_H[S_5] = (T_H[S_4] + T_H_y[S_4]) / 2
DELTAT[S_5] = T_H[S_5] - T_C[S_5]
T_C_y[S_5+S] = T_C_in
T_H_y[S_5] = T_H_in
h_H_y[S_5] = h_in
```

```
DELTAT_C[S_5] = T_C[S_5] - T_C_in
DELTAT_H[S_5] = T_H_in - T_H[S_5+S]
Call NH3H2O(123;T_H_in;P_H;x_out:T_x[S_5];P[S_5];x[S_5];h[S_5];s[S_5];u[S_5];v[S_5];q[S_5])
L_x[S_5] = 1

duplicate i = (S_5+1);(S_5+S)
        T_C[i] = (T_C[i - 11] + T_C_y[i - 11]) / 2
        T_H[i] = (T_H[i - 11] + T_H_y[i - 11]) /2
        T_avg[i] = (T_H[i-1] + T_C[i]) / 2
        T_bar_H[i] = (T_H[i-1] + T_H[i]) / 2
        T_bar_C[i] = (T_C[i-1] + T_C[i]) / 2
        CALL NH3H2O(128;T_bar_H[i];P_H;0:T_l[i];P_l[i];x_l[i];h_l[i];s_l[i];u_l[i];v_l[i];q_l[i])
        call thermophysical_properties(x_l[i];T_bar_H[i]:T_c_sol[i];P_c_sol[i];lambda_sol[i];mu_sol[i])
        call tube_flow(m_dot_H;mu_sol[i];T_H[i-1];T_H[i];P_H;D_in;lambda_sol[i];P_c_sol[i];L_tube_S;x_out:alpha_in[i];
                R_in[i];Re_D[i];u_m[i])
        call conduction_resistance(T_avg[i];D_out;D_in;L_tube_S:k_m[i];R_cond[i])
        call air_flow(T_C[i];T_C[i-1];T_avg[i];P;u_m;N_t_col;D_out;s_v;s_h;A_s_fin_tot;p_fin;th_fin;L_tube_S;k_m[i];A_tot:
                alpha_out[i];R_out[i];Re_out[i];eta_o[i];DELTAP[i])
        R_tot[i] = R_in[i] + R_cond[i] + R_out[i]
        UA[i] = 1 / R_tot[i]
        CALL NH3H2O(123;T_H[i];P_H;x_out:T_x[i];P[i];x[i];h[i];s[i];u[i];v[i];q[i])
        c_H[i] = ((h[i-1] - h[i]) / (T_x[i-1] - T_x[i])) * 1000
        call capacitance_rate(T_C[i];T_C[i-1];V_dot_C;m_dot_H;P;UA[i];c_H[i]:c_C[i];C_dot_C[i];C_dot_H[i];C_dot_min[i];C_dot_max[i])
        DELTAT[i] = T_H[i] - T_C[i]
        DELTAT_lm_cf[i] = (DELTAT[i] - DELTAT[i-1]) / ln (DELTAT[i] / DELTAT[i-1])
        P_HX[i] = (T_C[i-1] - T_C[i]) / (T_H[i-1] - T_C[i])
        R_HX[i] = (T_H[i-1] - T_H[i]) / (T_C[i-1] - T_C[i])
        F_HX[i] = LMTD_CF('crossflow_both_unmixed';P_HX[i];R_HX[i])
        DELTAT_lm[i] = DELTAT_lm_cf[i] * F_HX[i]
        q_dot[i] = UA[i] * DELTAT_lm[i]
        T_C_y[i-1] = T_C_y[i] + (q_dot[i] / C_dot_C[i])
        h_H_y[i] = h_H_y[i-1] - (q_dot[i] / (m_dot_H_tot * 1000))
        CALL NH3H2O(234;P_H;x_out;h_H_y[i]:T_H_y[i];P_y[i];x_y[i];h_y[i];s_y[i];u_y[i];v_y[i];q_y[i])
        L_x[i] = L_x[i-1] - (L_tube_S / L_tube)
end

S_6 = 5*S+6
T_C[S_6] = (T_C[S_5] + T_C_y[S_5]) / 2
T_H[S_6] = (T_H[S_5] + T_H_y[S_5]) / 2
```

```
DELTAT[S_6] = T_H[S_6] - T_C[S_6]
T_C_y[S_6+S] = T_C_in
T_H_y[S_6] = T_H_in
h_H_y[S_6] = h_in
DELTAT_C[S_6] = T_C[S_6] - T_C_in
DELTAT_H[S_6] = T_H_in - T_H[S_6+S]
Call NH3H2O(123;T_H_in;P_H;x_out:T_x[S_6];P[S_6];x[S_6];h[S_6];s[S_6];u[S_6];v[S_6];q[S_6])
L_x[S_6] = 1

duplicate i = (S_6+1);(S_6+S)
        T_C[i] = (T_C[i - 11] + T_C_y[i - 11]) / 2
        T_H[i] = (T_H[i - 11] + T_H_y[i - 11]) /2
        T_avg[i] = (T_H[i-1] + T_C[i]) / 2
        T_bar_H[i] = (T_H[i-1] + T_H[i]) / 2
        T_bar_C[i] = (T_C[i-1] + T_C[i]) / 2
        CALL NH3H2O(128;T_bar_H[i];P_H;0:T_l[i];P_l[i];x_l[i];h_l[i];s_l[i];u_l[i];v_l[i];q_l[i])
        call thermophysical_properties(x_l[i];T_bar_H[i]:T_c_sol[i];P_c_sol[i];lambda_sol[i];mu_sol[i])
        call tube_flow(m_dot_H;mu_sol[i];T_H[i-1];T_H[i];P_H;D_in;lambda_sol[i];P_c_sol[i];L_tube_S;x_out:alpha_in[i];
                R_in[i];Re_D[i];u_m[i])
        call conduction_resistance(T_avg[i];D_out;D_in;L_tube_S:k_m[i];R_cond[i])
        call air_flow(T_C[i];T_C[i-1];T_avg[i];P;u_m;N_t_col;D_out;s_v;s_h;A_s_fin_tot;p_fin;th_fin;L_tube_S;k_m[i];A_tot:
                alpha_out[i];R_out[i];Re_out[i];eta_o[i];DELTAP[i])
        R_tot[i] = R_in[i] + R_cond[i] + R_out[i]
        UA[i] = 1 / R_tot[i]
        CALL NH3H2O(123;T_H[i];P_H;x_out:T_x[i];P[i];x[i];h[i];s[i];u[i];v[i];q[i])
        c_H[i] = ((h[i-1] - h[i]) / (T_x[i-1] - T_x[i])) * 1000
        call capacitance_rate(T_C[i];T_C[i-1];V_dot_C;m_dot_H;P;UA[i];c_H[i]:c_C[i];C_dot_C[i];C_dot_H[i];C_dot_min[i];C_dot_max[i])
        DELTAT[i] = T_H[i] - T_C[i]
        DELTAT_lm_cf[i] = (DELTAT[i] - DELTAT[i-1]) / ln (DELTAT[i] / DELTAT[i-1])
        P_HX[i] = (T_C[i-1] - T_C[i]) / (T_H[i-1] - T_C[i])
        R_HX[i] = (T_H[i-1] - T_H[i]) / (T_C[i-1] - T_C[i])
        F_HX[i] = LMTD_CF('crossflow_both_unmixed';P_HX[i];R_HX[i])
        DELTAT_lm[i] = DELTAT_lm_cf[i] * F_HX[i]
        q_dot[i] = UA[i] * DELTAT_lm[i]
        T_C_y[i-1] = T_C_y[i] + (q_dot[i] / C_dot_C[i])
        h_H_y[i] = h_H_y[i-1] - (q_dot[i] / (m_dot_H_tot * 1000))
        CALL NH3H2O(234;P_H;x_out;h_H_y[i]:T_H_y[i];P_y[i];x_y[i];h_y[i];s_y[i];u_y[i];v_y[i];q_y[i])
        L_x[i] = L_x[i-1] - (L_tube_S / L_tube)
end
```

```
S_7 = 6*S+7
T_C[S_7] = (T_C[S_6] + T_C_y[S_6]) / 2
T_H[S_7] = (T_H[S_6] + T_H_y[S_6]) / 2
DELTAT[S_7] = T_H[S_7] - T_C[S_7]
T_C_y[S_7+S] = T_C_in
T_H_y[S_7] = T_H_in
h_H_y[S_7] = h_in
DELTAT_C[S_7] = T_C[S_7] - T_C_in
DELTAT_H[S_7] = T_H_in - T_H[S_7+S]
Call NH3H2O(123;T_H_in;P_H;x_out:T_x[S_7];P[S_7];x[S_7];h[S_7];s[S_7];u[S_7];v[S_7];q[S_7])
L_x[S_7] = 1

duplicate i = (S_7+1);(S_7+S)
      T_C[i] = (T_C[i - 11] + T_C_y[i - 11]) / 2
      T_H[i] = (T_H[i - 11] + T_H_y[i - 11]) /2
      T_avg[i] = (T_H[i-1] + T_C[i]) / 2
      T_bar_H[i] = (T_H[i-1] + T_H[i]) / 2
      T_bar_C[i] = (T_C[i-1] + T_C[i]) / 2
      CALL NH3H2O(128;T_bar_H[i];P_H;0:T_l[i];P_l[i];x_l[i];h_l[i];s_l[i];u_l[i];v_l[i];q_l[i])
      call thermophysical_properties(x_l[i];T_bar_H[i]:T_c_sol[i];P_c_sol[i];lambda_sol[i];mu_sol[i])
      call tube_flow(m_dot_H;mu_sol[i];T_H[i-1];T_H[i];P_H;D_in;lambda_sol[i];P_c_sol[i];L_tube_S;x_out:alpha_in[i];
            R_in[i];Re_D[i];u_m[i])
      call conduction_resistance(T_avg[i];D_out;D_in;L_tube_S:k_m[i];R_cond[i])
      call air_flow(T_C[i];T_C[i-1];T_avg[i];P;u_m;N_t_col;D_out;s_v;s_h;A_s_fin_tot;p_fin;th_fin;L_tube_S;k_m[i];A_tot:
            alpha_out[i];R_out[i];Re_out[i];eta_o[i];DELTAP[i])
      R_tot[i] = R_in[i] + R_cond[i] + R_out[i]
      UA[i] = 1 / R_tot[i]
      CALL NH3H2O(123;T_H[i];P_H;x_out:T_x[i];P[i];x[i];h[i];s[i];u[i];v[i];q[i])
      c_H[i] = ((h[i-1] - h[i]) / (T_x[i-1] - T_x[i])) * 1000
      call capacitance_rate(T_C[i];T_C[i-1];V_dot_C;m_dot_H;P;UA[i];c_H[i]:c_C[i];C_dot_C[i];C_dot_H[i];C_dot_min[i];C_dot_max[i])
      DELTAT[i] = T_H[i] - T_C[i]
      DELTAT_lm_cf[i] = (DELTAT[i] - DELTAT[i-1]) / ln (DELTAT[i] / DELTAT[i-1])
      P_HX[i] = (T_C[i-1] - T_C[i]) / (T_H[i-1] - T_C[i])
      R_HX[i] = (T_H[i-1] - T_H[i]) / (T_C[i-1] - T_C[i])
      F_HX[i] = LMTD_CF('crossflow_both_unmixed';P_HX[i];R_HX[i])
      DELTAT_lm[i] = DELTAT_lm_cf[i] * F_HX[i]
      q_dot[i] = UA[i] * DELTAT_lm[i]
      T_C_y[i-1] = T_C_y[i] + (q_dot[i] / C_dot_C[i])
```

```
    h_H_y[i] = h_H_y[i-1] - (q_dot[i] / (m_dot_H_tot * 1000))
    CALL NH3H2O(234;P_H;x_out;h_H_y[i]:T_H_y[i];P_y[i];x_y[i];h_y[i];s_y[i];u_y[i];v_y[i];q_y[i])
    L_x[i] = L_x[i-1] - (L_tube_S / L_tube)
end

S_8 = 7*S+8
T_C[S_8] = (T_C[S_7] + T_C_y[S_7]) / 2
T_H[S_8] = (T_H[S_7] + T_H_y[S_7]) / 2
DELTAT[S_8] = T_H[S_8] - T_C[S_8]
T_C_y[S_8+S] = T_C_in
T_H_y[S_8] = T_H_in
h_H_y[S_8] = h_in
DELTAT_C[S_8] = T_C[S_8] - T_C_in
DELTAT_H[S_8] = T_H_in - T_H[S_8+S]
Call NH3H2O(123;T_H_in;P_H;x_out:T_x[S_8];P[S_8];x[S_8];h[S_8];s[S_8];u[S_8];v[S_8];q[S_8])
L_x[S_8] = 1

duplicate i = (S_8+1);(S_8+S)
    T_C[i] = (T_C[i - 11] + T_C_y[i - 11]) / 2
    T_H[i] = (T_H[i - 11] + T_H_y[i - 11]) /2
    T_avg[i] = (T_H[i-1] + T_C[i]) / 2
    T_bar_H[i] = (T_H[i-1] + T_H[i]) / 2
    T_bar_C[i] = (T_C[i-1] + T_C[i]) / 2
    CALL NH3H2O(128;T_bar_H[i];P_H;0:T_l[i];P_l[i];x_l[i];h_l[i];s_l[i];u_l[i];v_l[i];q_l[i])
    call thermophysical_properties(x_l[i];T_bar_H[i]:T_c_sol[i];P_c_sol[i];lambda_sol[i];mu_sol[i])
    call tube_flow(m_dot_H;mu_sol[i];T_H[i-1];T_H[i];P_H;D_in;lambda_sol[i];P_c_sol[i];L_tube_S;x_out:alpha_in[i];
            R_in[i];Re_D[i];u_m[i])
    call conduction_resistance(T_avg[i];D_out;D_in;L_tube_S:k_m[i];R_cond[i])
    call air_flow(T_C[i];T_C[i-1];T_avg[i];P;u_m;N_t_col;D_out;s_v;s_h;A_s_fin_tot;p_fin;th_fin;L_tube_S;k_m[i];A_tot:
            alpha_out[i];R_out[i];Re_out[i];eta_o[i];DELTAP[i])
    R_tot[i] = R_in[i] + R_cond[i] + R_out[i]
    UA[i] = 1 / R_tot[i]
    CALL NH3H2O(123;T_H[i];P_H;x_out:T_x[i];P[i];x[i];h[i];s[i];u[i];v[i];q[i])
    c_H[i] = ((h[i-1] - h[i]) / (T_x[i-1] - T_x[i])) * 1000
    call capacitance_rate(T_C[i];T_C[i-1];V_dot_C;m_dot_H;P;UA[i];c_H[i]:c_C[i];C_dot_C[i];C_dot_H[i];C_dot_min[i];C_dot_max[i])
    DELTAT[i] = T_H[i] - T_C[i]
    DELTAT_lm_cf[i] = (DELTAT[i] - DELTAT[i-1]) / ln (DELTAT[i] / DELTAT[i-1])
    P_HX[i] = (T_C[i-1] - T_C[i]) / (T_H[i-1] - T_C[i])
    R_HX[i] = (T_H[i-1] - T_H[i]) / (T_C[i-1] - T_C[i])
```

```
    F_HX[i] = LMTD_CF('crossflow_both_unmixed';P_HX[i];R_HX[i])
    DELTAT_lm[i] = DELTAT_lm_cf[i] * F_HX[i]
    q_dot[i] = UA[i] * DELTAT_lm[i]
    T_C_y[i-1] = T_C_y[i] + (q_dot[i] / C_dot_C[i])
    h_H_y[i] = h_H_y[i-1] - (q_dot[i] / (m_dot_H_tot * 1000))
    CALL NH3H2O(234;P_H;x_out;h_H_y[i]:T_H_y[i];P_y[i];x_y[i];h_y[i];s_y[i];u_y[i];v_y[i];q_y[i])
    L_x[i] = L_x[i-1] - (L_tube_S / L_tube)
end

S_9 = 8*S+9
T_C[S_9] = (T_C[S_8] + T_C_y[S_8]) / 2
T_H[S_9] = (T_H[S_8] + T_H_y[S_8]) / 2
DELTAT[S_9] = T_H[S_9] - T_C[S_9]
T_C_y[S_9+S] = T_C_in
T_H_y[S_9] = T_H_in
h_H_y[S_9] = h_in
DELTAT_C[S_9] = T_C[S_9] - T_C_in
DELTAT_H[S_9] = T_H_in - T_H[S_9+S]
Call NH3H2O(123;T_H_in;P_H;x_out:T_x[S_9];P[S_9];x[S_9];h[S_9];s[S_9];u[S_9];v[S_9];q[S_9])
L_x[S_9] = 1

duplicate i = (S_9+1);(S_9+S)
      T_C[i] = (T_C[i - 11] + T_C_y[i - 11]) / 2
      T_H[i] = (T_H[i - 11] + T_H_y[i - 11]) /2
      T_avg[i] = (T_H[i-1] + T_C[i]) / 2
      T_bar_H[i] = (T_H[i-1] + T_H[i]) / 2
      T_bar_C[i] = (T_C[i-1] + T_C[i]) / 2
      CALL NH3H2O(128;T_bar_H[i];P_H;0:T_l[i];P_l[i];x_l[i];h_l[i];s_l[i];u_l[i];v_l[i];q_l[i])
      call thermophysical_properties(x_l[i];T_bar_H[i]:T_c_sol[i];P_c_sol[i];lambda_sol[i];mu_sol[i])
      call tube_flow(m_dot_H;mu_sol[i];T_H[i-1];T_H[i];P_H;D_in;lambda_sol[i];P_c_sol[i];L_tube_S;x_out:alpha_in[i];
            R_in[i];Re_D[i];u_m[i])
      call conduction_resistance(T_avg[i];D_out;D_in;L_tube_S:k_m[i];R_cond[i])
      call air_flow(T_C[i];T_C[i-1];T_avg[i];P;u_m;N_t_col;D_out;s_v;s_h;A_s_fin_tot;p_fin;th_fin;L_tube_S;k_m[i];A_tot:
            alpha_out[i];R_out[i];Re_out[i];eta_o[i];DELTAP[i])
      R_tot[i] = R_in[i] + R_cond[i] + R_out[i]
      UA[i] = 1 / R_tot[i]
      CALL NH3H2O(123;T_H[i];P_H;x_out:T_x[i];P[i];x[i];h[i];s[i];u[i];v[i];q[i])
      c_H[i] = ((h[i-1] - h[i]) / (T_x[i-1] - T_x[i])) * 1000
      call capacitance_rate(T_C[i];T_C[i-1];V_dot_C;m_dot_H;P;UA[i];c_H[i]:c_C[i];C_dot_C[i];C_dot_H[i];C_dot_min[i];C_dot_max[i])
```

```
        DELTAT[i] = T_H[i] - T_C[i]
        DELTAT_lm_cf[i] = (DELTAT[i] - DELTAT[i-1]) / ln (DELTAT[i] / DELTAT[i-1])
        P_HX[i] = (T_C[i-1] - T_C[i]) / (T_H[i-1] - T_C[i])
        R_HX[i] = (T_H[i-1] - T_H[i]) / (T_C[i-1] - T_C[i])
        F_HX[i] = LMTD_CF('crossflow_both_unmixed';P_HX[i];R_HX[i])
        DELTAT_lm[i] = DELTAT_lm_cf[i] * F_HX[i]
        q_dot[i] = UA[i] * DELTAT_lm[i]
        T_C_y[i-1] = T_C_y[i] + (q_dot[i] / C_dot_C[i])
        h_H_y[i] = h_H_y[i-1] - (q_dot[i] / (m_dot_H_tot * 1000))
        CALL NH3H2O(234;P_H;x_out;h_H_y[i]:T_H_y[i];P_y[i];x_y[i];h_y[i];s_y[i];u_y[i];v_y[i];q_y[i])
        L_x[i] = L_x[i-1] - (L_tube_S / L_tube)
end

S_10 = 9*S+10
T_C[S_10] = (T_C[S_9] + T_C_y[S_9]) / 2
T_H[S_10] = (T_H[S_9] + T_H_y[S_9]) / 2
DELTAT[S_10] = T_H[S_10] - T_C[S_10]
T_C_y[S_10+S] = T_C_in
T_H_y[S_10] = T_H_in
h_H_y[S_10] = h_in
DELTAT_C[S_10] = T_C[S_10] - T_C_in
DELTAT_H[S_10] = T_H_in - T_H[S_10+S]
Call NH3H2O(123;T_H_in;P_H;x_out:T_x[S_10];P[S_10];x[S_10];h[S_10];s[S_10];u[S_10];v[S_10];q[S_10])
L_x[S_10] = 1

duplicate i = (S_10+1);(S_10+S)
        T_C[i] = (T_C[i - 11] + T_C_y[i - 11]) / 2
        T_H[i] = (T_H[i - 11] + T_H_y[i - 11]) /2
        T_avg[i] = (T_H[i-1] + T_C[i]) / 2
        T_bar_H[i] = (T_H[i-1] + T_H[i]) / 2
        T_bar_C[i] = (T_C[i-1] + T_C[i]) / 2
        CALL NH3H2O(128;T_bar_H[i];P_H;0:T_l[i];P_l[i];x_l[i];h_l[i];s_l[i];u_l[i];v_l[i];q_l[i])
        call thermophysical_properties(x_l[i];T_bar_H[i]:T_c_sol[i];P_c_sol[i];lambda_sol[i];mu_sol[i])
        call tube_flow(m_dot_H;mu_sol[i];T_H[i-1];T_H[i];P_H;D_in;lambda_sol[i];P_c_sol[i];L_tube_S;x_out:alpha_in[i];
                R_in[i];Re_D[i];u_m[i])
        call conduction_resistance(T_avg[i];D_out;D_in;L_tube_S:k_m[i];R_cond[i])
        call air_flow(T_C[i];T_C[i-1];T_avg[i];P;u_m;N_t_col;D_out;s_v;s_h;A_s_fin_tot;p_fin;th_fin;L_tube_S;k_m[i];A_tot:
                alpha_out[i];R_out[i];Re_out[i];eta_o[i];DELTAP[i])
        R_tot[i] = R_in[i] + R_cond[i] + R_out[i]
```

```
    UA[i] = 1 / R_tot[i]
    CALL NH3H2O(123;T_H[i];P_H;x_out:T_x[i];P[i];x[i];h[i];s[i];u[i];v[i];q[i])
    c_H[i] = ((h[i-1] - h[i]) / (T_x[i-1] - T_x[i])) * 1000
    call capacitance_rate(T_C[i];T_C[i-1];V_dot_C;m_dot_H;P;UA[i];c_H[i]:c_C[i];C_dot_C[i];C_dot_H[i];C_dot_min[i];C_dot_max[i])
    DELTAT[i] = T_H[i] - T_C[i]
    DELTAT_lm_cf[i] = (DELTAT[i] - DELTAT[i-1]) / ln (DELTAT[i] / DELTAT[i-1])
    P_HX[i] = (T_C[i-1] - T_C[i]) / (T_H[i-1] - T_C[i])
    R_HX[i] = (T_H[i-1] - T_H[i]) / (T_C[i-1] - T_C[i])
    F_HX[i] = LMTD_CF('crossflow_both_unmixed';P_HX[i];R_HX[i])
    DELTAT_lm[i] = DELTAT_lm_cf[i] * F_HX[i]
    q_dot[i] = UA[i] * DELTAT_lm[i]
    T_C_y[i-1] = T_C_y[i] + (q_dot[i] / C_dot_C[i])
    h_H_y[i] = h_H_y[i-1] - (q_dot[i] / (m_dot_H_tot * 1000))
    CALL NH3H2O(234;P_H;x_out:h_H_y[i];T_H_y[i];P_y[i];x_y[i];h_y[i];s_y[i];u_y[i];v_y[i];q_y[i])
    L_x[i] = L_x[i-1] - (L_tube_S / L_tube)
end

S_11 = 10*S+11
T_C[S_11] = (T_C[S_10] + T_C_y[S_10]) / 2
T_H[S_11] = (T_H[S_10] + T_H_y[S_10]) / 2
DELTAT[S_11] = T_H[S_11] - T_C[S_11]
T_C_y[S_11+S] = T_C_in
T_H_y[S_11] = T_H_in
h_H_y[S_11] = h_in
DELTAT_C[S_11] = T_C[S_11] - T_C_in
DELTAT_H[S_11] = T_H_in - T_H[S_11+S]
Call NH3H2O(123;T_H_in;P_H;x_out:T_x[S_11];P[S_11];x[S_11];h[S_11];s[S_11];u[S_11];v[S_11];q[S_11])
L_x[S_11] = 1

duplicate i = (S_11+1);(S_11+S)
      T_C[i] = (T_C[i - 11] + T_C_y[i - 11]) / 2
      T_H[i] = (T_H[i - 11] + T_H_y[i - 11]) /2
      T_avg[i] = (T_H[i-1] + T_C[i]) / 2
      T_bar_H[i] = (T_H[i-1] + T_H[i]) / 2
      T_bar_C[i] = (T_C[i-1] + T_C[i]) / 2
      CALL NH3H2O(128;T_bar_H[i];P_H;0:T_l[i];P_l[i];x_l[i];h_l[i];s_l[i];u_l[i];v_l[i];q_l[i])
      call thermophysical_properties(x_l[i];T_bar_H[i]:T_c_sol[i];P_c_sol[i];lambda_sol[i];mu_sol[i])
      call tube_flow(m_dot_H;mu_sol[i];T_H[i-1];T_H[i];P_H;D_in;lambda_sol[i];P_c_sol[i];L_tube_S;x_out:alpha_in[i];
                R_in[i];Re_D[i];u_m[i])
```

```
        call conduction_resistance(T_avg[i];D_out;D_in;L_tube_S:k_m[i];R_cond[i])
        call air_flow(T_C[i];T_C[i-1];T_avg[i];P;u_m;N_t_col;D_out;s_v;s_h;A_s_fin_tot;p_fin;th_fin;L_tube_S;k_m[i];A_tot:
                alpha_out[i];R_out[i];Re_out[i];eta_o[i];DELTAP[i])
        R_tot[i] = R_in[i] + R_cond[i] + R_out[i]
        UA[i] = 1 / R_tot[i]
        CALL NH3H2O(123;T_H[i];P_H;x_out:T_x[i];P[i];x[i];h[i];s[i];u[i];v[i];q[i])
        c_H[i] = ((h[i-1] - h[i]) / (T_x[i-1] - T_x[i])) * 1000
        call capacitance_rate(T_C[i];T_C[i-1];V_dot_C;m_dot_H;P;UA[i];c_H[i]:c_C[i];C_dot_C[i];C_dot_H[i];C_dot_min[i];C_dot_max[i])
        DELTAT[i] = T_H[i] - T_C[i]
        DELTAT_lm_cf[i] = (DELTAT[i] - DELTAT[i-1]) / ln (DELTAT[i] / DELTAT[i-1])
        P_HX[i] = (T_C[i-1] - T_C[i]) / (T_H[i-1] - T_C[i])
        R_HX[i] = (T_H[i-1] - T_H[i]) / (T_C[i-1] - T_C[i])
        F_HX[i] = LMTD_CF('crossflow_both_unmixed';P_HX[i];R_HX[i])
        DELTAT_lm[i] = DELTAT_lm_cf[i] * F_HX[i]
        q_dot[i] = UA[i] * DELTAT_lm[i]
        T_C_y[i-1] = T_C_y[i] + (q_dot[i] / C_dot_C[i])
        h_H_y[i] = h_H_y[i-1] - (q_dot[i] / (m_dot_H_tot * 1000))
        CALL NH3H2O(234;P_H;x_out;h_H_y[i]:T_H_y[i];P_y[i];x_y[i];h_y[i];s_y[i];u_y[i];v_y[i];q_y[i])
        L_x[i] = L_x[i-1] - (L_tube_S / L_tube)
end

duplicate i = 1;(S+1)
        T_H_celsius[i] = T_H_y[i] - 273,15
        T_C_celsius[i] = T_C_y[i] - 273,15
end
duplicate i = (S_11);(S_11+S)
        T_H_celsius[i] = T_H_y[i] - 273,15
        T_C_celsius[i] = T_C_y[i] - 273,15
end

Q_11 = (h_H_y[S_11]- h_y[S_11+S]) * m_dot_H_tot "calculated heat transfer"

q_dot_10 = sum(q_dot[i];i=(S_11+1);(S_11+S))
theta_H = (T_H[S_11] - T_C[S_11])
theta_C = (T_H[S_11+S] - T_C[S_11+S])
DELTAT_LMTD = (theta_H - theta_c) / ln(theta_H/theta_C)
A_out_10 = A_tot * S
A_in_10 = pi * D_in * L_tube
```

```
U_out = q_dot_10 / (A_out_10 * DELTAT_LMTD)          "overall heat transfer coefficient with respect to the air side surface"
U_in = q_dot_10 / (A_in_10 * DELTAT_LMTD)            "overall heat transfer coefficient with respect to the inner tube area"
DELTAP = sum(DELTAP[i];i=(S_11+1);(S_11+S))          "pressure loss in all segments"
W_dot_fan = ((2 * DELTAP * V_dot_C) / eta_fan) / 1000 "fan work"
```

Scientific Paper

Development of the hybrid absorption heat pump process at high temperature operation

Anders Borgås

Norwegian University of Technology and Science

Abstract

Compression/absorption heat pumps with ammonia/water mixtures are identified as one of the most promising heat pump technologies for high temperature applications. They are especially suited for processes with high temperature lift, due to evaporation and condensation, and it enables the use of ammonia for higher temperatures than in conventional vapour-compression heat pumps. Compression/absorption heat pumps are also distinguished by high performances and are flexible considering capacity contrail and external changes. Two separate simulation models were developed; a two-stage compression/absorption model for heating process water from 100 °C to 150 °C utilizing waste heat at 50 °C, and an absorber model for heating air at 90 °C. Simulation results from the two-stage model indicated that high water content in the vapour to the compressor achieves the highest performances. Although pressure ratios are higher, higher circulation ratios causes smaller vapour mass flow rates, hence lower compressor work. The disadvantage are higher discharge temperatures and significantly lower vapour densities. Simulations with a desuperheater indicates that, unless the minimum temperature difference between mixture and heat sink occur at the absorber inlet, there is no gain by employing a desuperheater. Even when the minimum temperature difference is at the absorber inlet, the gain is small. Dimensioning the absorber gave some unrealistic results in terms of an extreme ratio between absorber height and width/length. It is difficult to determine whether the results are due to errors in the simulation model or if it is difficult to obtain a noteworthy result with the simulation parameters. However, it is worth mentioning that the air mass flow rate was 15 times as high as the mixture mass flow rate.

I. Introduction

Compression/absorption heat pumps with ammonia/water mixtures offer one of the most promising alternatives for high temperature heat pumps [1]. The heat pump cycle combines the conventional vapour-compression heat pump cycle and the absorption heat pump cycle. Vapour-compression cycles have limited temperature lifts, inflexible operating ranges, limited capacity control and temperature mismatches between heat sinks and heat sources, whereas absorption cycles have limited temperature ranges [2]. Combing these heat pump cycles reduces their individual limitations and offers a heat pump with advantages for some application areas. Hultén and Berntsson [3, 4] studied the compression/absorption heat pump cycle and summarized advantages:

- Small swept volume to the compressor
- High heat transfer coefficient
- Environmentally benign working fluids
- High COP
- Extra degree of freedom
- High working temperatures can be obtained
- The mixture temperature glide can be fitted to the gliding temperatures of heat source and heat sink

Several of the advantages come because of the ammonia/water mixture properties. Saturation temperatures of binary mixtures are

Master thesis • June 2014

determined by pressure and composition. Dif-

sorber model used to evaluate dimensions of a

Simulations with and without desuperheater was conducted for all scenarios.

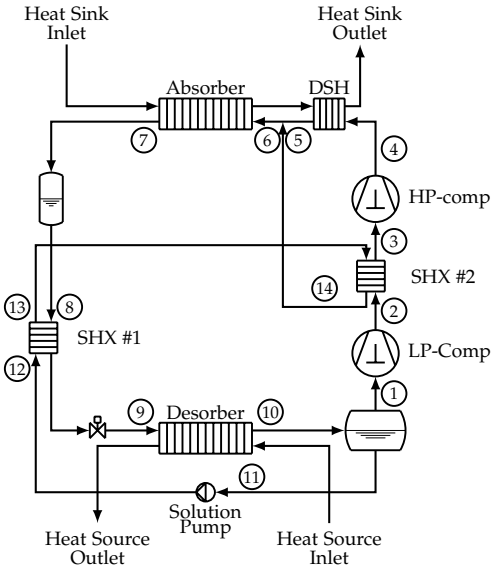

Figure 1: *Schematic diagram of the two-stage compression/absorption heat pump*

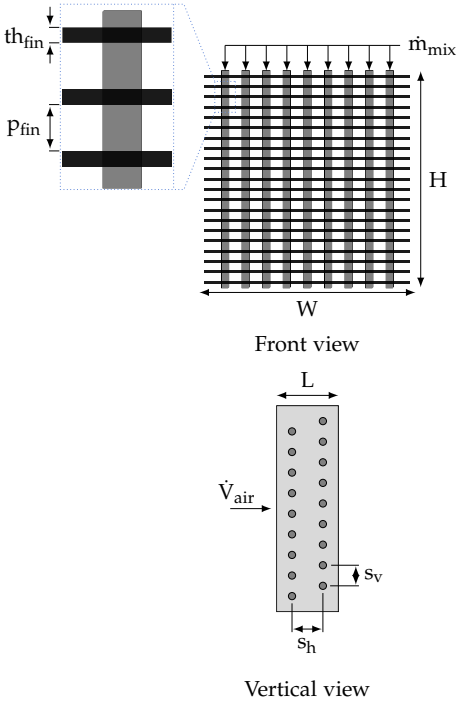

Figure 2: *Schematic diagram of the air cooled vertical tubular absorber*

Absorber simulation model The absorber simulation model is adapted from an EES model for a finned, annular tube cross-flow heat exchanger given by Nellis and Klein [9] The absorber model consist of 10 segments with similar dimensions. Mixture outlet parameters are the inlet parameters for the next segment. Thermophysical properties for the ammonia/water mixture were found using equations given by Thorin [10] and Conde-Petit [11]. Fin efficiencies were found with an approach that the actual fins acted like annular fins connected to the tube. Air inlet temperature was set to 90 °C and the maximum frontal air velocity was limited to 3.5 m/s. The conductance and total thermal resistance for each segment was calculated using equation (1) and (2).

$$UA = \frac{1}{R_{tot}} \tag{1}$$

$$R_{tot} = R_{in} + R_{cond} + R_{out} \tag{2}$$

The absorber model is cross-flow, thus need to be corrected with the *LMTD F* factor. The LMTD effectiveness, P_{HX}, and LMTD capacitance ratio R_{HX} is calculated:

$$P_{HX} = \frac{T_{C,out} - T_{C,in}}{T_{H,in} - T_{C,in}} \tag{3}$$

$$R_{HX} = \frac{\dot{C}_C}{\dot{C}_H} = \frac{T_{H,in} - T_{H,out}}{T_{C,out} - T_{C,in}} \tag{4}$$

The correction factor is found using an integrated EES function for a cross-flow with both fluids unmixed.

$$\Delta T_{lm} = \Delta T_{lm,cf} \cdot F_{HX} \tag{5}$$

$$\dot{Q} = UA \cdot \Delta T_{lm} \tag{6}$$

The transferred heat for each segment is corrected using equation (5) and (6), before the new calculated values are used in the next iteration. Mixture heat transfer coefficient is calculated using the Dittus-Boelter equation (equation 7), and the thermal resistance on the inner tube walls are calculated using equation 8.

$$\alpha_{mix} = 0.023 \cdot Re_D^{0.8} \cdot Pr^{0.4} \cdot \frac{\lambda_{liq}}{D_{in}} \tag{7}$$

$$R_{in} = \frac{1}{\alpha_{mix} \cdot \pi \cdot D_{in} \cdot L} \tag{8}$$

Reynolds number and Prandtl number is calculated using equation 9, 10, 11 and 12. The approach for the absorption process is that the mixture velocity decreases as vapour condenses and is absorbed into the liquid. The mixture velocity is adjusted so that the average density in each segment is the density of saturated liquid and saturated vapour times the fraction of liquid and vapour respectively.

$$Re_D = \frac{\rho_{liq} \cdot u_m \cdot D_{in}}{\mu_{liq}} \tag{9}$$

$$Pr = \frac{c_p \cdot \mu_{liq}}{\lambda_{liq}} \tag{10}$$

$$u_m = \frac{4 \cdot \dot{m}}{\rho_{avg} \cdot D_{in}^2} \tag{11}$$

$$\rho_{avg} = \rho_{liq} \cdot (1 - q) + \rho_{vap} \cdot q \tag{12}$$

Thermal resistance on the air-side surface is calculated using equation 13. Air heat transfer coefficient is found using an EES function for external flow over a staggered bank, while the fin efficiency is found using an EES function for annular fins with the assumption that the rectangular fins behave like annular fins.

$$R_{out} = \frac{1}{\eta_{overall} \cdot \alpha_{air} \cdot A_{tot}} \tag{13}$$

The conduction resistance is found by using equation 14.

$$R_{cond} = \frac{ln\left(\frac{D_{out}}{D_{in}}\right)}{2 \cdot \lambda \cdot \pi \cdot L_{tube}} \tag{14}$$

III. Simulation results

Two-stage model: Figure 3, 4, 5 and 6 shows the temperature profiles for the simulations with 93, 95, 97 and 99 weight-% of ammonia in the vapour in the compressor circuit, respectively. Blue heat sink temperature curves represent the temperature curves when the temperature difference at the absorber inlet and outlet is equal. Green heat sink temperature curves represent the temperature curves when the minimum temperature difference is at the absorber inlet, hence heat sink mass flow is reduced in order to maintain the minimum temperature difference. In all the simulation scenarios, the discharge temperature was limited to 180 °C for both compressors. COPs for the scenarios were 1.81, 1.79, 1.75 and 1.56, while the temperature difference at absorber inlet/outlet were 7 °C, 8 °C, 9.5 °C and 14 °C respectively. Table 1 shows an overview of results from simulations with no restrictions to the discharge temperature, while table 2 shows the increase and decreasing of some important parameters between simulation scenarios were the discharge temperature was limited to 180 °C and simulations where it was no limitation to the discharge temperature. Figure 7 shows temperature curves in one of the simulation scenarios with and without desuperheater. Vapour is cooled from 220 °C to 160 °C in the desuperheater, before mixing with liquid solution.

Table 1: *Summary of simulation results with no limitations to discharge temperature*

x_1 [-]	0.93	0.95	0.97	0.99
COP [-]	2.53	2.50	2.47	2.44
CR [-]	1.64	1.49	1.31	0.82
ZZ [-]	0.49	0.54	0.60	0.74
P_{abs} [bar]	25.0	29.5	36.5	53.5
PR [-]	4.92	4.70	4.34	3.66
ρ_1 [kg/m^3]	0.68	0.88	1.27	2.70
ρ_3 [kg/m^3]	2.70	3.45	4.55	8.33
T_4 [°C]	302.6	295.0	283.2	258.8
ΔW_{thr} [kW]	6.0	6.5	7.0	8.0
Q_{des} [kW]	60.5	60.0	59.5	59.5
q_6 [-]	0.33	0.35	0.39	0.52

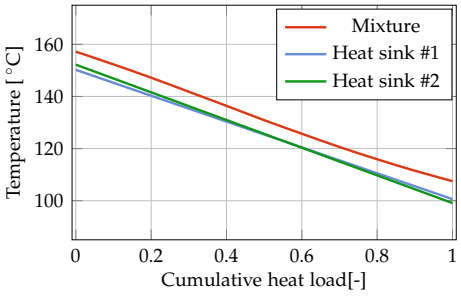

Figure 3: *Temperature versus cumulative heat load with $P_{desorber}$ = 1.03 bar and $P_{absorber}$ = 33 bar.*

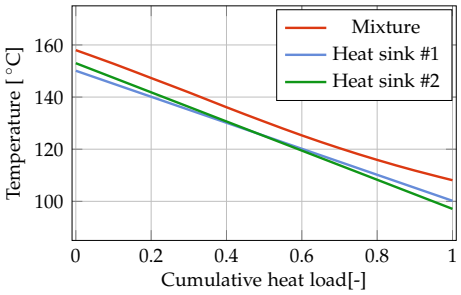

Figure 4: *Temperature versus cumulative heat load for with $P_{desorber}$ = 1.34 bar and $P_{absorber}$ = 38.5 bar.*

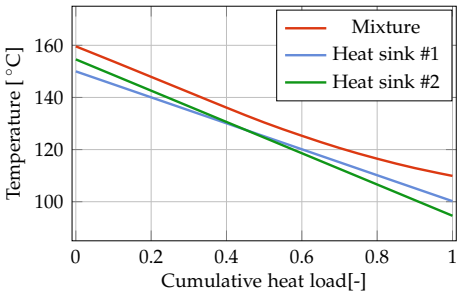

Figure 5: *Temperature versus cumulative heat load with $P_{desorber}$ = 1.94 bar and $P_{absorber}$ = 47.5 bar.*

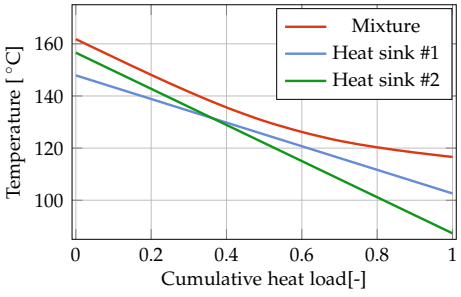

Figure 6: *Temperature versus cumulative heat load with $P_{desorber}$ = 4.0 bar and $P_{absorber}$ = 70 bar.*

Table 2: *Difference in simulation results for the scenarios with discharge temperatures restricted to 180 °C and no limitation*

x_1 [-]	0.93	0.95	0.97	0.99
Δ PR[b)]	13.0	12.5	12.3	12.6
Δ COP[a)]	39.6	39.8	40.6	56.8
Δ W_{thr}[b)]	37.4	37.3	38.0	42.5
Δ CR[a)]	54.3	59.5	78.4	149.7
Δ ZZ[b)]	13.3	13.0	13.8	13.5

[a)] Percentage increase
[b)] Percentage decrease

(a) *Without desuperheater*

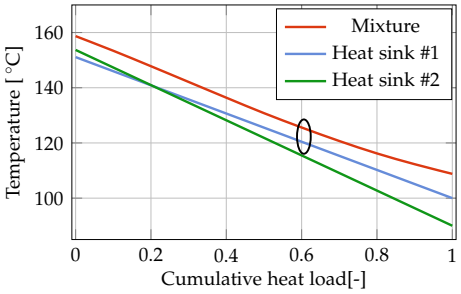

(b) *With desuperheater*

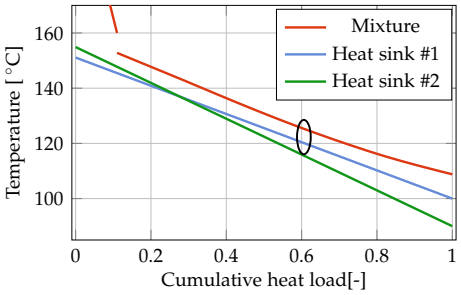

Figure 7: *Temperature versus cumulative heat load with and without desuperheater when P_{des} = 1.94 bar and P_{abs} = 41 bar.*

Absorber model: In order to maintain a relatively large mixture heat transfer coefficient, the number of tubes was limited to 24. Table 3 shows the simulations results for different number of tube rows and columns with a staggered arrangement and a tube spacing of 60 mm.

Table 3: *Heat exchanger geometries and simulation results with 60 mm tube spacing*

Scenario	#1	#2	#3	#4
N_{row} [-]	4	6	8	12
N_{col} [-]	6	4	3	2
W [m]	0.30	0.42	0.54	0.78
H [m]	2.00	1.45	1.30	1.05
L [m]	0.42	0.30	0.24	0.18
H_{tot} [m]	20.0	14.5	13.0	10.5
p_{fin} [mm]	7.5	4.0	3.0	2.0
A [m^2]	646	854	1044	1368
$\dot{V}_{air}$ [m^3/s]	2.10	2.13	2.46	2.87
α_{mix} [W/m^2-K]	1208	1205	1173	1145
α_{air} [W/m^2-K]	69	66	62	56
U_y [W/m^2-K]	8.9	6.7	5.7	4.2
ΔP [Pa]	371	248	187	125
W_{fan} [kW]	3.1	2.1	1.8	1.4
$T_{mix,out}$ [°C]	101.2	100.7	100.2	101.0
$T_{air,out}$ [°C]	139.7	139.6	133.4	126.3

Spray drying case: Table 4 shows the simulation results from the spray drying case. Air was used as heat source and heat sink medium, and air inlet temperature in the desorber was set to 35 °C. Ammonia concentration in the saturated vapour was 97.5 weight-%, overall ammonia concentration 0.75 and absorber pressure was 45 bar.

Table 4: *Simulation results from spray drying case*

P_{des}	1.03 bar
P_{abs}	45.0 bar
x_{vap}	0.975
ZZ	0.75
$\dot{m}_{mix}$	0.11 kg/s
$\dot{m}_{air,des}$	1.57 kg/s
$\dot{m}_{air,abs}$	1.82 kg/s
CR	0.50
$\dot{Q}_{abs}$	100.0 kW
$W_{LP\text{-}comp}$	31.2 kW
$W_{HP\text{-}comp}$	37.8 kW
W_{pump}	0.2 kW
W_{fan}	2.0 kW
COP	1.45
COP w/fan	1.40

IV. Discussion

Figure 3, 4, 5 and 6 showed that the overall ammonia concentration has a larger impact on the linearity of the temperature curves than the absorber pressure. The temperature difference at the absorber inlet and outlet increased as the ammonia concentration in the vapour increased. Increasing the limitation to the discharge temperature resulted in lower absorber pressures and lower overall ammonia concentrations. Although absorber pressures decreased, lower overall ammonia concentrations resulted in more linear mixture temperature curves.

In all simulations, the requirement to heat pump heating capacity was 100 kW, thus the total mixture mass flow rates was adjusted according to calculated enthalpy differences. However, simulation results indicated that the mixture mass flow between the different scenarios only had minor differences. As the pressure ratio increased for increasing ammonia concentration in the vapour, the specific compressor work decreased but the COP also decreased. Since the circulation ratio decreased and the total mixture mass flow rate was approximately the same, a larger quantity of the total mixture mass flow rate went through the compressor circuit, hence the decrease in COP. COP increased for all scenarios when the limitation to the discharge temperature increased. This increases was a result of lower pressure ratio, thus lower specific compressor work, but also a result of the increasing circulation ratios. Mixture mass flow rates only had minor variations in simulation scenarios when the limitation the discharge temperature was increased, hence a smaller mass flow rate through the compressor circuit.

There was a significant difference between vapour densities in the scenarios. Results presented in table 1 show that with an x_{vap} of 0.99, the vapour density is four times higher than with an x_{vap} of 0.93. Although the differences in circulation ratios, hence difference in vapour

mass flow rates, is quite substantial the difference in volumetric flow rates is large. If one disregards volumetric losses in the compressor the difference in volumetric flow rates to the LP-compressor is reduced to three times as high. Increasing the limitation to the discharge temperature decreases the volumetric flow rate to the LP-compressor by 20-25 % for all scenarios, while the volumetric flow rate to the HP-compressor is reduced by 8-10 %. The smaller reduction for the HP-compressor can be explained by a lower absorber pressure, hence lower intermediate pressure resulting in a smaller vapour density

Evaluating figure 7 shows that with the approach that the mixing of vapour and liquid solution is adiabatic and in equilibrium before the absorber, only moves the starting point of the mixture temperature curve in the absorber. Since the heat available in the desuperheater is equal to the reduction in heat in the absorption process, the water outlet temperature cannot be higher if the mass flow rate is unchanged. Since the mixture temperature curve is unchanged, the minimum temperature difference between mixture and water occur at the same location in the heat exchange. It means that in order to achieve a higher water outlet temperature, the minimum temperature difference must occur at the outlet for the original process.

Absorber simulations showed that by increasing the number of tube rows, maintained the total number of tubes, resulted in:

- air pressure drop and fan work decreased
- fin pitches can be smaller
- total air-side surface area increased
- volumetric air flow rate can be increased, however lowering the air outlet temperature
- absorber height decreases, while width and length increases

The geometries listed in table 3 are not entirely realistic due to the extreme ratio between absorber height and width/length. It is difficult to determine whether the somewhat strange simulation results is due to problems is with the simulation model or if the processes is difficult to optimize for the simulation parameters. However, there are some factors that may have contributed to the results.

- The air mass flow rate was approximately 15 times higher than the air mass flow rate.
- High thermal resistance in absorber material.
- Limited frontal air velocity.

In the spray drying case the temperature difference between heat source and heat sink may have been to large resulting in low COP. The ammonia concentration in the vapour had to be 97.5 weight-% to avoid sub-atmospheric pressure, and it resulted in a pressure ratio of 6.6 for the compressors.

V. Conclusion

- Overall ammonia concentration is more significant than for the linearity of the temperature curves than the pressure.
- A high water content in the vapour to the compressor results in higher COP and lower absorber pressure.
- A low water content in the vapour to the compressor results in lower pressure ratios, discharge temperatures and compressor volumes.
- With no limitations the discharge temperature, COP increases by approximately 40 %, pressure ratios by 12 - 13 % and absorber pressures by 23 - 25 % for all scenarios, compared to simulations with the discharge temperature limited to 180 °C
- With the assumptions in the model, a desuperheater will only be beneficial if

the minimum temperature between mixture and heat sink occur at the absorber inlet. Even then, the gain is small.

- Absorber simulations did not give any realistic absorber geometries due to the extreme ratio between absorber height and width/length.

- The simulation inputs for the spray drying case may not have been optimal for the process

Nomenclature

Latin letters		
A	Area	m^2
c_p	specific heat capacity	kJ/kg-K
COP	coefficient of performance	-
CR	circulation ratio	-
D	diameter	m
DSH	desuperheater	-
F_{HX}	correction factor	-
H	height	m
HP	high-pressure	-
L	length	m
LMTD	logat	m
LP	low-pressure	-
$\dot{m}$	mass flow rate	kg/s
N_{col}	number of tube columns	-
N_{row}	number of tube rows	-
P	pressure	bar
p_{fin}	fin pitch	mm
P_{HX}	LMTD capacitance ratio	-
Pr	Prandtl number	-
PR	pressure ratio	-
q	vapour quality	-
$\dot{Q}$	heat transfer rate	kW
R	thermal resistance	m^2-K/W
R_{HX}	LMTD effectiveness	-
Re_D	Reynolds number	-
s_h	horizontal tube spacing	mm
s_v	vertical tube spacing	mm
SHX	solution heat exchanger	-
T	temperature	°C or K
th_{fin}	fin thickness	mm
u_m	mean velocity	m/s
U_y	overall heat transfer coefficient	W/m^2-K
UA	conductance	W/m^2-K
$\dot{V}$	volumetric flow rate	m^3
W	work / width	kW or m
x	ammonia concentration	-
ZZ	overall ammonia concentration	-
Greek letters		
α	heat transfer coefficient	W/m^2-K
η	fin efficiency	-
λ	thermal conductivity	W/m-K
μ	dynamic viscosity	Pa-s
ρ	density	kg/m^3
Subscripts		
abs	absorber	-
C	cold	-
comp	compressor	-
cond	conduction	-
des	desorber	-
H	hot	-
in	inner	-
liq	liquid	-
mix	mixture	-
out	outer	-
thr	throttling	-
tot	total	-
vap	vapour	-

References

[1] O Brunin, M Feidt, and B Hivet. "Comparison of the working domains of some compression heat pumps and a compression-absorption heat pump". In: *International Journal of Refrigeration* 20.5 (1997), pp. 308 –318.

[2] J. Kim et al. "Experimental study of operating characteristics of compression/absorption high-temperature hybrid heat pump using waste heat". In: *Renewable Energy* 54.0 (2013), pp. 13 –19.

[3] M. Hultén and T. Berntsson. "The compression/absorption cycle - influence of some major parameters on COP and a comparison with the compression cycle". In: *International Journal of Refrigeration* 22 (1999), pp. 91–106.

[4] M. Hultén and T. Berntsson. "The compression/absorption heat pump cycle - conceptual design improvments and ccomparison with the compression cycle". In: *International Journal of Refrigeration* 25 (2002), pp. 487–497.

[5] L. Itard and C. Machielsen. "Considerations when modelling compression/resorption heat pumps". In: *International Journal of Refrigeration* 17.7 (1994), pp. 453 –460.

[6] S. R. Nordtvedt. "Experimental and theoretical study of a compression/absorption heat pump with ammonia/water as working fluid". PhD thesis. Norwegian University of Science and Technology, 2005.

[7] O. M. Ibrahim and S. A. Klein. "Thermodynamic Properties of Ammonia-Water Mixtures". In: *ASHRAE Trans.: Symposia* 21,2 (1993), p. 1495.

[8] T. Sveine, S. Grandum, and H. Baksaas. "Design of high temperature absorption/compression heat pump". In: *Natural Working Fluids, IIR - Gustav Lorentzen conference*. 1998.

[9] G. Nellis and S. Klein. *Heat Transfer*. Cambridge University Press, 2009.

[10] E. Thorin. "Thermophysical Properties of Ammonia/Water Mixtures for Prediction of Heat Transfer Areas in Power Cycles". English. In: *International Journal of Thermophysics* 22.1 (2001), pp. 201–214.

[11] D. M. R. Conde-Petit. *Thermophysical Properties of NH_3 + H_2O solution for the industrial design of absorption refrigeration equipment*. Tech. rep. M. Conde Engineering, 2004.